Advancements in material removal mechanism and surface integrity of high speed metal cutting: A review

Bing Wang[1,2,*], Zhanqiang Liu[1,2,**], Yukui Cai[1,2], Xichun Luo[3], Haifeng Ma[1,2], Qinghua Song[1,2], Zhenhua Xiong[4]

([1] *School of Mechanical Engineering, Shandong University, Jinan 250061, China*

[2] *Key Laboratory of High Efficiency and Clean Mechanical Manufacture of MOE/Key National Demonstration Center for Experimental Mechanical Engineering Education, Jinan 250061, China*)

[3] *Centre for Precision Manufacturing, DMEM, University of Strathclyde, Glasgow, UK*

[4] *State Key Laboratory of Mechanical System and Vibration, School of Mechanical Engineering, Shanghai Jiao Tong University, Shanghai 200240, China*

*Corresponding author, Telephone: +86-15275134008, Email: sduwangbing@sdu.edu.cn

**Corresponding author, Telephone: +86-531-88393206, Email: melius@sdu.edu.cn

Abstract

The research and application of high speed metal cutting (HSMC) is aimed at achieving higher productivity and improved surface quality. This paper reviews the advancements in HSMC with a focus on the material removal mechanism and machined surface integrity without considering the effect of cutting dynamics on the machining process. In addition, the variation of cutting force and cutting temperature as well as the tool wear behavior during HSMC are summarized. Through comparing with conventional machining (or called as normal speed machining), the

advantages of HSMC are elaborated from the aspects of high material removal rate, good finished surface quality (except surface residual stress), low cutting force, and low cutting temperature. Meanwhile, the shortcomings of HSMC are presented from the aspects of high tool wear rate and tensile residual stress on finished surface. The variation of material dynamic properties at high cutting speeds is the underlying mechanism responsible for the transition of chip morphology and material removal mechanism. Less surface defects and lower surface roughness can be obtained at a specific range of high cutting speeds, which depends on the workpiece material and cutting conditions. The thorough review on pros and cons of HSMC can help to effectively utilize its advantages and circumvent its shortcomings. Furthermore, the challenges for advancing and future research directions of HSMC are highlighted. Particularly, to reveal the relationships among inherent attributes of workpiece materials, processing parameters during HSMC, and evolution of machined surface properties will be a potential breakthrough direction. Although the influence of cutting speed on the material removal mechanism and surface integrity has been studied extensively, it still requires more detailed investigations in the future with continuous increase in cutting speed and emergence of new engineering materials in industries.

Keywords: High speed metal cutting; Material deformation; Material removal mechanism; Surface integrity; Cutting force and temperature; Cutting tools

1. Introduction

Mechanical machining, as a subtractive manufacturing operation, is one of the most widely used manufacturing processes. Although some emerging manufacturing processes, such as additive manufacturing, have advanced beyond rapid prototyping to the manufacture of structural and functional components, the dominant role of machining is still irreplaceable owing to its flexibility [1], good surface quality [2], high material removal rate [3], and the capability to machine nearly all types of materials [4].The global machining market is estimated to be worth over $400 billion by the year 2022 with an annual growth rate of 6-7% [5], which indicates the large demand for machining and the necessity to reduce the machining cost.

The development of machining process is generally aimed at improvements in production efficiency and product quality and at cost reduction. To achieve these goals, high performance machining has been pursued by both academia and industries. Extensive research involving experiments [6], analytical modeling [7], and numerical simulation [8] of machining process has been conducted to understand the interaction between cutting tools and workpiece materials. In particular, comparing with the experimental research, analytical modeling and simulation of machining processes are important in the present digital manufacturing era, due to their low cost and capability to serve as a basis for digital twins. The machining performance has been progressing steadily through the optimization of process parameters and advancement of cutting tools and machining equipment [9].

High speed machining (HSM), which was first proposed by Salomon on 1931 [10], has been promoting the development of machining processes at a faster pace.

Owing to its unique technical advantages, it has been one of the most popular research topics in the field of metal cutting. The most prominent benefit of HSMC is the significantly higher processing efficiency induced by the high cutting speed [11]. In recent decades, a substantial number of studies reported that machined surface quality can be improved using HSMC when appropriate process parameters are selected [12-14]. With the development of ultra-hard cutting tools and HSMC equipment, the cutting speed has been increased by several times [2].

HSMC has great potentials in the manufacture of high-value added products such as aviation components, where large quantities of difficult-to-machine materials are widely used. For example, titanium and nickel-based alloys are dominant materials used in aviation engines owing to their good physical and mechanical properties. However, their machinability is pretty poor leading to deteriorated surface quality and low production rate [15]. Thin-walled complex structures with light weight are commonly employed in aviation industries, for which high material removal rate is extremely necessary [16]. The advantages of HSMC, including the low cutting force and high machining efficiency, can satisfy the requirements for manufacturing such aviation components.

Fig. 1 presents the evolution and application of HSMC from the perspectives of machining tool, spindle speed, cutting speed, material removal rate, industrial application, and the division of cutting speed range. With the development of machine tools, starting from the earliest and manual ones (i.e., the first and second generations as shown in Fig. 1) to the CNC machine tools (i.e., the third and fourth

generations as shown in Fig. 1), the spindle speed and associated cutting speed and material removal rate have been increased by over one hundred times [9]. The development of electro-spindle with higher rotation speeds has further increased the cutting speed in recent decades. The potential technical superiorities of HSMC, including the higher production rate and lower machining cost, have been presented in industrial applications. Meanwhile, the emergence and advancement of HSMC has expanded the capability of machining processes from processing easy-to-cut materials to processing difficult-to-machine materials such as superalloys [2,17] and brittle materials [18].

Nevertheless, the limitations of fundamental understanding of HSMC, especially the material removal mechanism and machined surface integrity, have restricted full utilization and further expansion of HSMC in industrial applications. The material dynamic properties and surface plastic deformation at high cutting speeds during HSMC have not been understood clearly. Consequently, process planning in HSMC is restricted by the insufficient knowledge. Furthermore, the cutting speed range that can be achieved in the shop floor is always limited by some known or unknown conditions. For example, when a favorable aspect of HSMC is used like reducing the surface roughness at high cutting speeds, tensile residual stress may be formed on the machined surface or the cutting tool life may be significantly decreased as a sacrifice. A balance between the pros and cons of HSMC must be determined reasonably to make full use of this advanced processing technology [11,15,19]. Research on HSMC considering more practical conditions

that used in industries is a prerequisite to make such as a balance.

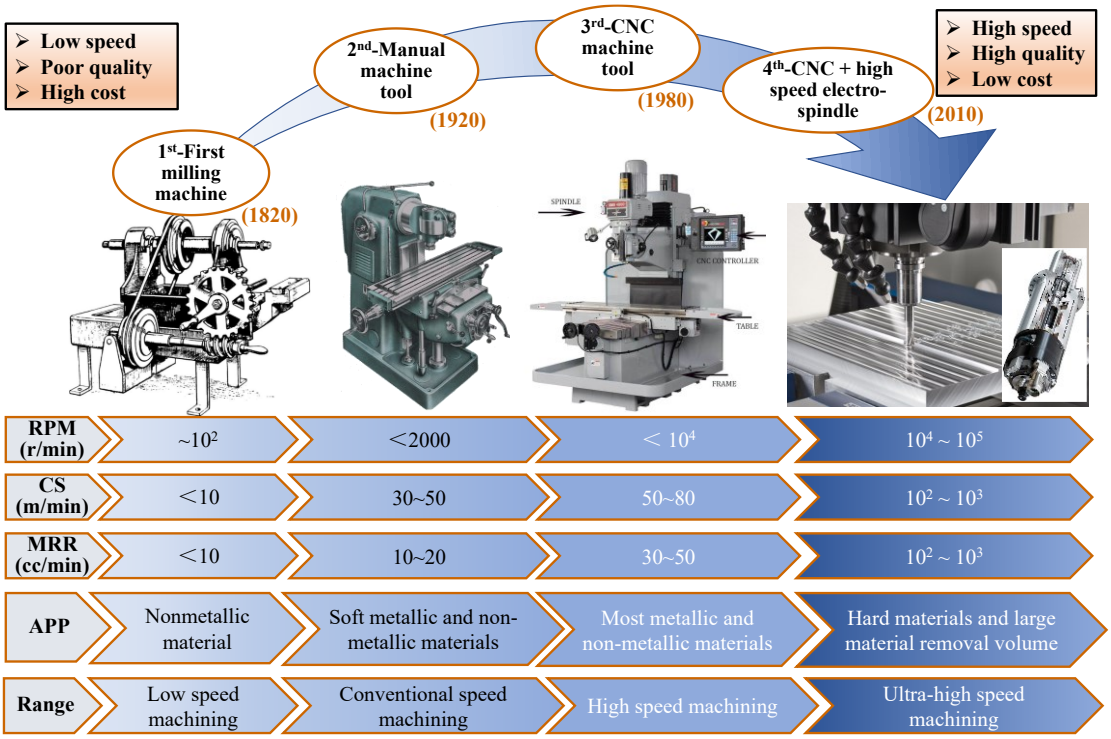

Fig. 1. Evolution and application of high speed metal cutting. (Note: CNC- computer numerical control, RPM-revolutions per minute, CS-cutting speed, MRR-material removal rate, APP-application)

In addition, the evaluation on the machined surface quality has evolved from macro parameters, such as the surface roughness and surface defects, to micro or nano levels such as the crystalline features and phase transformations. Advanced material characterization tools, including Transmission Electron Microscopy (TEM) and Electron Back-Scattered Diffraction (EBSD), make it possible to get deeper insights into the underlying mechanisms of material removal and machined surface formation during HSMC.

We acknowledge at the outset that there have been several noteworthy review papers on HSMC in recent decades [2,3,20], and they were mainly focused on the

experimental results and process modeling while lacked micro-mechanism analysis due to the limitation of microscopic observation tools at that time. The relationships among material removal mechanism, machined surface integrity, and processing parameters have also not been understood clearly. To address the research gap that still occurs, this article is aimed at reviewing the state-of-the-art of HSMC to elaborate its pros and cons for the first time, and at highlighting the challenges in its practical application. In particular, the material removal mechanism and machined surface integrity of HSMC are addressed. The dynamic deformation behavior of workpiece material, microstructural evolution of machined surface, and thermal-mechanical loading characteristics in HSMC, are systematically reviewed and correlated to understand the technical advantages and current research limitations of HSMC. Although there have been some prominent achievements until now, a few potential research directions are recommended, which demonstrate the urgent need to continue the development of HSMC for both academia and industries.

The paper is organized in six sections (Sections 2-7) followed by future research directions and conclusions. Section 2 outlines the definition and history of HSMC, and some technical methods to achieve high cutting speeds. Section 3 and Section 4 present the material removal mechanism and machined surface integrity during HSMC, respectively. The cutting force and cutting temperature, in addition to the tool wear behavior and mechanism are discussed in Section 5 and Section 6, respectively. The pros and cons of HSMC are elaborated from the above aspects. Several typical application cases of HSMC in industries are presented in Section 7.

At last, the future research directions on HSMC are discussed and the conclusions are drawn highlighting still-to-be-tackled challenges. Fig. 2 shows the framework of this review paper.

It needs to be noted that the "HSMC" involved in this review paper is limited to high speed metal cutting while excluding the abrasive machining, and the effect of cutting dynamics (i.e., vibration of the cutting tool and workpiece) on the machining process is also excluded. To keep the review scope in a focus, HSMC that achieved in the machining modes of orthogonal cutting, turning, and milling are reviewed in this paper. The main content of this paper, especially the material removal mechanism and machined surface integrity of HSMC, is put on the research progress made after the publication of the handbook of high-speed machining technology in the year 2013 [21].

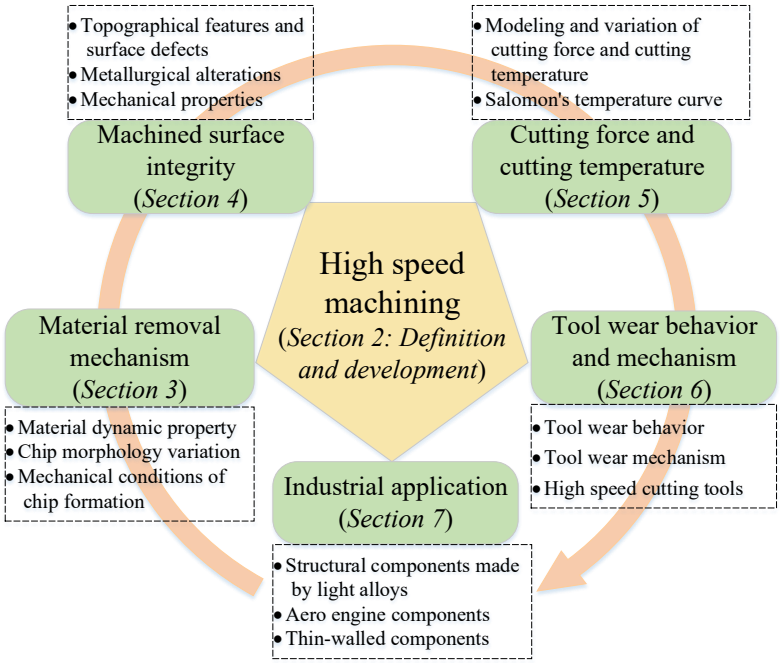

Fig. 2. The framework of this review paper.

2. Definition and development of HSMC

2.1 Definition

Dr. C. Salomon was granted a German Patent about HSMC in 1931 and first proposed the hypothesis based on a series of experiments that cutting temperatures begin decreasing above a certain cutting speed [10]. Salomon's cutting temperature curve indicated that there is a cutting speed range (also called death valley) where machining cannot be performed owing to the excessively high temperatures and associated severe cutting tool wear. Initially, HSMC was defined as machining at cutting speeds higher than the death valley. Nevertheless, the existence of Salomon's curve and its occurrence condition are still being debated in the metal cutting field as open questions [22]. Detailed discussion about the research progress on Salomon's curve will be discussed in Section 5.2.

The cutting speed range in HSMC is a relative concept, and it depends on the cutting processes, workpiece materials and cutting tools used [23]. It was once recommended that machining within a speed range of 500 m/min-7,000 m/min [11] or machining with a spindle rotation speed higher than 8,000 r/min [24] belongs to HSMC. Schulz and Moriwaki [3] defined HSMC as machining whereby cutting speeds are five to ten times higher than conventional cutting speeds. Nevertheless, the above division of cutting speed range for HSMC does not consider specific cutting conditions and workpiece materials.

Fig. 3 shows the milestones of development for HSMC, covering several typical findings contributed to advancement of HSMC at different eras. Since

Salomon proposed the concept of HSMC, its development was slow due to limited performance of available machining equipment for nearly half century. Through considering inertia effect of material deformation at ultra-high cutting speeds, Arndt [25] proposed a new cutting force model adaptable for ultra-high speed machining (UHSMC). After that, based on HSMC experiments, Icks [26,27] suggested that the cutting speed range between 1000 m/min and 10,000 m/min belongs to HSMC and it depends on the machining process.

The consistent increase in spindle rotation speed resulted in a prosperous development of HSMC in the 1990s. Schulz [23,28] verified that precipitation hardening plays an important role in the transformation of chip formation from continuous to segmented and the associated cutting speed range of HSMC. A fixed classification into three ranges of cutting speeds was once suggested as conventional machining (0-500 m/min), HSMC (500 m/min-10,000 m/min), and UHSMC (>10,000 m/min) [11]. Tönshoff et al. [29,30] recommended that HSMC be defined as machining at cutting speeds with an essential overstepping of conventional speeds. They proposed that a substantial decrease of production costs caused by increase in cutting speed is an important characteristic entering the range of HSMC. Nevertheless, there was no clarity on what can be considered as a substantial decrease in production costs.

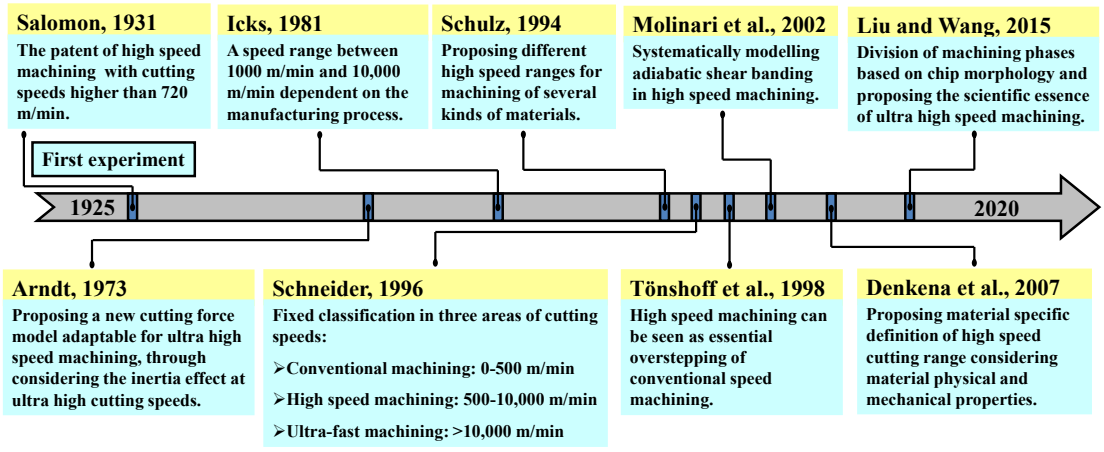

Fig. 3. The milestones of development for academic research on high speed machining [3,10,**Error! Bookmark not defined.**-31,35,36].

The machining mechanism and scientific essence of HSMC have been more focused on in recent decades. Molinari et al. [31] modelled adiabatic shear banding in HSMC based on the previous work performed by Recht [32], Komanduri et al. [33], and Davies et al. [34]. Denkena [35] developed a predictive model of critical cutting speed for HSMC considering physical and mechanical properties of workpiece materials. According to Denkena's model, the critical cutting speed mainly depends on material thermal-physical properties of density, specific heat, thermal conductivity, and material mechanical property of tensile strength. Based on a series of experiments as well as analytical modeling and numerical simulation of HSMC, Liu and Wang [36-38] suggested a division of machining phases based on chip morphology and material deformation mechanism, and proposed the scientific essence of brittle fracture of workpiece materials during UHSMC. The development of fundamentals about HSMC is beneficial for getting deep insights into it and has also significantly promoted its application.

Besides the above achievements, the handbook of high-speed machining technology edited by King [21] systematically summarized HSMC from the aspects of general theory and industrial application. Some other researchers, including Tlusty [39], Smith and Tlusty [40], Schmitz and Donalson [41], Movahhedy and Mosaddegh [42] focused on the characteristics of cutting dynamics during HSMC of different workpiece materials to maximize the machining performance.

New definitions of HSMC have been formulated in compliance with advanced knowledge. The machining process enters a new regime only when the deformation behavior of workpiece material undergoes a significant transformation. The material localized deformation behavior within adiabatic shear bands (ASBs) is distinctly different from the uniform plastic deformation of continuous chips [31,34]. Consequently, the existence of ASBs and associated formation of serrated chips have been identified as an indication of HSMC and gradually accepted by academia [43,44]. It needs to be noted that although the critical cutting speed for adiabatic shear is relatively low for certain workpiece materials such as titanium alloys owing to their poor thermal properties, it can still be regarded as HSMC once the cutting speed is higher than that for ASB formation. With a constant increase in the cutting speed, workpiece materials undergo ductile to brittle transition due to the embrittlement effect of the high strain rate. Consequently, the material deformation mechanism transforms from adiabatic shear to brittle fracture, which can be regarded as the indication of UHSMC [36,37]. Therefore, HSMC can be defined as machining with a cutting speed higher than that for ASB formation, whereas UHSMC can be

defined as machining with a cutting speed higher than that for fragmented chip formation induced by workpiece material embrittlement.

A consensus has been reached that the high speed in HSMC is preferably referred to a combined economic and performance target, rather than merely a technical parameter [11]. It is difficult to define HSMC by a specific cutting speed range, which is always varied for different cutting conditions. Consequently, high performance machining is put forward [11] to get the maximum output from machining processes by adjusting machining parameters.

2.2 Test methods to achieve high cutting speeds

Besides using a high-speed spindle directly, high cutting speeds can be achieved by different methods as seen in Fig. 4. A large diameter of cutting tool or workpiece can help to increase linear cutting speeds if a high-speed spindle is not available. Wang et al. [36] installed a disk workpiece with 130 mm in diameter to the spindle of a machine tool through a tool shaft as shown in Fig. 4a. This method can achieve high cutting speeds at relatively low spindle speeds. A cutting speed range of 50 m/min to 8,000 m/min was obtained by Wang et al. during machining of different workpiece materials such as Inconel 718 and aluminum alloy 7050-T7451.

Simultaneous rotations of spindle and workpiece in an opposite direction can increase the linear cutting speed effectively. Zhou et al. [45] adopted a machining tool with double spindles rotating oppositely to achieve a maximum cutting speed of 30,000 m/min, as seen in Fig. 4b. The finished surface quality of pure aluminum

A1199 and aluminum alloy A5056 were studied at this high cutting speed.

Modifying Split Hopkinson Pressure Bars (SHPB) or Taylor Bar is common method to realize high cutting speeds, as high-pressure gas can generate very high impact speeds. Either cutting tool or specimen can be set as a moving element, and the cutting depth can be adjusted precisely through fixing the relative position between workpiece and cutting tool. HSMC generated by high-pressure gas is also called as ballistic machining. Sutter et al. [46], Sutter and List [47] developed a ballistic machining setup shown in Fig. 4c, and performed HSMC experiments of titanium alloy Ti6Al4V over a wide speed range from 300 m/min to 4,400 m/min. Considering that the ballistic machining is realized by a linear movement between the cutting tool and workpiece, in-situ measurement or observation of machining process with a high-speed camera can be conveniently conducted, and this is a prominent advantage compared with other HSMC methods. Ye et al. [48] established a ballistic machining setup using a light-gas gun shown in Fig. 4d that can provide cutting speeds up to 12,000 m/min, and carried out HSMC experiments on AISI 1045 steel. The highest cutting speed was achieved by Arndt [25] as 8,000 ft/s (equivalent to 146,304 m/min) using the ballistic machining method, whereby the inertia effect of material deformation caused by the ultra-high cutting speed was revealed. Wuertemberger [49] reported an ultra-high speed test setup based on a rocket propulsion, which can achieve ultra-high speeds up to 10,000 m/s. Although the setup was applied to study the wear behavior of high-speed rocket sleds, it can still provide some inspiration for designing new HSMC setups to obtain higher

cutting speeds.

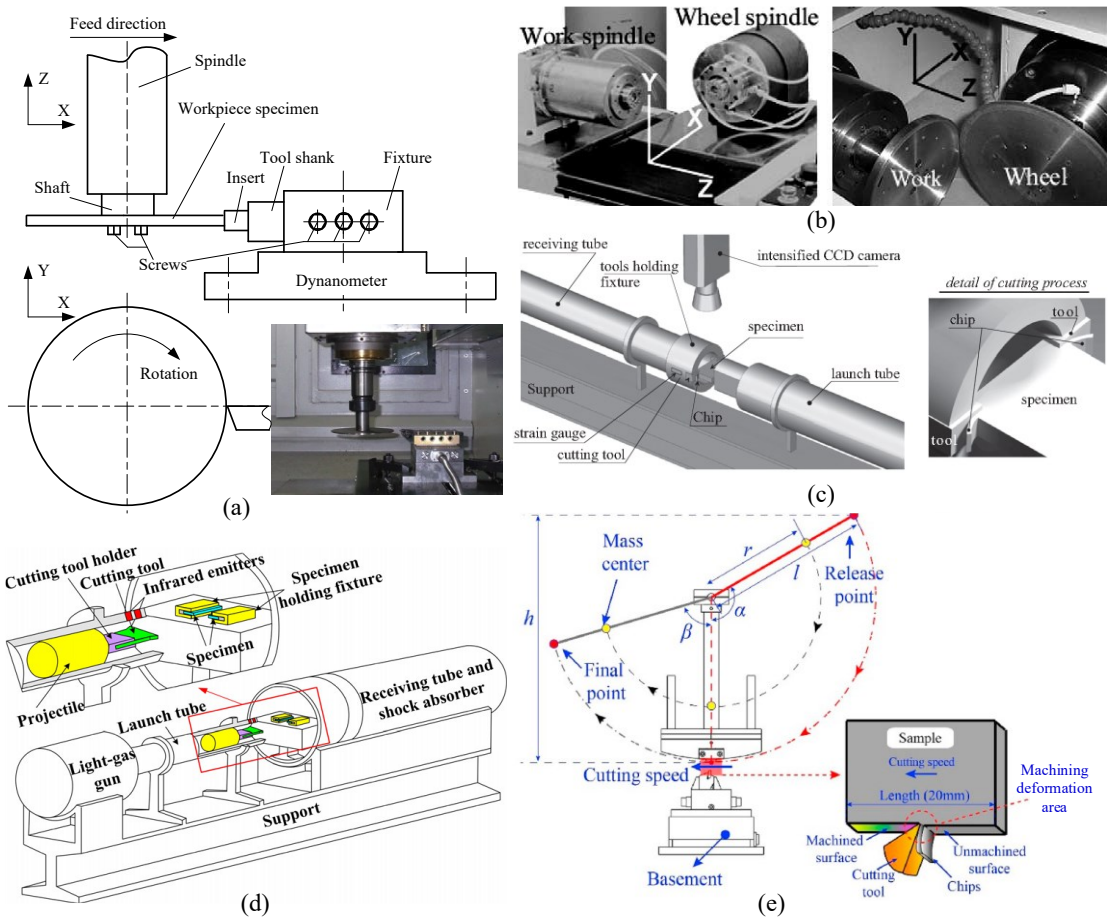

Fig. 4. Different methods to achieve high cutting speeds. (a) High speed machining achieved with a large diameter of workpiece [36]. (b) High speed machining achieved by double spindles [45]. (c) and (d) Ballistic machining setups [46-48]. (e) Pendulum based Cutting Test setup [50,51].

A recent work performed by Xu et al. [50,51] reported that a Pendulum based Cutting Test (PbCT) setup, as shown in Fig. 4e, was used to investigate the effect of varying cutting speed on chip morphology and surface integrity. Although the maximum cutting speed of 140 m/min they obtained was not very high, it provided a simple and feasible way to achieve continuously varying cutting speed in a single cutting step. Similarly, the ballistic machining setup shown in Fig. 4c,d can also

generate continuously changed cutting speed because decaying speed of moving bodies (either cutting tool or workpiece) occurs in both PbCT and ballistic machining setup.

Among different methods to achieve high cutting speeds as shown in Fig. 4, those realized based on machining tools (as shown in Fig. 4a,b) may work better than the others, because the machine tools possess higher rigidity and precision. Nevertheless, the modifying SHPB and ballistic machining setup also have their own advantages as they can be combined with in-situ measurement more easily. It is difficult to determine which method is the best to perform HSMC experiments, and one should choose the most suitable method based on specific research purpose.

High performance machining equipment that can provide high cutting speeds is a foundation for both fundamental research and industrial application of HSMC. No longer simply seeking higher cutting speeds, different sensors have been integrated with machining tools or setups to monitor the machining process or realize in-situ measurement of process parameters. For example, force sensors, acoustic emission sensors, high-speed cameras, and thermal imagers can be used to monitor the machining process of HSMC. Multi-sensor fusion has been promoting the development of machining performance [52-55], and it will also be a hot topic in the future research of HSMC to further develop the process superiorities.

3. Material removal mechanism during HSMC

The material deformation behavior and associated removal mechanism during HSMC present distinctly different characteristics compared with those during conventional machining. Consequently, the serrated or fragmented chips produced at high cutting speeds are different from the continuous ribbon chips commonly formed at conventional speeds. The formation of serrated or fragmented chips is generally favorable to the machining process from the perspectives of material removal and chip disposal.

3.1 Material dynamic properties under high speed loading

HSMC has been recognized as a nonlinear dynamic deformation process accompanied by large strain, large strain rate and high temperature in cutting deformation areas [2, 56 - 58]. Modeling of material dynamic properties is a foundation for characterizing the material deformation behavior during HSMC. Particularly, accurate description of material constitutive model is a prerequisite for numerical simulation of machining process.

Mechanical tests on material deformation behavior are bases for evaluating dynamic properties of workpiece materials during metalworking process including HSMC. According to the range of strain rate of material deformation during different metalworking processes, different mechanical tests can be used to develop material models [36]. With the strain rate increasing from 10^{-8} /s to higher than 10^{7} /s, material response can be divided into three sections as static response, quasi-static response and dynamic response. The dynamic response is sub-divided into intermediate strain rate range and high strain rate range [59].

SHPB test is the most widely used method to establish constitutive models of work materials in HSMC [60,61], because the strain rate range of SHPB test overlaps with that in HSMC. Different types of specimens, including standard cylindrical specimens [61,62], hat-shaped specimens [63,64], and pressure-shear plates [65,66], have been attempted in SHPB tests to study material dynamic deformation behavior. Nevertheless, with the cutting speed increasing further to UHSMC range, the strain rate of material deformation can be higher than 10^6 /s [67] approaching that in high-speed impact test.

Johnson-Cook (JC) constitutive model is the most commonly used form to describe material dynamic deformation in machining process [68]. One reason is that JC model is a thermal viscoplastic model suitable for material deformation where the strain rate is over a wide range from 10^3 to 10^6 s^{-1}. Another reason is that the effects of strain, strain rate and temperature are considered in separated ways in JC model, leading to easy calibration for the JC model coefficients. JC model has been applied in numerical simulations of machining process for different workpiece materials such as titanium alloys [58], superalloys [69], aluminum alloys [61], steels [70] and composites [71]. It is found that the effect of thermal softening exceeds the effects of strain and strain rate hardening during high speed loading or HSMC process. As a result, the material is deformed more easily in a localized shear band, which indicates that HSMC provides more suitable conditions for deformation of workpiece materials.

JC model has been modified in different forms to describe material dynamic deformation more precisely. Table 1 lists several typical modified JC constitutive models suitable for different materials. Different factors, such as softening effect caused by dynamic recrystallization [72], strain softening [74], strain rate softening [69], and coupling effects between strain rate and temperature [61,77] are considered in these modified models. For instance, Calamaz et al. [74] used a modified JC model considering strain softening effect in finite element (FE) simulation of machining Ti6Al4V, and proved the reliability of the modified material model. Wang et al. [61] established a modified JC constitutive model of aluminum alloy 7150-T7451 considering the coupling effects between strain rate and temperature. Through comparing FE simulation results of machining process using both JC model and modified JC model, a higher predictive accuracy of the modified material model is verified.

Table 1. Several typical modified JC constitutive models[*].

References	Work materials	Modified JC models	The highest strain rate	Remarks
Andrade et al. [72], Fu et al. [73]	OFHC, 7050-T7 451	$\sigma = (A + B\varepsilon^n)(1 + C\ln(1 + \frac{\dot{\varepsilon}}{\dot{\varepsilon}_0}))\mathrm{x}$ $(1 - (\frac{T - T_r}{T_m - T_r})^m)(\frac{1}{1 - (1 - \frac{(\sigma_f)_{rec}}{(\sigma_f)_{def}})u(T)})$	10^4 s^{-1}	Considering softening effect induced by dynamic recrystallization

Calamaz et al. [74]	Ti6Al4V	$\sigma = (A + B\varepsilon^n(\frac{1}{\exp(\varepsilon^a)}))(1 + C\ln\frac{\dot{\varepsilon}}{\dot{\varepsilon}_0})\text{x}$ $(1-(\frac{T-T_r}{T_m-T_r})^m)(D+(1-D)\tanh(\frac{1}{(\varepsilon+S)^c}))$	10^3 s^{-1}	Considering strain softening effect
Sheikh-Ahmad and Bailey [75]	Pure titanium	$\tau = B\gamma^n(1 + C\ln\frac{\dot{\gamma}}{\dot{\gamma}_0})(\alpha e^{\beta(\frac{T_m-T}{T_m-T_r})})$	10^2 s^{-1}	Modifying strain hardening and thermal softening effects
Li et al. [76]	1045 steel	$\sigma = (A(HRC) + B\varepsilon^{n(HRC)})(1 + C\ln\frac{\dot{\varepsilon}}{\dot{\varepsilon}_0})\text{x}$ $\exp(-(\frac{T^* - m_1}{m_2})^2)$	10^4 s^{-1}	Considering the effect of hardness on strain hardening effect
Wang et al. [69]	Inconel 718	The strain rate coefficient C is modified to $C = C_1 - (C_2 + C_3\sin(\frac{i-5000}{3000}\pi))\text{x}$ $\sin(\frac{T-500}{150}\pi)$	10^4 s^{-1}	Considering strain rate softening effect
Ugodilinwa et al. [77]	Haynes 282	$\sigma = (A + B\varepsilon^n)(1 + C_1\ln\dot{\varepsilon})\times$ $\exp\left[(\lambda_1 + \lambda_2\ln\dot{\varepsilon})(T - T_r)\right]$	10^3 s^{-1}	Considering coupling effects between strain rate and temperature
Wang et al. [61]	7050-T7 451	$\sigma = \left(A + B\varepsilon^n\right)\left[1 - \frac{\tanh(\varepsilon)}{\exp(\varepsilon^p)}\cdot m_1\ln\left(\frac{T}{T_r}\right)\right]\times$ $\left[1 + C\left(1 - \left(\frac{T}{T_m}\right)^{m_2}\right)\ln\left(\frac{\dot{\varepsilon}}{\dot{\varepsilon}_0}\right)\right]\left[1 - (\frac{T-T_r}{T_m-T_r})^{m_3}\right]$	10^4 s^{-1}	Considering coupling effects between strain/strain rate and temperature

[*]Nomenclature: σ -flow stress (MPa); $(\sigma_f)_{rec}$, $(\sigma_f)_{def}$ -flow stress just prior and after recrystallization; u(T)-step function of local temperature; τ -shear stress (MPa); ε - equivalent strain; γ -shear strain; $\dot{\varepsilon}$ -equivalent strain rate; $\dot{\gamma}$ -shear strain rate; $\dot{\varepsilon}_0, \dot{\gamma}_0$ -reference strain rate; T-local temperature (K); T_r-room temperature (K); T_m-melting temperature of workpiece material

(K); A, B, n, C, m, m_1, m_2, m_3- JC constitutive parameters; D, S, λ, α, β-material constants.

Note: The specific parameter values can be tracked in corresponding references.

Based on the viewpoint from Astakhov [3,9], mechanical machining can be regarded as purposeful fracture between the removed layer material and bulk workpiece. Machining conditions that are favorable to material fracture can help improve the machining efficiency. Material fracture is determined by the combined influences of the stress state, strain rate, and temperature. The effect of the stress state on material fracture that occurs during mechanical tests [78] or machining processes [79-81] has been studied, whereby material fracture strain models considering the stress state effect have been developed. The effects of the strain rate and temperature on material dynamic fracture and corresponding fracture strain models have been focused on in recent years through SHPB tests. It has been acknowledged that material fracture strain decreases with either increasing the strain rate or decreasing the temperature [82]. An increase in the strain rate promotes the ductile to brittle transition of ductile materials. Through investigating the effects of the strain rate and stress triaxiality on the equivalent fracture strain of Ti6Al4V, Wang et al. [64] proposed a fracture strain model with an exponential expression of the strain rate as Eq. (1).

$$\bar{\varepsilon}_f = (0.097 + 0.118\mathrm{e}^{-2.764\eta})(1 + 0.217\ln\frac{\dot{\varepsilon}}{\dot{\varepsilon}_0})^{-0.125} \tag{1}$$

where η is the stress triaxiality, $\dot{\varepsilon}$ and $\dot{\varepsilon}_0$ are the loading strain rate and the reference strain rate, respectively.

Micro-mechanism analysis of material fracture at high speed loading can help understand the material failure behavior during HSMC. The cross-sectional microstructures of the fracture surface for Ti6Al4V tested from 0.001 /s (i.e., quasi-static loading) to 16,000 /s revealed that the dominant material fracture mechanism transforms from transgranular fracture to mixed intergranular fracture and transgranular fracture, and then to intergranular fracture [83]. It indicates that ductile to brittle transition occurs for metal with increasing the strain rate.

3.2 Material deformation behavior and material removal mechanism

As the cutting speed increases, the chip morphology evolves from continuous to serrated and then to fragmented. From the perspectives of material removal rate, chip disposal, and machining automation, serrated and fragmented chips are preferable to continuous chips. This is one of the technical superiorities of HSMC. Fig. 5 presents the main research methods for identifying the chip formation mechanism in HSMC including experimental research, analytical modeling, and numerical simulation.

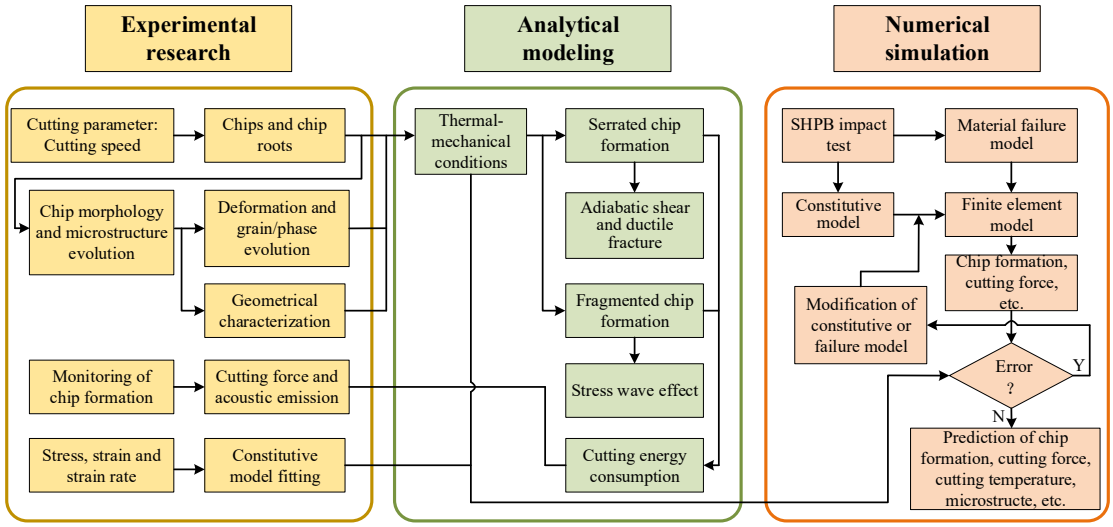

Fig. 5. Research methods about chip formation mechanism during high speed metal cutting.

Experimental research of chips is the most common method for understanding the chip formation mechanism during HSMC. However, it is high-cost and time-consuming. The chip morphology variation and associated microstructure evolution can be studied by analyzing the chips and chip roots produced at different cutting speeds. Geometrical parameters such as the chip thickness, serrated frequency, and degree of chip serration are commonly used to characterize chip morphologies quantitatively [84]. The variations in grain size/orientation and phase transformation within chips can be analyzed to reveal the microstructural evolution [85,86]. In-situ observation of chip formation with high-speed cameras and online measurement of cutting force and acoustic emission are efficient methods for monitoring the material removal behavior during HSMC [47,55]. In recent years, with the development of digital image correlation (DIC) technique, inverse constitutive modeling of chip deformation using coupled DIC and finite element method (FEM) has been a research hotspot [87].

Analytical modeling and numerical simulation are effective for obtaining deeper insights into the scientific essence of chip formation and are more cost-efficient than experimental methods. The modeling of thermal-mechanical conditions for serrated and fragmented chip formation provides a basis for the theoretical research of chip formation mechanism. The adiabatic shear and ductile fracture theory [88-90] and the stress wave effect [36,91] have been acknowledged as efficient theories to explain the formation mechanisms of serrated chips and fragmented chips, respectively. The cutting energy consumption for chip formation can also be theoretically modeled as a function of process parameters.

FEM is the main tool for numerical simulation of HSMC due to its suitability of analyzing severe plastic deformation process and high computational efficiency. Accurate material models, including constitutive model [59,92,93] and friction model [94], are important to guarantee the reliability of simulation results. With numerical simulation, the parameters of cutting force, cutting temperature, and microstructural evolution can also be predicted along with chip formation process. The relationships among experimental research, analytical modeling, and numerical simulation of chip formation in HSMC are illustrated in Fig. 5.

Fig. 6 presents the chip formation process during HSMC of Ti6Al4V and Inconel 718 [95,96]. Both experimental and numerical simulation results are shown in Fig. 6. With the cutting speed increasing, the chip morphology of both Ti6Al4V (Fig. 6a-d) and Inconel 718 (Fig. 6e-h) evolves from continuous to serrated and then to fragmented. The transition speed of chip morphology depends on workpiece

materials. Adiabatic shear theory and periodic fracture were popular perspectives to explain serrated chip formation mechanism. Through analyzing the mechanical conditions on chip free surface and tool tip region, Wang and Liu [89] proposed a mixed mechanism of adiabatic shear and ductile fracture (Fig. 6i) and successfully solve the dispute of the above two famous theories. For the material on chip free surface located at Point A shown in Fig. 6i, positive stress triaxiality occurs and ductile fracture criterion expressed by Eq. (2) is suitable for evaluating material failure. Regarding the material within the tool tip area located at Point B shown in Fig. 6i, negative stress triaxiality occurs and adiabatic shear is apt to be initiated. Adiabatic shear criterion expressed by Eq. (3) is adaptable to evaluate the occurrence of plastic deformation instability.

$$\bar{\varepsilon}_f = f(\eta, \dot{\varepsilon}, T) \tag{2}$$

where T is the deformation temperature which is not considered in Eq. (1). The ductile fracture criterion considering all the effects of strain rate, stress state and temperature was presented in [80].

$$\frac{d\tau}{dV} = \left.\frac{\partial \tau}{\partial \gamma}\right|_{\dot{\gamma},T} \cdot \frac{d\gamma}{dV} + \left.\frac{\partial \tau}{\partial \dot{\gamma}}\right|_{\gamma,T} \cdot \frac{d\dot{\gamma}}{dV} + \left.\frac{\partial \tau}{\partial T}\right|_{\gamma,\dot{\gamma}} \cdot \frac{dT}{dV} = 0 \tag{3}$$

where τ is the shear flow stress, γ is the shear strain, $\dot{\gamma}$ is the shear strain rate, and $d\tau/dV$ implies the total differential calculation of shear flow stress over the cutting speed.

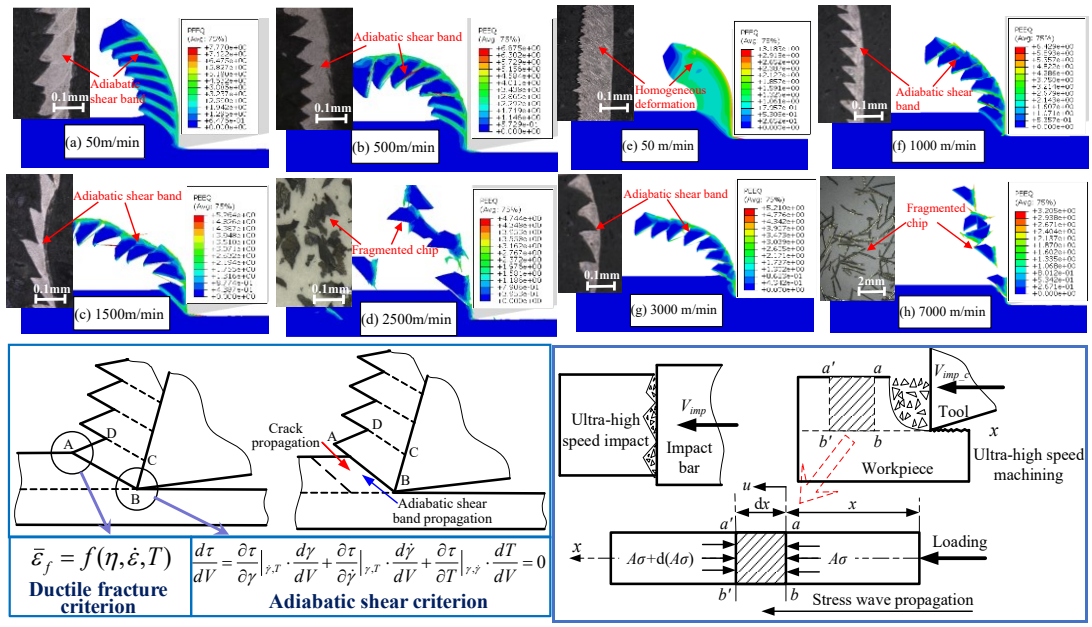

(i) (j)

Fig. 6. Chip formation process during high speed machining of (a-d) Ti6Al4V [95], (e-h) Inconel 718 [96], and formation mechanisms of (i) serrated chip [89], (j) fragmented chip [37].

Three different conditions occur for serrated chip formation based on the criteria of Eqs. (2) and (3). One is that the Eq. (2) is satisfied while Eq. (3) is not satisfied, which means ductile fracture occurs on the chip free surface without ASB formation. With continuous movement of the cutting tool, the ductile fracture propagates from the chip free surface to the tool tip until completed formation of a chip segment. The second condition is that the Eq. (3) is satisfied while Eq. (2) is not satisfied, which means adiabatic shear is responsible for the serrated formation instead of ductile fracture. The ASB propagates along the primary shear zone to the chip free surface. The third condition is that Eq. (2) and Eq. (3) are satisfied simultaneously. The ductile fracture formed on the chip free surface and the ASB formed on the tool tip propagated towards each other until they encounter as seen in Fig. 6i. Through comparing with experimental results of critical cutting speeds for

HSMC of different workpiece materials [80,89], it was proved that an error of less than 10% exists for the predictive results obtained with Eqs. (2) and (3).

Embrittlement of ductile materials at high strain rate loading leads to different chip formation mechanisms compared to low strain rate loading. Through analyzing stress wave propagation within a slender cylindrical sample loaded by impact, Von Karman and Duwez [97] concluded that there was a critical impact speed, over which ductile to brittle transition of deformed material occurs and brittle fracture becomes the dominant failure mode instead of plastic deformation. Zhou et al. [45] studied the effect of cutting speed on material removal mechanism during machining of pure aluminum A1199 and aluminum alloy A5056. They found that ductile metals are expected to behave elastically throughout most of their strength ranges, and become brittle when cutting speed is beyond the static plastic wave propagation rate in workpiece materials. Apparently, taking advantage of material embrittlement at ultra-high cutting speeds, the cutting energy consumption caused by material plastic deformation can be reduced when removed layer material turns into chips. Kuznetsov [98] also proposed that material embrittlement is enhanced with increasing the cutting speed, leading to a less time scale for material plastic deformation and reduction of material deformation energy.

A prediction model of critical cutting speed for UHSMC, as expressed as Eq. (4), at which the fragmented chips are formatted by ductile to brittle transition has been developed based on stress wave propagation theory as shown in Fig. 6j [37]. Cleavage and crystalline fracture were observed as the dominant failure mechanism

for chip formation during UHSMC, and all these features are typical brittle fracture characteristics [37,67].

$$V_{UHSM} = \int_0^{e_u} \sqrt{\frac{d\sigma_0/de}{\rho}} de \tag{4}$$

where V_{UHSMC} is the critical cutting speed of UHSMC, $d\sigma_0/de$ is the slope of the tangent line corresponding to the point of stress σ_0 on the engineering stress-strain curve of workpiece material, e_u is the strain corresponding to the tensile strength of workpiece material, and ρ is the workpiece material density.

Based on the model of Eq. (4), the predictive results of V_{UHSMC} for three workpiece materials (i.e., Ti6Al4V, Inconel 718, and 7050-T7451 aluminum alloy) have an error of 4.8%, 6.0%, and 16% compared with experimental results. Nevertheless, the model of Eq. (4) is limited to the prediction of critical cutting speed for orthogonal cutting mode, and the stress wave propagation is assumed to be within a one-dimensional removed material layer. A general model adaptable to more complicated machining processes and considering more practical cutting conditions is still needed.

Wang et al. [37,99] developed cutting energy consumption models for serrated and fragmented chip formation during HSMC and UHSMC, as shown in Fig. 7a. As expressed by Eq. (5), the cutting energy consumption for serrated chip formation mainly includes the plastic deformation energy in the primary shear zone, friction energy of the tool-chip interface, and chip kinetic work. Comparatively, the cutting energy consumption for fragmented chip formation mainly includes the local kinetic energy of chip fragments and the fracture surface energy expressed by Eq. (6). The

variation in cutting energy consumptions for several typical ductile metals such as aluminum 7050-T7451, Inconel 718, and Ti6Al4V are presented in Fig. 7b-d, respectively. The predicted results of cutting energy consumption for both serrated and fragmented chips present good agreement with experimental results as shown in Fig. 7. The errors between the predicted and experimental results are less than 10% for the above three workpiece materials.

$$E = \int_0^{\gamma} \tau(\gamma, \dot{\gamma}, T) d\gamma + \frac{\bar{\tau}_s A_s V_c \sin\beta}{a_c a_w V \cos(\phi + \beta - \gamma_0)} + \frac{\rho V^2 \sin^2\phi}{2\cos^2(\phi - \gamma_0)} \tag{5}$$

where $\bar{\tau}_s$ is the average shear stress in the primary shear zone, A_s is the sectional area of the primary shear zone along the cutting edge, V_c is the chip sliding speed, a_w is the cutting width, and β is the friction angle.

$$E' = \frac{\rho \dot{\varepsilon}^2}{A'^2} + \chi A' \tag{6}$$

where A' is the ratio of the fragment chip surface area to its volume which can be obtained by Eq. (7), χ is the specific surface energy for the workpiece material.

$$A' = \left(\frac{2\rho \dot{\varepsilon}^2}{\chi}\right)^{1/3} \tag{7}$$

The cutting energy consumption for brittle regime machining in UHSMC is significantly lower than that for ductile regime machining in HSMC. This indicates the advantage of UHSMC in terms of energy savings. For example, the cutting energy consumption for chip formation during machining of 7050-T7451 at a speed of 8,000 m/min decreases by 19% compared to that at 4,000 m/min, whereas the machining efficiency increases to two times. Meanwhile, the cutting energy consumption for chip formation during machining of Inconel 718 at a speed of 8,000

m/min is less than that at 5,000 m/min by 35%, whereas the machining efficiency increases by 60%.

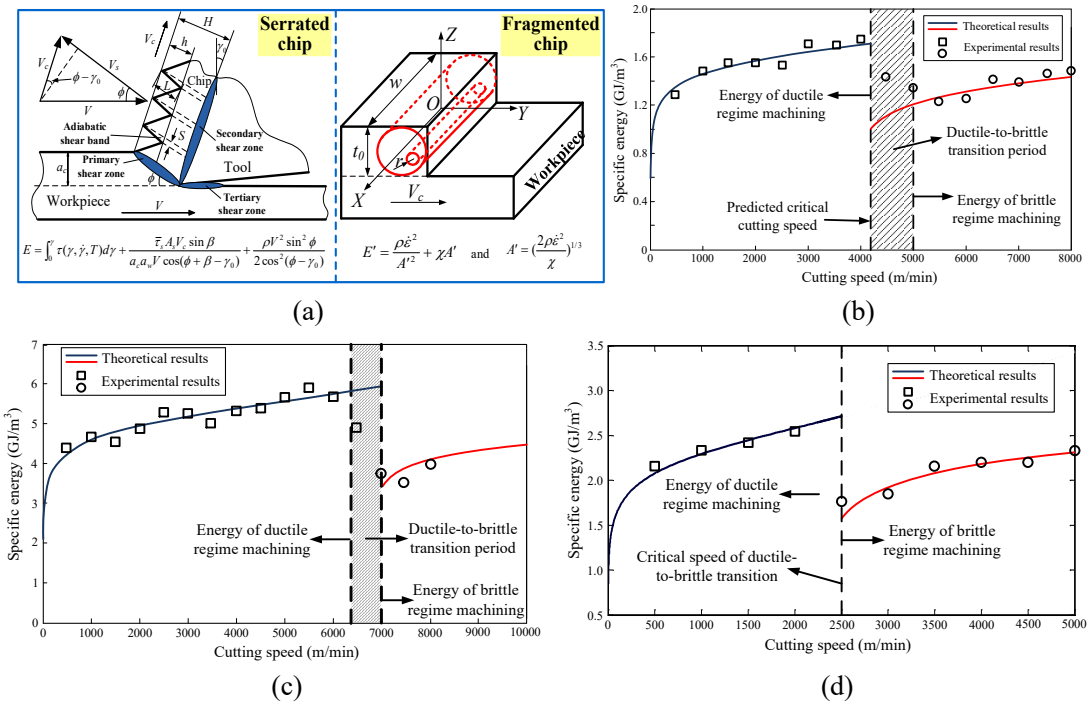

Fig. 7. (a) Cutting energy consumption models for serrated and fragmented chips formation during high speed machining [37], and variation of cutting energy consumption for (b) aluminum 7050-T7451, (c) Inconel 718 and (d) Ti6Al4V [99,100].

The observation and characterization of the microstructures within chips at a micro level can help obtain deeper insights into the chip formation and material removal mechanism during HSMC. With the aid of TEM, Duan and Zhang [101] carried out an in-depth investigation into the microstructures and formation mechanism of ASB within serrated chips of hardened AISI 1045 steel produced during HSMC. Based on different microstructures, two types of ASBs (i.e., deformed and transformed shear bands) were identified in the formation of serrated

chips. The deformed ASBs are generated by purely severe plastic shear, while the transformed ASBs are produced by recrystallization process.

Following this method, Liu et al. [102] attempted to reveal the formation mechanism of serrated chips during HSMC of titanium alloy Ti6Al4V. As shown in Fig. 8, the Scanning Electron Microscopy (SEM) morphologies for the ASBs were similar for the serrated chips formed for the cutting speeds from 250 m/min to 500 m/min. However, the microstructures within ASBs were significantly different at different cutting speeds through observation with TEM and Focused Ion Beam (FIB) techniques. Columnar grains with the size of hundred nanometers were produced by severe plastic deformation in ASBs at the cutting speed of 250 m/min (as shown in Fig. 8a,b), which belongs to the deformed ASB classified by Duan and Zhang [101]. At this condition, the cutting temperature within chips did not reach the recrystallization temperature, thus no recrystallization, recovery, or phase transformation took place [103,104]. The thermal softening was not prominent leading to a relatively high cutting force as well. Equiaxed nano-grains generated by the effect of recrystallization were observed at the cutting speed of 375 m/min as shown in Fig. 8c,d. With the cutting speed increasing to 500 m/min, the grain size within ASBs increased due to the growth of recrystallized nano-grains at higher cutting temperatures.

With the popularization of composites used in aerospace, the material removal mechanism during HSMC of composites, including metal matrix [105] and ceramic matrix [4] ones, has also attracted more attention by both academia and industries.

Bejjani et al. [106] studied the microstructural evolution within ASBs of serrated chips formed during HSMC of titanium metal matrix composite (Ti-MMC). They reported that the microstructure inside the ASBs was composed of elongated and equiaxed nano-sized grains attributed to rotational dynamic recrystallization, which is similar with the phenomenon in HSMC of titanium alloy.

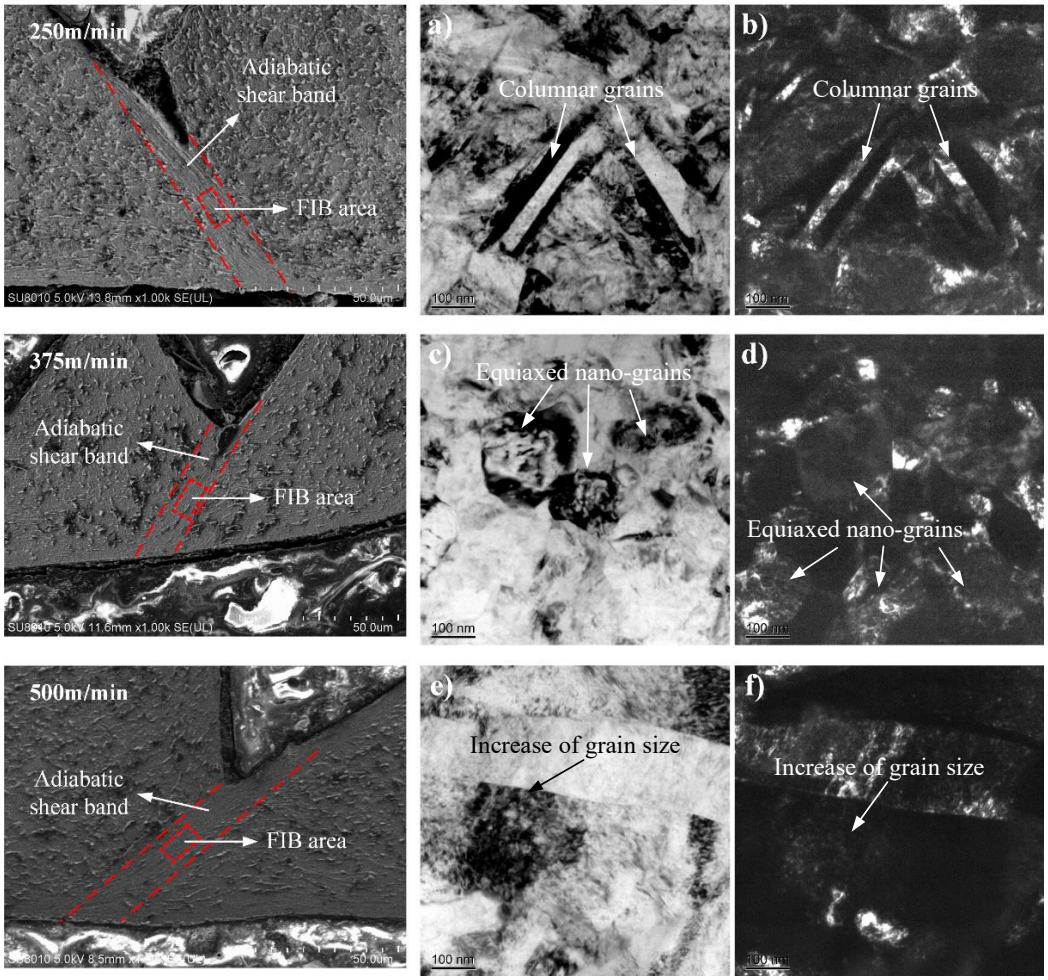

Fig. 8. Microstructural evolution in ASBs of serrated chips formed during HSMC of Ti6Al4V at different cutting speeds. (a) Bright field and (b) dark field images at 250 m/min. (c) Bright field and (d) dark field images at 375 m/min. (e) Bright field and (f) dark field images at 500 m/min [102].

Although the above research is beneficial for understanding the formation mechanism of serrated chips during HSMC of different workpiece materials, some limitations or research gaps still occur implying potential research directions in this field. For instance, the relationship or mapping is still not clear among the specific microstructures formed in chips, deformation conditions such as the strain, strain rate, and state of stress, in addition to the cutting conditions. Furthermore, it has not been focused enough on the dependence of material removal mechanism and associated microstructural evolution on inherent attributes of workpiece material. Original specific microstructures, thermal-physical-mechanical properties and isotropy/anisotropy of workpiece materials may result in different removal mechanism during HSMC process.

Effective numerical simulation of the microstructure within chips can help to predict material removal behavior and achieve distributions of microstructure field prior practical machining process. Through developing a Mechanical Threshold Stress (MTS) based internal state variable (ISV) constitutive model, the grain size distributions within ASBs and segments of serrated chips were successfully predicted during HSMC of commercially pure titanium [107] and nickel-based Waspaloy [108], as shown in Fig. 9. In their model, the flow stress depends on the microstructure including the dislocation density and mean grain size. The influences of dislocation drag, dynamic recovery, and dynamic recrystallization are also taken into consideration. When the grain size is smaller than a critical value, an inverse Hall-Petch effect caused by grain boundary sliding is included in the model to

simulate serrated chip formation. It can be seen from Fig. 9 that ultrafine grains distributed within the ASBs of serrated chips can be successfully predicted for both two workpiece materials.

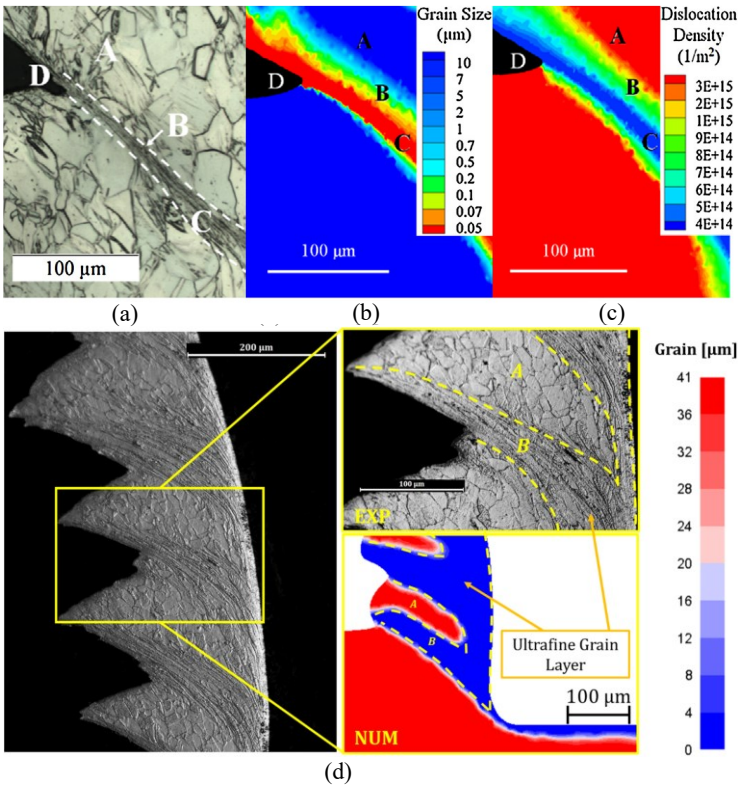

Fig. 9. (a) Optical micrograph of chip microstructure in ASB formed during HSMC of commercially pure titanium at a cutting speed of 100 m/min, and simulated (b) grain size and (c) dislocation density distribution [107]. (d) Predicted and experimental micrographs of microstructure distribution in serrated chip during machining of Waspaloy at a cutting speed of 70 m/min [108].

However, an apparent limitation of the present physically-based constitutive model is the need to calibrate an excessive number of parameters in addition to the significant dependence of the prediction capability of the model on the calibration accuracy. The development of more efficient physically-based constitutive models is likely to remain a potential research direction for the simulation of HSMC process. In

addition, the present research about material removal behavior and associated mechanism in HSMC is mainly limited to two-dimensional cutting. Material removal mechanism in three-dimensional cutting that is widely used in practical applications needs further study.

4. Machined surface integrity in HSMC

The excellent surface integrity of the final machined component is a main superiority of HSMC. Surface integrity is commonly used to characterize machined surface quality. It mainly includes surface topography, metallurgical alteration, and mechanical property [15]. In general, surface topography primarily affects the contact condition and stress concentration of machined components, while the metallurgical alteration within the machining-affected area determines the surface mechanical properties, which will further affect the component service performance [109,110].

Cutting speed is the main variable that affects the machined surface integrity during HSMC. The scope of this review about machined surface integrity during HSMC is marked by the dashed line in Fig. 10. The variation in the surface geometrical characteristics, microstructural characteristics, and mechanical properties (mainly refers to residual stress here) at high cutting speeds will be emphasized. The effects of the other cutting parameters, cutting environments and cutting tools on the machined surface integrity are not covered in this review paper.

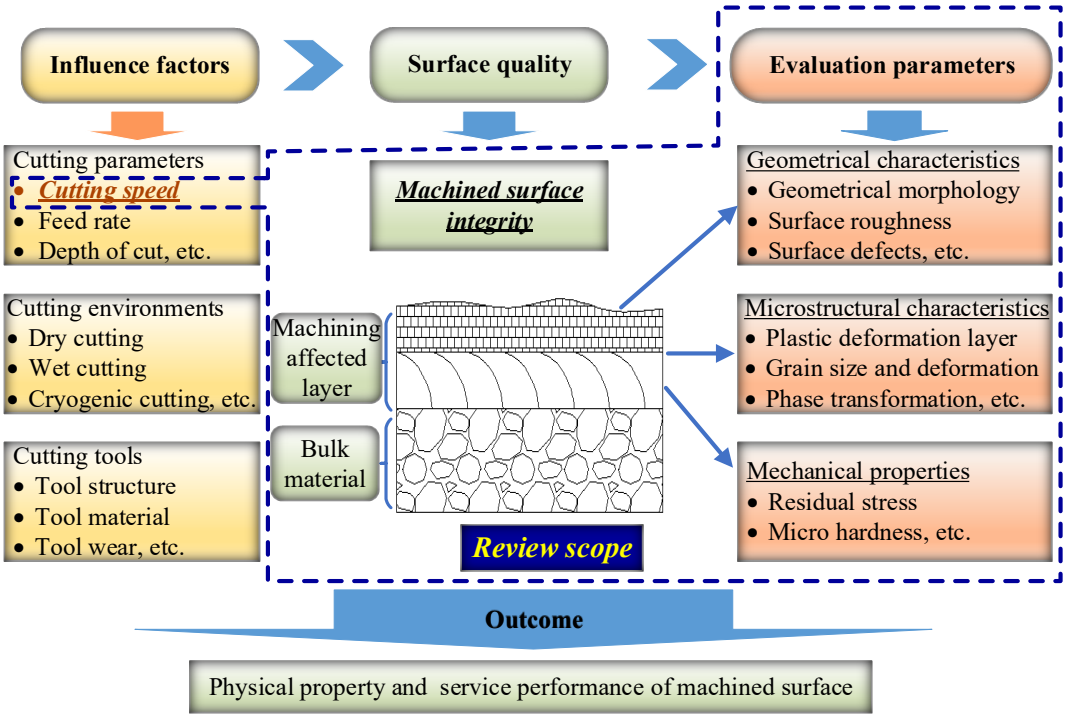

Fig. 10. Review scope of machined surface integrity in HSMC.

4.1 Machined surface topography and surface defects generated during HSMC

4.1.1 Machined surface topography

Surface roughness is the most widely used parameter to characterize the geometrical characteristics of machined surfaces. Regarding assembled machined surfaces, an excessively high surface roughness is likely to induce extreme friction and wear. For load bearing components, a rough surface may induce more severe stress concentrations at asperities, which then result in micro-cracks more easily under external loadings [111]. A smoother surface with lower surface roughness is generally preferred in most mechanical components. The cutting speed is an important process parameter that determines the finished surface roughness by

affecting the material deformation behavior and the contact conditions between the cutting tool and finished surface.

Su et al. [112] performed high speed orthogonal cutting experiments over a speed range from 120 m/min to 1,200 m/min on a high strength alloy steel Aermet100. They revealed an underlying reason for the variation in the micro-topography of machined surface by correlating the chip morphology and machined surface micrograph at different cutting speeds. As shown in Fig. 11, the results indicate that although the machined surface roughness increases as the cutting speed increases from 120 m/min to 200 m/min, it then decreases consistently when the cutting speed increases from 200 m/min to 1,200 m/min. The variation in machined surface roughness is recognized as being induced by micro-waves formed on the surface, which is determined mainly by the degree of chip serration. Complete chip serration at a cutting speed of 1,200 m/min generates the lowest surface roughness, which implies the applicability of HSMC in practical production.

An experimental research on HSMC of Ti6Al4V also concluded that the machined surface roughness decreased with increasing of the cutting speed over a range of 420 m/min-1,020 m/min [113]. Decrease of cutting force and serrated chip thickness are two main reasons contributed to the decrease of machined surface roughness at high cutting speeds. Zhou et al. [114] studied the machined surface roughness in high speed turning of Inconel 718 at different cutting speeds, and presented that the variation of machined surface roughness also depends on the cutting tools used. CBN tools coated with titanium nitride (TiN) can induce a

reduction of surface roughness from over 0.5 μm to 0.3 μm with increasing the cutting speed from 200 m/min to 350 m/min, while uncoated CBN tools did not induce significant variation of machined surface roughness.

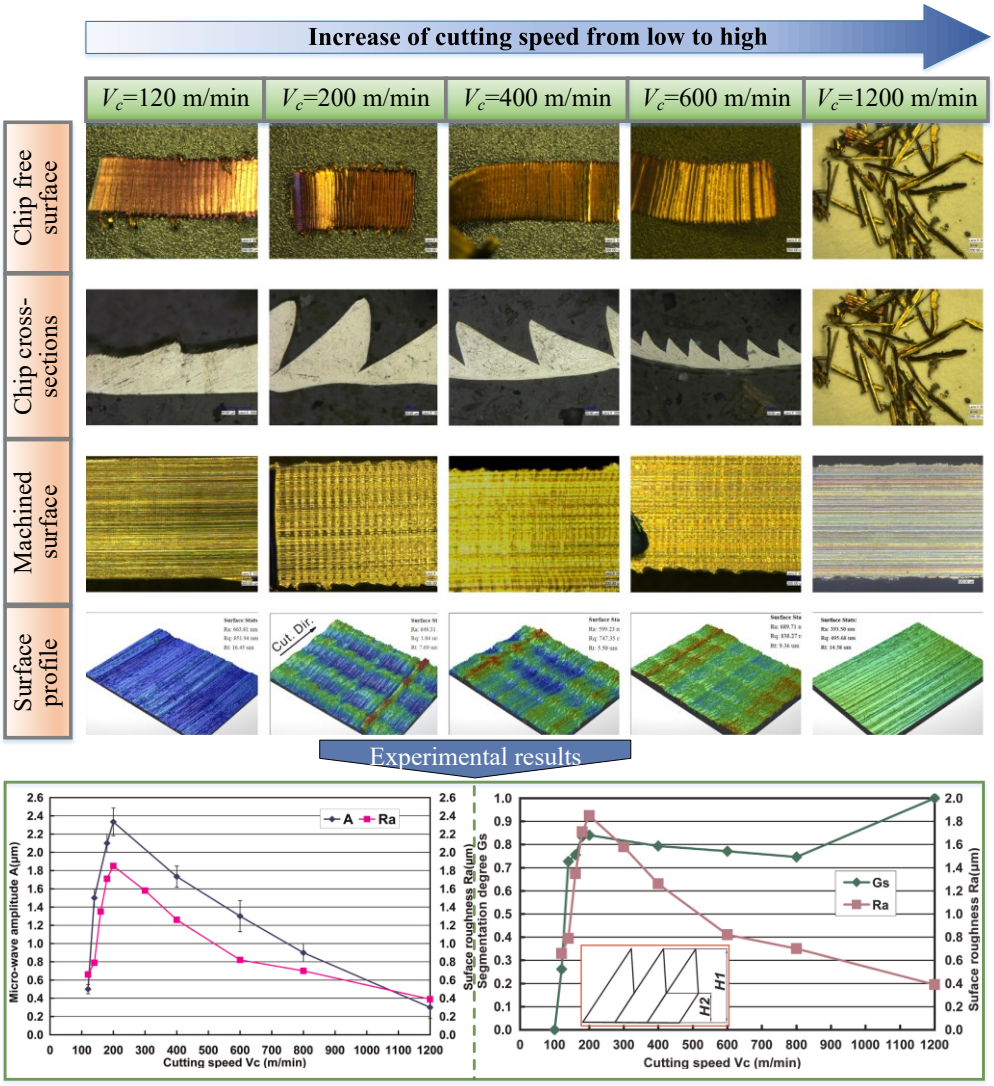

Fig. 11. Evolution of geometrical characteristics of machined surface and corresponding chip morphologies during high speed machining of Aermet100 [112].

4.1.2 Machined surface defects

Various surface defects induced by the interaction between the cutting tool and workpiece material are commonly observed on machined surfaces during machining

processes. These defects will function as weakening locations that cause the initiation and propagation of cracks and premature failure of machined components [115]. Thus, a clear understanding of the types of surface defects and the prevention of their formation through selecting appropriate cutting parameters can effectively use the technical advantages of HSMC.

The surface defects formed during HSMC of different workpiece materials such as steels [48], nickel-based alloys [116,117], titanium alloys [118,119], and aluminum alloys [67] have been studied. Fig. 12 presents the typical surface defects formed on machined surfaces during HSMC of two types of nickel-based superalloys (AD 730™ [117] and Inconel 718 [36,120]) under different cutting conditions. Cavities and carbide cracking are two main types of surface defects for the two workpiece materials, as shown in Fig. 12a,b,h,j). The cavities are generally formed because of the pull-out of hard precipitates and carbides from the surface or developed in association with tool wear, e.g., irregular wear near the tool nose or adhesion of workpiece material on the cutting edge [117]. Cracked carbides that remain on machined surfaces tend to induce the formation of micro-cracks and deteriorate the machined surface quality. Built-up-edge (BUE) debris detached from the cutting edge is easily re-deposited on the machined surface and induces debris defects. Meanwhile, surface tears and material dragging are likely to occur when detached cracked carbides or BUE are re-deposited and dragged on the machined surface in the subsequent cutting steps.

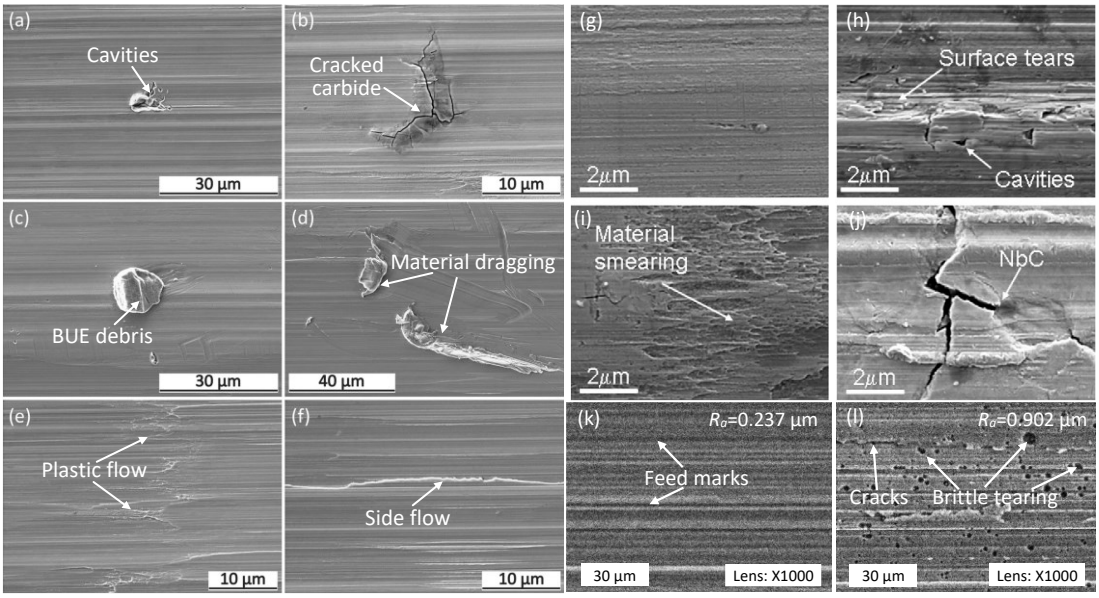

Fig. 12. Typical surface defects formed on the machined surface during HSMC of nickel-based superalloy at different cutting conditions. (a-f) Turning, workpiece material: AD 730™, cutting speed 300 m/min, feed rate 0.2 mm/r, depth of cut 0.25 mm [117]. (g-j) Turning, workpiece material: Inconel 718, cutting speed 90 m/min (g-machined with new tool, h-machined with worn tool) and 300 m/min (i-machined with new tool, j-machined with worn tool), feed rate 0.2 mm/r, depth of cut 0.25 mm [120]. (k,l) Orthogonal cutting, workpiece material: Inconel 718, cutting speed 800 m/min (k) and 7,000 m/min (l), uncut chip thickness 0.1 mm [36].

As excessive cutting temperature or microstructural inhomogeneity is inclined to induce plastic flow or side flow defects, as shown in Fig. 12e,f [121]. Especially, severe tool wear that occurs during HSMC of difficult-to-machine materials intensifies the defect formation associated with non-uniform plastic flow [119]. When the cutting speed increases to the range of UHSMC (e.g., a cutting speed of 7,000 m/min as shown in Fig. 12l), embrittlement of workpiece material occurs and the material removal is dominated by brittle fracture. The defects also evolve from

plastic deformation types to brittle fracture. Owing to the brittle fracture, the surface roughness generated at the cutting speed of 7,000 m/min is significantly higher than that at 800 m/min.

It is noteworthy that the optimum cutting conditions for the inhibition of surface defects differ across different studies even for the same workpiece material. For example, M'Saoubi reported that a good surface finish was obtained during machining of Inconel 718 at a relatively low cutting speed of 90 m/min (as shown in Fig. 12g) due to the lower cutting temperature, whereas Wang et al. [36] observed that a high cutting speed of 800 m/min produced machined surface with less defects as shown in Fig. 12k. Ye et al. [48] also reported that a high cutting speed of 4,000 m/min produced a smoother surface than that at a speed of 1,800 m/min during HSMC of 1045 steel. This is attributed to the fact that higher cutting speeds result in a shorter time for the plastic deformation of machined surface, whereby the plastic flow becomes limited resulting in a higher quality of surface integrity [122].

It can be concluded that the cutting speeds at which lower cutting temperatures and less plastic deformation are generated can help suppress the formation of surface defects during ductile regime machining. Meanwhile, when the cutting speed exceeds the critical value of UHSMC, brittle regime machining occurs and the surface quality deteriorates. It is recommended that UHSMC be applied in the rough and semi-finish machining processes rather than in the final finish process. Nevertheless, the means to achieve effective trade-offs between machining

efficiency and surface defects with proper process planning for different workpiece materials is still under debate.

4.2 Metallurgical alterations of machined surface

4.2.1 Microstructural alteration

Metallurgical alterations of machined surfaces have attracted more attention in recent decades and been gradually recognized as a significant surface integrity parameter that determines surface properties and performance. Ultrafine grains are prone to be generated by severe plastic deformation during machining processes. The higher plastic strain and plastic strain rate generated in HSMC provide a favorable condition for the formation of ultrafine grains on the machined surface. Guo et al. [123] mapped the relationships among deformation rate, strain, and temperature in machining processes (Fig. 13). They summarized the dependence of microstructural alteration and microhardness on the deformation parameters, i.e., strain and deformation rate. It is evident that the range of deformation rate and strain in HSMC can help produce ultrafine grains and micro/nano-sized cell structures.

Different research on several kinds of workpiece materials [50,51,104,108,124,125] has demonstrated that high cutting speeds can generate ultrafine grains on the machined surface and subsurface. Xu et al. [50] investigated the microstructural alterations on the machined surface of nickel-based superalloy Inconel 718 over a speed range from 50 m/min to 140 m/min using the PbCT setup as seen in Fig. 4e. It was reported that the severe deformation depth within the

machining-affected area increased with increasing the cutting speed in a certain range. The extent of plastic deformation within the machining-affected layer was characterized using a strain contour map through calculating local misorientation variations within each grain and weighted by grain size. Their results proved that the depth of plastic deformation area under machined surface became larger with the increase of cutting speed. It can be expected that with the increase of local misorientation variations within each grain, refined grains would be formed within a coarse grain when low-angle boundaries transformed to high-angle boundary.

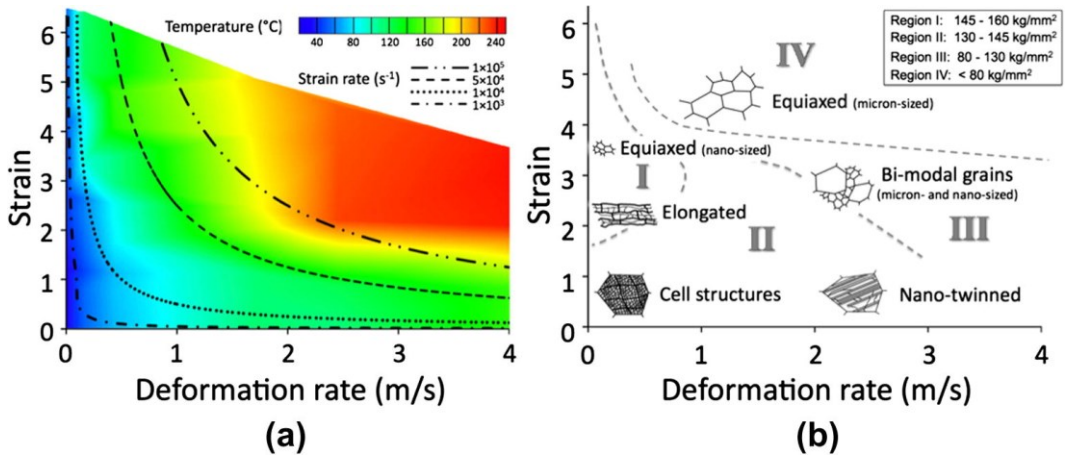

Fig. 13. Deformation-microstructure map derived from machining experiments showing (a) deformation parameters (strain, strain rate, temperature) accessed and (b) microstructures and hardness recorded in the different deformation regions [123].

Velásquez et al. [125] performed a close observation on the cross-section of machined surface and sub-surface generated during HSMC of titanium alloy Ti6Al4V with a cutting speed range from 20 m/min to 420 m/min. Fig. 14a-d presents the comparison of cross-sections of machined surface at the cutting speed of 20 m/min and 260 m/min. Three areas of the machining-affected region were defined as bulk material (P1), moderate plastic deformation layer (P2), and ultrafine grain layer (P3).

The layer thicknesses of both P3 and P2+P3 increase with the cutting speed increasing within the investigated speed range in [125]. Imbrogno et al. [108] summarized the effect of strain rate (i.e., cutting speed) on material deformation mechanisms through analysis of the machined surface microstructures during machining of nickel-based Waspaloy. As shown in Fig. 14e,f, with the cutting speed increasing, the material deformation mechanism of machined surface evolves from slip bands formation caused by mobile dislocations, to formation of elongated dislocation cell structures, and then to the formation of sub-micron grains and recrystallization.

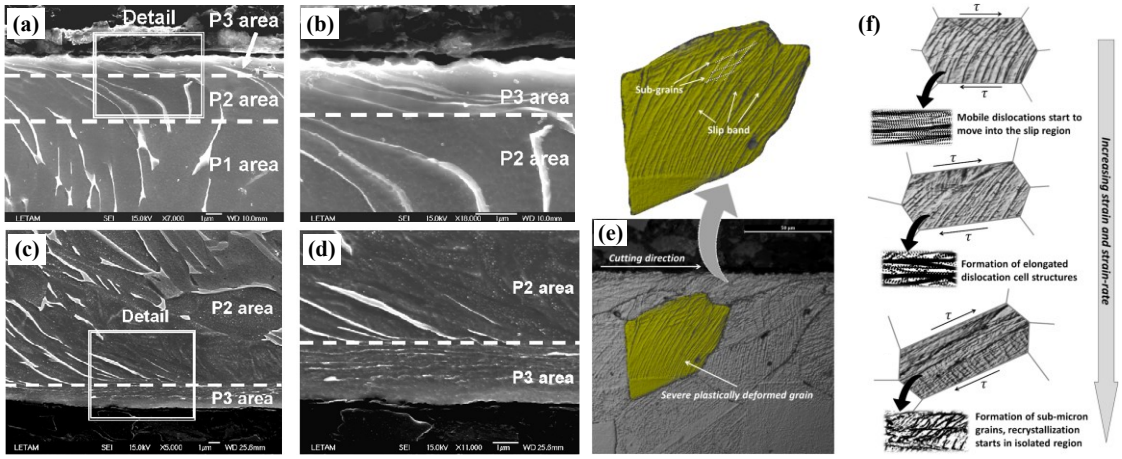

Fig. 14. Machined surface microstructures of titanium alloy Ti6Al4V produced at (a,b) cutting speed of 20 m/min and (c,d) cutting speed of 260 m/min (adapted from [125], Note: P1, P2, and P3 areas refer to bulk material, moderate plastic deformation layer, and ultrafine grain layer, respectively; Fig. (b) and Fig. (d) are the enlarged views for the square area marked in Fig. (a) and Fig. (c), respectively). (e) Typical machined surface microstructure of nickel-based Waspaloy, and (f) the effect of strain rate (i.e., cutting speed) on deformation mechanisms during machining of Waspaloy [108].

The conclusions of Xu et al. [50] and Velásquez et al. [125] indicate that high cutting speeds produce a deeper modified layer and may deteriorate surface integrity

from the perspective of metallurgical alteration. However, the cutting speed range addressed in the above-mentioned research is less than 1,000 m/min, and a more extensive study is required to cover a wider cutting speed range to reveal the speed effect on the microstructural alterations of machined surface. Furthermore, whether the ultrafine grain layer formed on the machined surface is good or not is also inconclusive and needs to be studied further.

Different conclusions were reported in the research of Neugebauer et al. [126] and Zhang and Yin [127] about the speed effect on the microstructural alteration of machined surfaces. Neugebauer et al. [126] observed that an increase in the cutting speed from 150 m/min to 2,000 m/min induced an increase in the temperature within cutting chips and decreased specific forces, and consequently reduced the subsurface damage of workpiece. Based on the material embrittlement caused by high strain rates ($>10^3$ s^{-1}) during HSMC, a "skin effect" of subsurface damage was proposed by Zhang and Yin [127] to explain the decrease in the damaged layer thickness of machined surfaces at high cutting speeds. It implies that an increase of cutting speed above a critical value is favorable for improving the surface integrity. An experimental and numerical research was performed by Wang et al. [124] on the microstructural evolution during HSMC of Ti6Al4V over a speed range of 100 m/min-300 m/min. The models of Zener-Hollomon and Hall-Petch were used to simulate the variations of grain size and micro-hardness within the machining-affected layer generated at different cutting speeds. It was observed that more refined grains and associated larger micro-hardness were produced on the

machined surface of Ti6Al4V at higher cutting speeds.

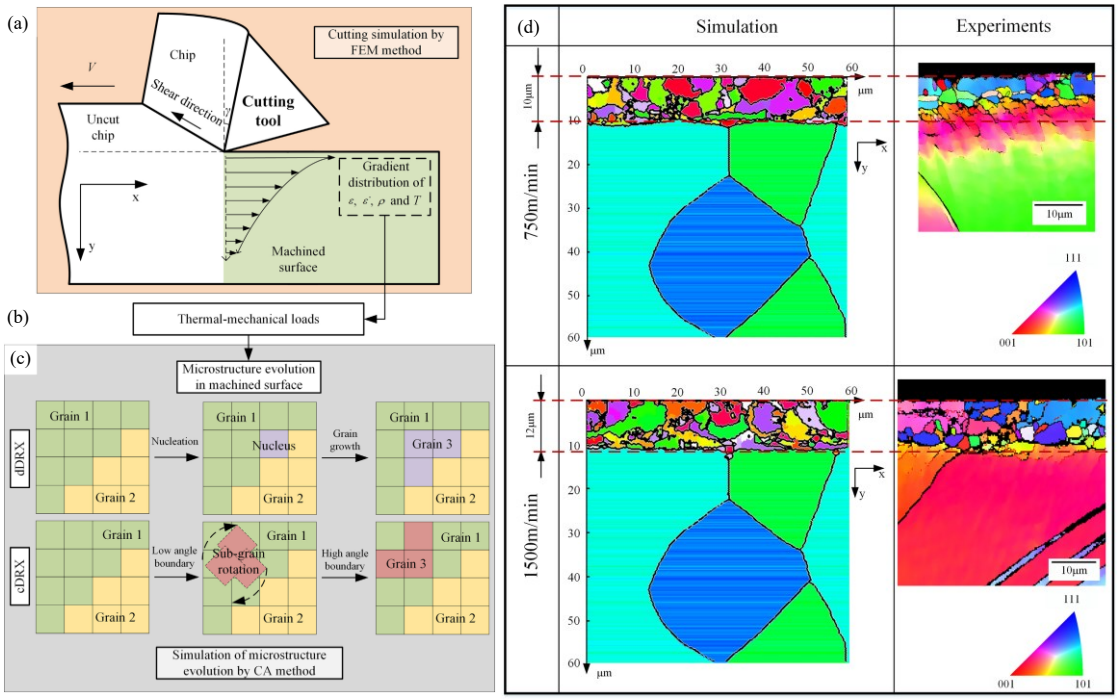

Fig. 15. Prediction of microstructure gradient distribution on machined surface during HSMC of OFHC with coupled FEM and CA method. (a) FEM simulation of HSMC. (b) Extraction of thermal-mechanical loadings from FEM results. (c) CA simulation of microstructure evolution with mixed mechanisms of cDRX and dDRX. (d) Comparison of simulation and experimental results of microstructure distribution at different cutting speeds [128].

A recent research of Liu et al. [128] demonstrated the feasibility of predicting the microstructure gradient distribution on machined surface generated in HSMC using a coupled FEM and cellular automata (CA) method. A unified material model is adopted to describe both the constitutive behaviors and microstructure evolution during machined surface formation. A combined mechanism of continuous dynamic recrystallization (cDRX) and discontinuous dynamic recrystallization (dDRX) is considered to characterize grain refinement and growth [129,130]. The detailed

operation procedure of this approach and numerical simulation examples for HSMC of oxygen-free high-conductivity copper (OFHC) at two high cutting speeds (i.e., 750 m/min and 1,500 m/min) are presented in Fig. 15. The good agreement between the experimental and simulation results is demonstrated to express the gradient microstructures of the machined surface. Nevertheless, the coupled FEM and CA method is limited to pure or single-phase materials such as OFHC. Future research needs to focus more on the simulation of general engineering materials with multiple phases, for which phase transformations should be considered.

4.2.2 White layer formation

The formation of white layer, which is a typical modified layer on the machined surface of nickel-based alloys and hardened steels, also depends on the cutting speed during HSMC. The white layer formation has been acknowledged as being detrimental to the performance and service life of mechanical components. The suppression of its formation with appropriate cutting parameters is significant for improving the properties of finished surfaces.

The white layer formed on a machined surface may not be continuous [131], and aggressive cutting conditions or severe tool wear are likely to induce a continuous and thick white layer. The morphology and microstructure of typical white layers formed on machined surfaces during HSMC of nickel-based superalloy AD 730™ and titanium alloy Ti6Al4V are presented in Fig. 16 [117,132]. A relatively uniform white layer can be observed for both two materials, as shown in

Fig. 16a,c. Here, a high cutting speed of 300 m/min was used for machining of AD 730™ superalloy and a 0.5 mm worn insert was used for machining of Ti6Al4V. Nano-crystalline microstructures were identified within the white layer of AD 730™ superalloy using Electron Channeling Contrast Imaging (ECCI), as shown in Fig. 16b. The thickness of the white layer formed on the machined surface of Ti6Al4V (Fig. 16c) is significantly larger than that of AD 730™ superalloy owing to the poor thermal properties of titanium alloys [47,95]. It is difficult to resolve the ultrafine grains at nano-meters level because the dimension of microstructures in the white layer approaches the resolution limit of backscattered electron SEM. Clearer microstructures can be captured using TEM with a higher magnification. As shown in Fig. 16d-f, as the distance from the machined surface increases, the mean grain size increases to approximately 200 nm in the transition region between the white layer and swept grain, and approximately 500 nm in the swept grain region.

Similar with the formation of ASBs in serrated chips, adiabatic shear localization has been recognized as a dominate factor for the white layer formation during machining of different workpiece materials. This opinion is supported by Chen et al. in HSMC of nickel-based superalloy AD 730™ [117], Barry and Byrne in turning of hardened steel [133], Bushlya et al. [30] in HSMC of Inconel 718, Chen et al. [31] in broaching of Inconel 718, Du et al. [134] in HSMC of nickel-based superalloy FGH 95, Veldhuis et al. [135] in turning of the powder metallurgical nickel-based superalloy ME 16, and Wusatowska-Sarnek et al. [136] in milling of powder metallurgical nickel-based superalloy IN100. The great plastic deformation

work and high strain rate loading accompanied with high cutting temperatures are apt to induce localized shear deformation in the superficial layer of machined surface. Consequently, grain refinement takes place to accommodate with the severe localized plastic strain and leads to the formation of nano-crystalline microstructures within the white layer.

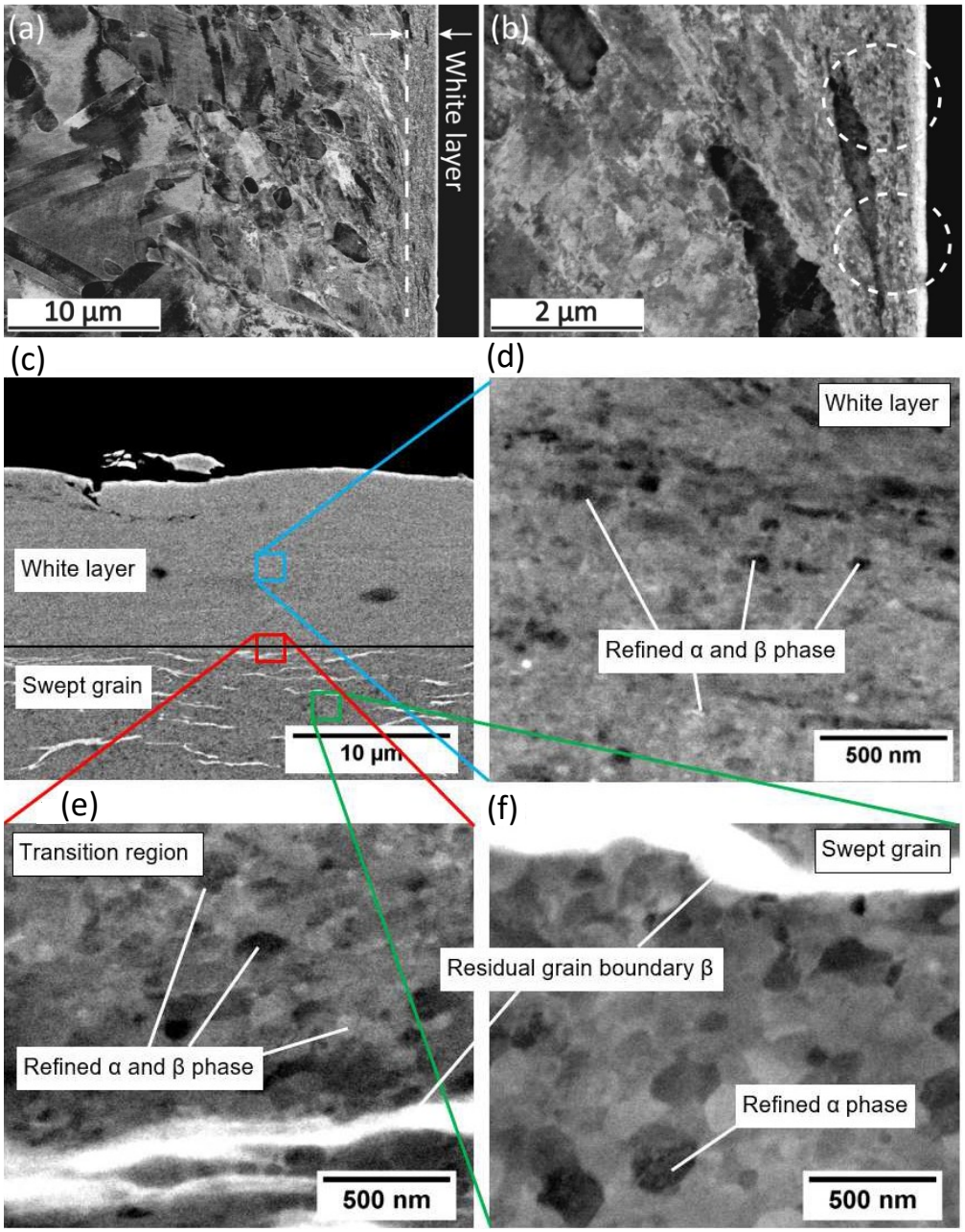

Fig. 16. Electron Channeling Contrast Imaging (ECCI) SEM micrographs of (a) white layer formed on the machined surface during HSMC of nickel-based superalloy AD 730™ at a cutting

speed of 300 m/min, and (b) nano-crystalline microstructure as marked by dash lines within the white layer [117]; (c) Cross-sectional Backscattered Electron SEM images of the white layer and deformed region on the machined surface during HSMC of titanium alloy Ti6Al4V. Higher magnification images of (d) the white layer, (e) the transition region between white layer and swept grain and (f) the swept grain [132].

Liao et al. [137] investigated the formation mechanism of white layer for a nickel-based superalloy S135H under severe plastic deformation induced by machining process. Their results show that the white layer was composed of a graded microstructure, which includes a dynamic recrystallized layer formed by nano-crystallized grains and a dynamic recovery layer formed by sub-grain microstructures. Although grain refinement occurred within the superficial surface of white layer, γ' phase dissolution also occurred leading to distinctly different properties of white layer from bulk material. Based on cyclic compression tests using micropillars, it was found that the white layer has lower strength and increased ductility compared to the bulk material. As a result, the white layer formation weakens the mechanical properties of machined surface and is expected to be avoided in machining process. However, the influence of cutting speed on the white layer formation of S135H was not covered in [137] and needs to be further studied.

The effect of cutting speed on the white layer formation of another typical nickel-based superalloy FGH95 was reported in [134]. Through a close examination on the cross-sections of white layer formed on the machined surface, a thin white layer with about several micros in thickness was formed on the machined surface

during HSMC of FGH95. A transition zone with moderate plastic deformation distributed between the white layer and bulk material. Less γ' phase was observed within the white layer and transition zone. With the cutting speed increasing from 1,000 m/min to 3,500 m/min, the white layer thickness was found to decrease by about 20%, which indicates that high cutting speeds can inhibit the formation of white layers [134]. Consequently, appropriate selection of cutting parameters can help to alleviate the negative effect of white layer formation. Nevertheless, other post treatment processes may be required if the white layer is expected to be removed completely.

4.2.3 Phase transformation

Phase transformation has also been recognized as an important factor affecting the metallurgical alterations. Due to a short time interaction between the cutting tool and workpiece under high cutting speeds, the phase transformation on the machined surface presents different characteristics compared to common heat treatment and forming processes [138].

Based on phase transformation dynamics, rapid heating and cooling phase transformation models were proposed to explain the phase variations on machined surface during HSMC of Ti6Al4V from 50 m/min to 600 m/min [139].TEM observation results, as shown in Fig. 17, verified phase transformation of $\alpha \rightarrow \beta$ during HSMC of Ti6Al4V. Compared to the orientation relationship between α and β phases in bulk material, it changed from classical Burgers orientation relationships

of $(0001)_\alpha//(110)_\beta$ and $[11\text{-}20]_\alpha//[111]_\beta$ to new orientation relationships of $(01{-}10)_\alpha//(110)_\beta$, $[0001]_\alpha//[111]_\beta$. The phase transformations occurred in both ASB and tool-chip interface of serrated chips, and machined surfaces are shown in Fig. 19. It was reported that the β phase ratio increased from 8% to 90% in the machined surface layer generated over the high cutting speed range of 50 – 600 m/min.

Nevertheless, the current research on the phase transformation behavior of machined surface during HSMC is still limited, and which kind phase is better for the service performance of machined surface is also unclear. Effective prediction and control of phase transformations will be important and needs further research.

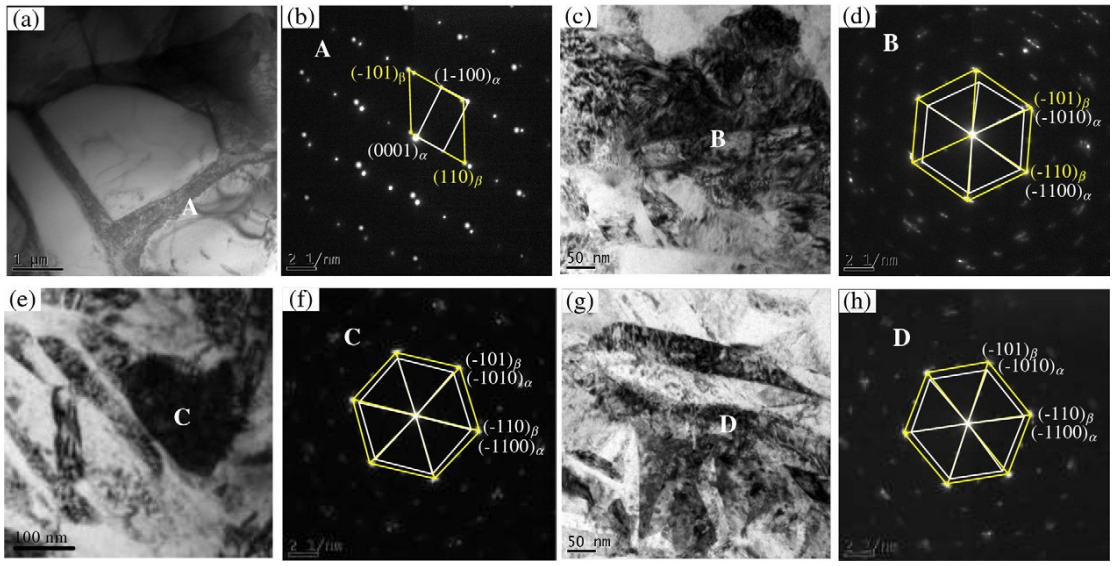

Fig. 17. Phase transformations during HSMC of Ti6Al4V. (a), (c), (e) and (g) are the bright field TEM images of bulk material, tool-chip interface of serrated chip produced at 200 m/min, ASBs of serrated chip produced at 500 m/min, and machined surface formed at 600 m/min, respectively. (b), (d), (f) and (h) are the SAED patterns of corresponding regions, respectively [139].

It is clear from the preceding discussion that researchers are trying to get deeper insights into the microstructural alterations of machined surface generated in HSMC, as the microstructure determines final physical and mechanical properties of machined components. With the advancement of material observation and characterization tools, evaluation of machined surface integrity has been expanded from macro level to micro and nano levels. Application of new engineering materials, such as powder metallurgy superalloys, metal matrix and ceramic matrix composites, also raises urgent needs for effective assessment of machined surface integrity of such new materials. It is anticipated that this research direction will still be popular in the near future driven by the machining requirements of industrial sectors.

4.3 Residual stress distribution within machined surface layer

Residual stress has significant influence on the mechanical behavior, particularly the fatigue performance, of machined components [140,141]. For thin-walled components, residual stress also impacts the dimensional accuracy and determines the subsequent assembly quality [142]. Fractographic analysis of mechanical components demonstrates that fatigue failures are generally nucleated on the surface or subsurface of components. As a result, the residual stress generated within the machining-affected layer is critical for assuring the service performance of finished components.

Compressive residual stress is preferred on the finished surface during machining process. A compressive residual stress can increase the threshold values

of allowed alternating stress for a specific fatigue life. Comparatively, a tensile residual stress indicates a reduction of allowed alternating stress during working [143,144]. Too high tensile residual stress generated on the machined surface will be detrimental to the fatigue performance and lead to a premature failure of mechanical components and even disasters. Furthermore, the effect of residual stress is particularly prominent for high cycle fatigue regime because the working stress is too low to substantially relax the residual stress generated during machining process [145].

The plastic deformation of machined surface and cutting heat that propagates into the workpiece are the main causes of residual stress generation. In general, the cutting heat and associated thermal effect are apt to induce tensile residual stress, whereas plastic deformation and associated mechanical loading tend to generate compressive residual stress [19]. Jacobson et al. [146] observed that an increase in the strain rate at high cutting speeds can generate more mechanical work, which would result in compressive residual stresses. Meanwhile, more severe plastic deformation at high cutting speeds generates more heat leading to tensile residual stress formation. The final state of the residual stress on the machined surface would be determined by the above two competing factors.

The residual stress profiles within machining-affected layers of Inconel 718 during a turning process at different cutting speeds were investigated by Schlauer et al [147]. Low residual stress and small distribution depth of the residual stress were generated at a low cutting speed of 10 m/min. With increasing the cutting speed to

410 m/min and 810 m/min, although larger compressive residual stresses were produced at a deeper subsurface, a layer exhibiting very high tensile residual stresses was also generated on the superficial surface which is not expected. The layer with high tensile residual stress may become a hidden danger in service. Similar residual stress profiles were also reported by Guerville and Vigneau [148] and Derrien and Vigneau [149] in milling experiments of Inconel 718 at different speeds. As seen in Fig. 18a, the maximum tensile residual stress on the machined surface at a cutting speed of 200 m/min is nearly three times that generated at a cutting speed of 18 m/min. The orthogonal cutting experiments on Ti6Al4V with a wide speed range from 20 m/min to 660 m/min also presented a similar trend for the variation of residual stress [125]. It can be seen from Fig. 18b that the residual stress in both two directions evolve from compressive to tensile with increasing the cutting speed, which indicates that the residual stress generated at high cutting speeds may be detrimental to service performance of machined surface.

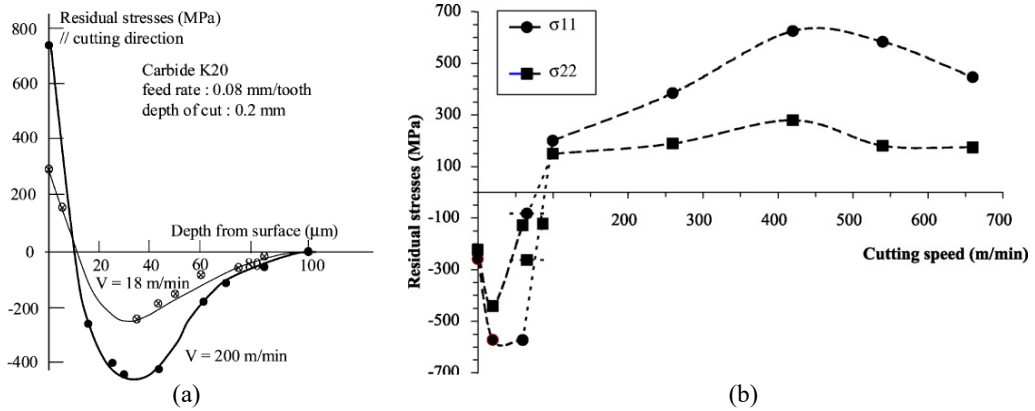

Fig. 18. Effect of cutting speed on the residual stress generated on the machined surface during (a) milling of Inconel 718 [149] and (b) orthogonal turning of Ti6Al4V [125].

FEM based modeling has been widely used to predict the residual stress profile

on the machined surface generated during HSMC process [150]. Some of the work includes predicting the effects of cutting parameters [151], tool-edge configurations and tool wear [152], single and sequential cuts [153], chip serration [154], and material constitutive parameters [155] on residual stresses for various materials such as steels [151], aluminum alloys [154,155], titanium alloys [152], and nickel-based superalloys [152,153]. Some work appeared in adopting hybrid methods combined with FEM based simulations to model the residual stress generation [156-158].

Generally, numerical simulation on residual stress generation in machined surface during HSMC is limited to single cutting pass on very short length and time scales due to the exceedingly high computational cost. To break this limitation, Wang et al. [153] proposed a concept of equivalent loading which enables an efficient modeling approach to predict residual stress in an actual machined surface by incorporating multiple cutting passes and crossing different length and time scales, as shown in Fig. 19a-d. With this method, the residual stress profiles generated at different cutting speeds are obtained for machining of Inconel 718 as shown in Fig. 19e. Although the highest cutting speed investigated by Wang et al. [153] is limited to 120 m/min, their research still suggests a useful method to acquire the residual stress generation on machined surface produced at higher cutting speeds combined with multiple cutting passes.

Based on the above discussion, there are still some limitations in predicting residual stresses during HSMC. The simulations of steps following machining process have not been fully considered, e.g., the cooling and recovery related

microstructural effects on residual stress evolution. In addition, simulations of practical machined part distortions and residual stress generation in HSMC with cutting fluid or Minimal Quantity Lubrication (MQL) will also be potential research directions.

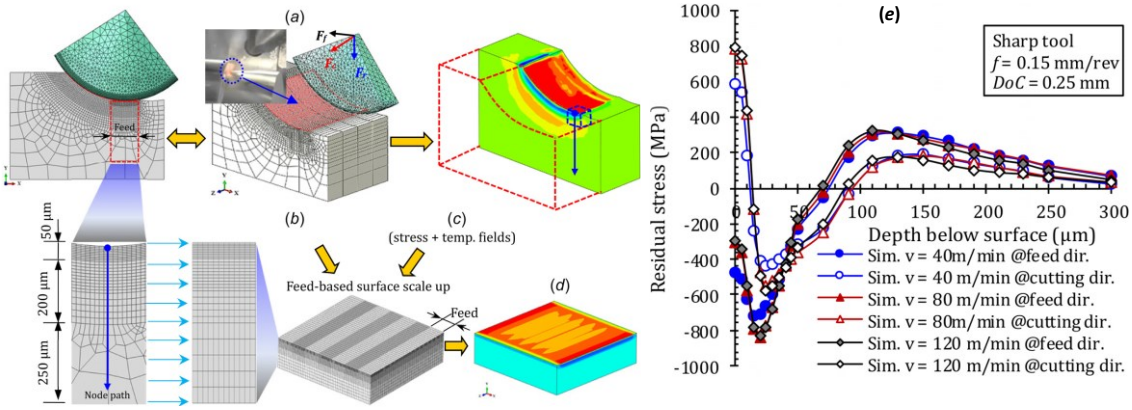

Fig. 19. Geometry models, mesh design, and FEA implementation procedure for prediction of residual stress in machining Inconel 718 superalloy. (a) Microscale single-pass cutting. (b) Spatial resolution. (c) Equivalent loading. (d) Residual stress fields. (e) Simulation results of residual stress at different cutting speeds [153].

Considering the residual stress profiles generated during HSMC, some other post-treatment processes, such as rolling, shot and shotless peeing, can help to introduce compressive residual stresses to replace the tensile residual stress formed during machining process [159-161]. Hua et al. [110] have presented that the machined surface of HSMC can be strengthened effectively and the fatigue life can be prolonger significantly using a low plasticity burnishing (LPB) post-treatment. Selection of appropriate cutting tool angles may also help to suppress the generation of tensile residual stresses [15]. Process planning of multiple cutting passes, e.g., rough and finish machining, and associated post strengthening treatment to achieve a

compressive residual stress on the machined surface are important to improve the service performance of machined components. Efficient modeling of the evolution of residual stress state in the above sequential processes is urgent to be studied driven by industrial needs.

5. Cutting force and cutting temperature during HSMC

5.1 Cutting force

In the cutting speed range of HSMC, thermal softening caused by chip plastic deformation is beneficial to weaken material deformation resistance, which then reduces the cutting force. When the cutting speed increases to the range of UHSMC, brittle fracture of removed layer material also helps to keep the cutting force at a low level [37,98].

According to orthogonal cutting experiments conducted by Denkena et al. [35], a dependence of cutting force and feed force on the cutting speed is presented in Fig. 20a. Both of cutting force and feed force decrease with the cutting speed increasing, and these two force components are asymptotic to constant beyond a certain boundary speed. Denkena et al. [35] expressed the relationship between cutting force and cutting speed by an exponential equation as Eq. (8).

$$F_c(V_c) = F_{c\infty} + F_{c\,\mathrm{var}} e^{-(2V_c/V_{HSC})} \tag{8}$$

where the cutting force is decomposed into a cutting speed-independent component $F_{c\infty}$ and a cutting speed-dependent variable $F_{c\,\mathrm{var}} e^{-(2V_c/V_{HSC})}$. The cutting force converges asymptotically to the cutting speed-independent component when the

cutting speed increases to a critical value. The V_{HSC} is defined as the boundary or critical cutting speed of HSMC here.

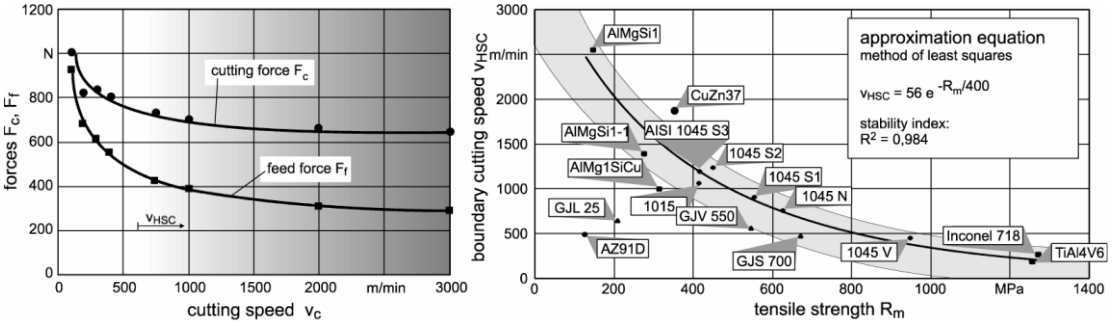

Fig. 20. (a) Variation of cutting force versus cutting speed during machining of 1045 steel;(b) the effect of tensile strength of work materials on the boundary cutting speed of HSMC (adapted from [35]).

Furthermore, Denkena et al. [35] found that the boundary cutting speed presents a strong dependency on the tensile strength which can be expressed by Eq. (9).

$$V_{HSC} = 56e^{-(R_m/400)} \tag{9}$$

where R_m is the material tensile strength. Fig. 20b shows the boundary cutting speed for a broad variety of workpiece materials with tensile strength values varying from 151 MPa to 1,275 MPa. A higher tensile strength leads to a lower boundary cutting speed. The values of boundary cutting speed of HSMC calculated based on Eq. (9) are close to that obtained based on serrated chip formation [89,95].

Taking mechanical and thermal properties of workpiece materials into consideration, Neugebauer et al. [126] modified the model of boundary cutting speed V_{HSC} of HSMC as Eq. (10).

$$V_{HSC} = 0.025\frac{T_m\sqrt{c_p\rho\kappa}}{R_m} \tag{10}$$

where T_m is the melting temperature of workpiece materials, c_p is the specific heat

capacity, and κ is the thermal conductivity.

However, the boundary cutting speed V_{HSC} obtained by both Denkena et al. [35] and Neugebauer et al. [126] did not consider the effects of other cutting parameters on the boundary cutting speed. The cutting parameters such as the feed speed, the depth of cut and cutting tool angles have significant influences on the boundary cutting speed, too. In addition, Klocke and Hoppe [162] found that the cutting force exhibits an increase for high cutting speeds after a local minimum, and different workpiece materials correspond to different cutting speeds for the minimum cutting force. Nevertheless, the maximum cutting force was still at low cutting speed in the experiments of Klocke and Hoppe [162], and the cutting force presented a decrease trend in a wide range of cutting speeds. Consequently, the effect of cutting speed on the cutting force still needs a more comprehensive research to reveal the interactions among cutting speed, material dynamic properties and the cutting force.

Fig. 21 presents the results of specific cutting force for Ti6Al4V obtained in different experiments [47,163-169]. It can be observed that a rapid drop of mean cutting force occurred corresponds to the cutting speed range of 0.5 m/s-10 m/s (i.e., 30 m/min-600 m/min). This could be explained by the predominant effect of thermal softening of the work material as a result of a strong localized heating and low thermal conductivity for Ti6Al4V. The drop of cutting force slows down ranging from the cutting speed of 10 m/s to 40 m/s (i.e., 600 m/min-2,400 m/min), and then it tends to be asymptotic to a constant. Sutter and List [47] proposed that the effect of dynamic strain hardening and strain rate hardening is more competitive than the

thermal effects when the cutting speed is higher than 2,400 m/min, which limits a further drop of specific cutting force with cutting speed increasing. Based on the chip formation mechanism discussed in Section 3.2, the ductile to brittle transition of Ti6Al4V occurs at a cutting speed higher than 2,500 m/min, which can support the explanation of Sutter and List.

Numerical simulations of HSMC of different workpiece materials, such as Ti6Al4V, Inconel 718 and aluminum alloy 7075, have also verified the decreasing trend of cutting force with increasing the cutting speed [95,170-172].

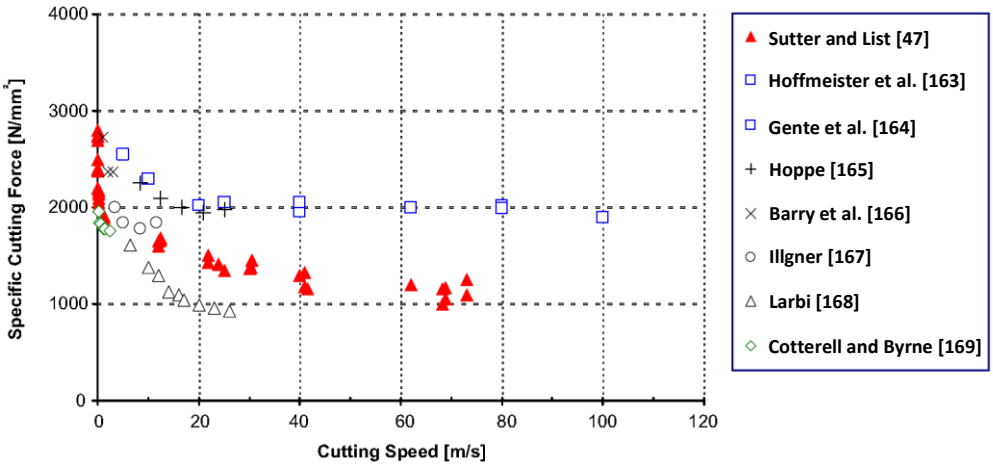

Fig. 21. Specific cutting force evolution for Ti6Al4V obtained in different experiments [47, 163-169].

Another advantage of HSMC is that the friction coefficient on the tool-chip interface decreases with increasing the cutting speed. This trend is supported by the experimental results of Sutter and Molinari [173] as shown in Fig. 22. Sutter and Molinari [173] utilized a ballistic machining setup to achieve cutting speeds higher than 50 m/s (i.e., 3,000 m/min) in machining 42CrMo4 steel. They found that the friction coefficient at the tool-chip interface decreased with increasing the cutting

speed at both cutting depths of 0.2 mm and 0.5 mm. Other researchers also found the decrease of friction coefficient at high cutting speeds, such as Findley and Reed [174] for lead-antimony alloy (the friction coefficient decreases from 0.85 to 0.3 with cutting speed from near zero to 780 m/min), Tanaka et al. [175] for steel (the friction coefficient decreases from 0.6 to 0.18 with cutting speed from near zero to 8,000 m/min) and Recht [176] for 4340 steel (the friction coefficient decreases from 0.6 to 0.26 with cutting speed from 240 m/min to 2,160 m/min).

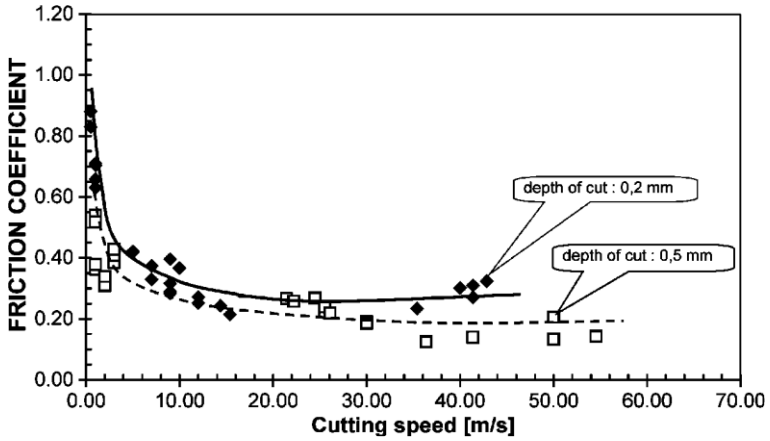

Fig. 22. Experimental evolution of friction coefficient at the tool-chip interface for a wide range of cutting speeds [173].

Recht [176] explained the reduction of friction coefficient as being due to melting at the asperities between tool-chip interface. Neugebauer et al. [126] proposed that at very high cutting speeds and normal forces, the sliding surfaces between tool and chip are separated by a lubricating film of molten workpiece material, which may help reduce the friction coefficient to very low values. However, considering the embrittlement of work materials at very high cutting speeds, the above postulations seem to be inapplicable for UHSMC. The decreasing adhesion

between tool-chip interface at ultra-high cutting speeds is a more possible reason contributed to the reduction of friction coefficient.

5.2 Cutting temperature

Decrease of cutting temperature when the cutting speed exceeds a critical value is the root for Salomon's assumption of HSMC. Fig. 23 shows the schematic of Salomon's cutting temperature curve versus cutting speed. With the cutting speed increasing, three cutting regimes can be divided as conventional cutting, critical cutting and high-speed cutting (i.e., HSMC). In the conventional cutting regime where the cutting speed is less than the critical value, the cutting temperature increases with the cutting speed increasing. Although the cutting temperature is not very high, machining is not recommended in this speed range due to a low machining efficiency. The critical cutting area (i.e., the death valley) is not suitable for application due to high cutting temperature that is apt to cause severe tool wear and deteriorating machining precision. Once the cutting speed is beyond the critical value, the cutting temperature decreases with the cutting speed increasing further. HSMC regime is the ideal machining region because it processes dual advantages of high efficiency and low temperature.

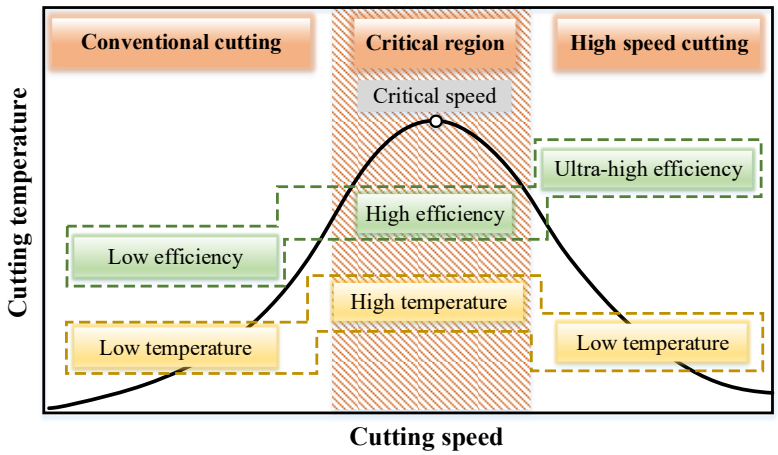

Fig. 23. Schematic of Salomon's cutting temperature curve versus cutting speed.

Finding the occurrence conditions of Salomon's curve is a prerequisite to make full use of the technical advantages of HSMC. However, the controversy on the existence of Salomon's cutting temperature curve has never stopped. The cutting heat generated in machining process [177,178], the cutting heat distributions in the cutting tool, the workpiece and the chip [179,180], in addition to the cutting temperatures of workpiece and cutting tool [181,182], have been the research focus of HSMC in recent decades.

Different opinions have been presented on the occurrence of Salomon's cutting temperature curve. Which kind of cutting mode that may support Salomon's assumption, and whether the cutting temperature refers to the temperature of cutting tool or that of workpiece have not reached a consensus until now. Based on a series of cutting experiments, McGee [183,184] pointed out that the cutting temperature increased steadily with the cutting speed increasing until the melting temperature of workpiece material, while no decrease trend of the cutting temperature occurred with the cutting speed increasing further. The conclusion of McGee was supported by the research of Dewes et al. [185]. Komanduri et al. [186] studied the variation of

cutting temperature on the tool-chip interface, and concluded that the cutting temperature increased with the cutting speed increasing without any decrease. Radulescu and Kapoor [187] proposed that the cutting temperature on the tool-chip interface has positive correlation with the cutting speed, and this correlation is suitable to both continuous and interrupted cutting modes. Longbottom and Lanham [22] made a comprehensive review on relevant research about Salomon's assumption about cutting temperature, and suggested that Salomon's assumption may not be suitable for the tool-chip interface temperature, while it may be adaptable for the variation of temperature on workpiece surface.

The interrupted machining may be a necessary condition for the tenability of Salomon's assumption about cutting temperature. Through high speed milling experiments of aluminum alloy, Schultz [188] found that a large amount of cutting heat is dissipated by the fast-moving chips, leading to a low temperature on the machined surface at high milling speeds. Dagiloke et al. [189] and Chen et al. [190] reported that high milling speeds lead to a decrease of heat transfer time from heat sources into workpiece, which then results in low temperatures on the workpiece surface in HSMC. O'Sullivan and Cotterell [191] found that the temperature on workpiece surface could be decreased at a not very high speed as about 220 m/min during machining of aluminum. Palmai [192] proposed that Salomon's assumption is valid for the variation of cutting temperature during interrupted machining such as milling, and developed an empirical cutting temperature model which is consistent with Salomon's results, but the underlying reason for the cutting conditions that

support Salomon's assumption was not given.

A decrease of cutting heat distribution proportion may also lead to decrease of cutting temperature in either workpiece surface or cutting tool. Richardson et al. [193] performed milling experiments on aluminum alloy 7449 with a wide cutting speed ranging from 300 m/min to 3,000 m/min, and revealed that the workpiece surface temperature decreased substantially due to a reduction of 83% for the heat distribution into the workpiece. The distribution proportions of cutting heat within cutting deformation zones are also different in different literatures. Shaw [194] proposed that 90% of the total cutting heat flows into cutting chips, while the rest 10% of the cutting heat flows into the workpiece and cutting tool equally. Another research reported that 80% percent of the total cutting heat is taken away by cutting chips, while the rest 20% flows into workpiece and cutting tool [195].

Astakhov [9,196] suggested that Péclet criterion, which is defined as the ratio of the product of cutting speed and cutting depth to thermal diffusivity of work material, can be used to understand the cutting heat distribution in metal cutting process. The Péclet number *Pe* is a similarity number and it characterizes the relative influence of the cutting parameters with respect to the thermal properties of work material on cutting heat distribution. Astakhov [196] found that the Péclet number *Pe* is much larger than 10 for commonly used cutting parameters, indicating that over 95% of the cutting heat was dissipated by cutting chips. Nevertheless, only the cutting heat source of primary deformation zone was considered in the Péclet criterion. The effects of cutting heat generated on the tool-chip interface and tool-workpiece

contact area should also be considered.

Although the cutting heat distributions in cutting chips, cutting tool and workpiece have not come to a consensus, a large amount of total cutting heat flowing into cutting chips has been recognized as a main reason leading to a relative low temperature on workpiece surface. If a larger proportion of cutting heat can be dissipated by cutting chips with the cutting speed increasing, it is possible for reduction of cutting temperatures of workpiece surface and cutting tool.

Jiang et al. [197] has tried to reveal the cutting conditions and associated mechanism for the tenability of Salomon's assumption. As shown in Fig. 24, a scenario of interrupted cutting mode was considered for the modeling of temperatures of cutting inserts and workpiece surface during HSMC of AISI 1045 steel. They found that the time ratio of cutting to non-cutting has significant effect on the cutting heat accumulation within cutting inserts and workpiece surface, which then leads to variation of cutting temperatures in corresponding areas.

With the time ratio of cutting to non-cutting increasing from 1/5 to 1/19, the highest temperature of cutting tool decreased from over 700 ℃ to less than 100 ℃. Increase of non-cutting time in a cutting period is beneficial for cutting heat dissipation, which can relieve the cutting heat accumulation occurred within cutting time. Meanwhile, the predominant role of cutting heat dissipation and a faster moving heat source at higher cutting speeds can decrease the temperature on workpiece surface as seen in Fig. 24. The conclusion of Jiang et al. [197] provides an underlying explanation for Salomon's temperature curve, and can instruct design and

manufacture of cutting tools and optimization of cutting parameters.

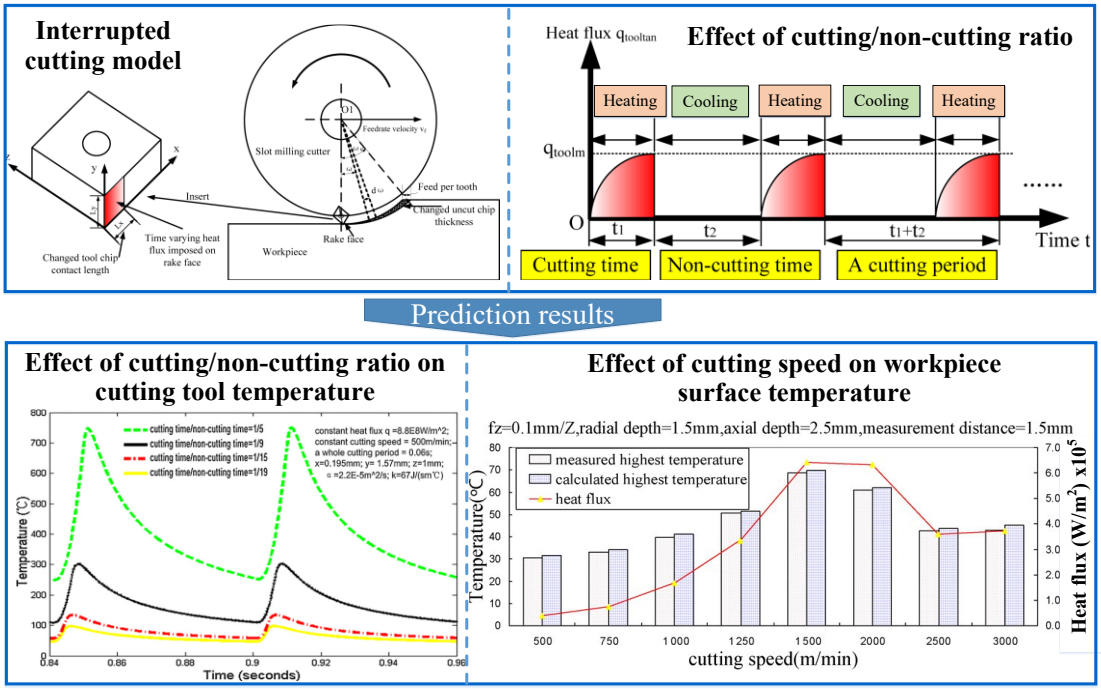

Fig. 24. Heat flux, measured and calculated temperatures of cutting tool and workpiece surface during high speed machining [197].

Based on the above discussion, the cutting heat generation and distribution, as well as the cutting temperatures of workpiece and cutting tool during HSMC process, need to be theoretically modelled and predicted more precisely. Meanwhile, accurate measurement of the cutting temperature within a tiny deformation zone at ultra-high cutting speeds is still a great challenge.

6. Tool wear behavior and mechanism in HSMC

Regarding the cons of HSMC or the most critical challenge for application of HSMC in industries, one can think of the severe tool wear under extreme thermal-mechanical loading conditions, especially during machining of difficult-to-machine materials. Inappropriate selection of cutting tools may restrict

the other advantages of HSMC. Understanding tool wear behavior and associated wear mechanism can instruct design and fabrication of cutting tools adaptable for HSMC, and recommend suitable tools for machining of specific work material. The tool wear behavior and mechanism in HSMC of difficult-to-machine materials such as titanium and nickel-based alloys are emphasized here.

Rahman et al. [198] summarized the wear behavior of different cutting tools in a review on HSMC of titanium alloys. It was found that the tool wear rate progress rapidly during machining titanium alloys with conventional cutting tools, and it is difficult to perform machining at cutting speeds higher than 60 m/min. Due to chemical reaction with the elements in titanium alloys at high temperatures, some tool materials, such as ceramic, diamond and cubic boron nitride (CBN) with binder material, are also not suitable for HSMC of titanium alloys. Comparatively, binder-less CBN tools present a prominently long tool life than other tools especially at high cutting speeds.

A research on high-speed milling of titanium alloy TA15 using diamond (PCD) and PCBN tools demonstrated a dramatic reduction of cutting tool life when the cutting speed just increased from 250 m/min to 350 m/min [199]. Shalaby and Veldhuis [200] compared the wear and tribological performance of four different ceramic tools in HSMC of nickel-based superalloy Inconel 100, and found that the tool life of all investigated tools decreased by up to 90% as seen in Fig. 25a-d. Meanwhile, their results indicate that SiAlON ceramic outperformed other ceramic

tool materials and can be used in machining of nickel-based superalloys at relatively high cutting speeds.

The tool wear mechanism during HSMC has also been widely focused on, and proved to rely on the tool material, machining mode, and cutting parameters [201-203]. Based on high speed milling experiments of an aerospace titanium alloy Ti-6242S using uncoated cemented carbide tools [204], flank wear and excessive chipping on the flank edge were reported as the main tool failure modes. Attrition, adhesion and diffusion were found as the main wear mechanisms of PCD and PCBN tools in high speed milling of titanium alloys [199,205]. Regarding a near-beta titanium alloy Ti5553, abrasive and adhesive wear mainly contribute to the severe tool wear at high cutting speed, and built-up-edge formation is also a common problem [206]. During HSMC of aluminum alloys, tungsten carbide with cobalt binder (WC-Co) tools are apt to appear unexpected chipping followed by catastrophic failure due to the chemical reaction between aluminum and cobalt at high cutting temperatures [207]. Coatings are recommended to be applied on tool materials containing cobalt for HSMC of aluminum alloys. When machining of nickel-based superalloys, adhesive wear and coating peeling are the main mechanisms for tool wear and premature failure at high cutting speeds [201,208].

To improve the performance of cutting tools at high cutting speeds, developing new tool materials and applying cooling assistance are still important. As seen in Fig. 25e, a high-pressure cooling jet can achieve over seven times longer tool life while the cutting speed doubles [209]. Meanwhile, chips are fractured more easily due to

the impact of high-pressure jet. Increase in coolant pressure also tends to reduce the adhesion tendency between tool and work material, and subsequently improve cutting tool life during HSMC of titanium alloys using coated carbide tools and PCD tools [210,205]. Cryogenic cooling and minimum quantity lubrication (MQL) have also been proved as effective ways to alleviate tool wear rate during HSMC of different work materials [206,211-213].

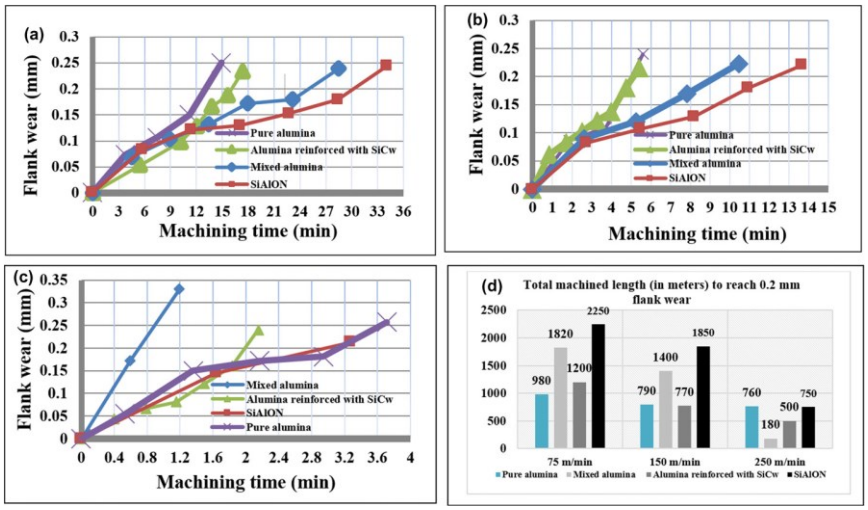

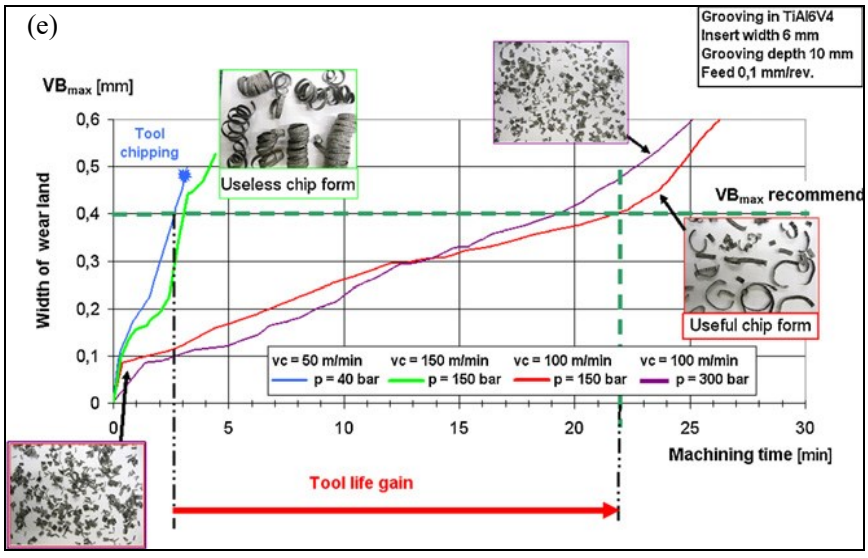

Fig. 25. Tool life of different ceramic tools in machining of superalloy Inconel 100 at different cutting speeds (a) V_c=75 m/min, (b) V_c=150 m/min, (c) V_c=250 m/min, (d) total cutting length at

different cutting speeds to reach 0.2 mm flank wear [200]; and (e) effect of cutting speed and flushing conditions on tool wear in machining Ti6Al4V [209].

Under the demand of eco-friendly manufacturing, high speed dry machining is recommended in recent decades. Advanced tool coatings can help to achieve higher cutting speeds without coolants. Similar with the review on tool wear behavior and mechanism in HSMC, the tool coatings that are adaptable for HSMC of titanium and nickel-based alloys are particularly commented. The coatings suitable for HSMC should be helpful for reducing the friction which can decrease the heat generation on the tool-chip interface. They also need to have excellent thermal barrier performance which can prevent the heat diffusion into cutting tools to guarantee high wear resistance of cutting tools at high temperatures. Compared to other coatings, (Ti,Al)N possesses a lower thermal conduction coefficient and a considerably enhanced oxidation stability, which makes it be one of the best coating materials for HSMC tools used in machining of difficult-to-machine materials such as titanium and nickel-based alloys [2,214]. Through adding oxygen to (Ti,Al)N coatings to form TiAlON, it can enhance the cutting tool performance further [215], because TiAlON offers a higher abrasion resistance due to the formation of Al_2O_3 during HSMC.

Generally, oxide PVD coatings have combined advantages of a reduction of friction at elevated temperatures and excellent wear resistance, so the heat generation can be decreased and the adherence of workpiece materials on the tool rake face can be suppressed at high cutting speeds [216-218]. In addition, soft tool coatings that

are made of solid lubricants, such as MoS_2 and tungsten carbide/carbon (WC/C) coatings, are useful to reduce the friction coefficient between tool-chip interface and then to lower the cutting forces and temperatures [219,220]. Consequently, the tool wear rate is decreased and higher cutting speeds can be achieved.

With the emergence of advanced cutting tools and new engineering materials, the tool wear behavior and mechanism during HSMC under different combinations of cutting tool and workpiece materials needs further study. To develop new advanced cutting tool materials and structures as well as tool coatings, that can achieve high cutting speeds without coolant, will always be important for production.

7. Application of HSMC in industries

Typical cases for the application of HSMC in industries are presented in this section to show the feasibility of HSMC in practical manufacturing. One of the advantages of HSMC is high material removal volume in manufacturing of components. Under the requirements of safety and economic efficiency, the application of light-weight components has been increased dramatically, which makes HSMC play a more significant role in the industries. Furthermore, with the development of advanced materials with higher strength and toughness, high-efficient machining of mechanical component made of such materials raise more challenges for HSMC. Thin-walled components with light weight and high

strength are particularly popular in high value-added products such as those of aviation industries.

A typical application of HSMC in manufacturing of multi-frame monolithic component used in aircraft is shown in Fig. 26a,b [221]. The aircraft frame was made of aluminum alloy 7075 in an oversaturated state, and it was fabricated from a block workpiece with dimensions of 60 mm x1,190 mm x 1,215 mm. The weight of the finished frame was 3.15 kg while that of the initial workpiece was 243 kg, meaning that the weight of the final product was 1.3% of the initial workpiece and 98.7% of the workpiece material was removed as chips. The basic criteria for assessing the manufacturing precision included the wall thickness tolerance of +/- 0.2 mm on the largest machined surface with dimensions of 300 mm x 300 mm, and the surface roughness R_a less than 0.6 μm. Using HSMC process with a spindle rotational speed of 15,000 rpm, excessive material on the workpiece was removed with high efficiency, while the dimensional accuracy (the wall thickness tolerance less than 0.2 mm), the surface roughness (R_a=0.272 μm) and waviness of the machined surface were successfully guaranteed [221].

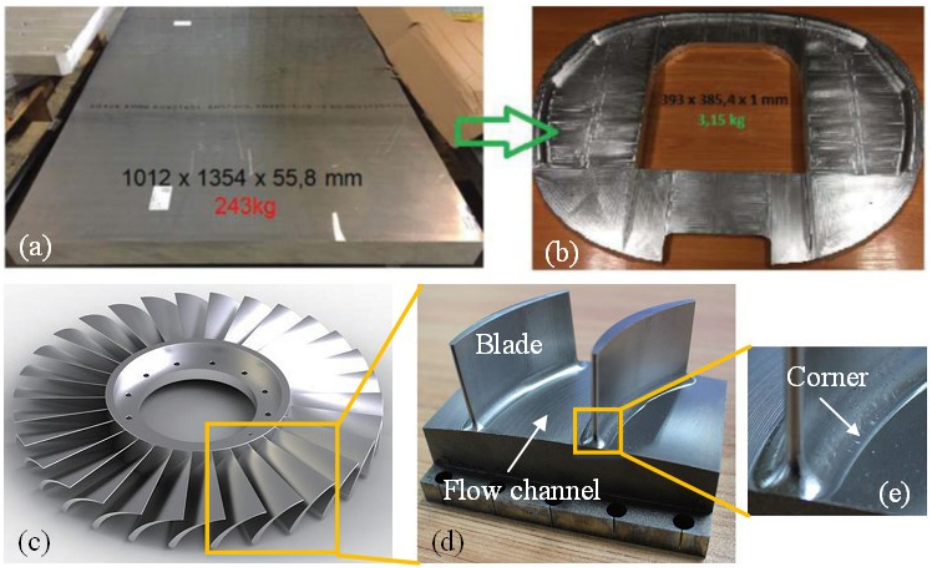

Fig. 26. Typical components manufactured using high speed machining. (a) An aluminum alloy 7075 block. (b)Aircraft frame structure [221]. (c-e) Blisk made of titanium alloy Ti6Al4V and a simplified workpiece [222].

Thin-walled complex surface structures, such as the blisk shown in Fig. 26c, are commonly used in aero engines. A simplified blisk component (Fig. 26d,e) made of Ti6Al4V was manufactured to prove the feasibility of HSMC [222]. A linear cutting speed about 100 m/min was adopted in the machining process. It was found that both the dimensional tolerance (less than 0.1 mm) and surface roughness (R_a=1.298 μm) of the finished part, especially the corner structures, can meet the requirements of customers.

Cutting tool companies have been promoting the application of HSMC through development of advanced cutting tools. Besides the new cutting tool materials introduced in Section 6, integral ultra-hard cutting tools have been emerged in recent years and applied in HSMC of hard-to-cut materials [223]. As seen in Fig. 27a,b, solid ceramic end milling tools have been successfully used in machining of superalloy

components with thin-walled and complex surface structures at high cutting speeds [224,225]. SiAlON is the main material to fabricate solid ceramic milling tools due to its excellent combination of strength and toughness. The cutting speeds achieved by these solid ceramic milling tools are ten times higher than that obtained using tungsten carbide tools with the same geometrical parameters, while the tool life is improved by two to three times [223,226]. The SiAlON solid milling tools have also presented excellent cutting performance in HSMC of additively manufactured titanium alloys [227]. Meanwhile, Wang et al. [228] developed four different kinds of solid ceramic end milling tools made of Al_2O_3+TiC, Al_2O_3+(W,Ti)C, Si_3N_4 and Ti(C,N), and employed them in HSMC of hardened steel. Their results demonstrated that all the solid ceramic tools possess longer tool life and produce better surface finish than tungsten carbide tools.

Integral PCD tools were also developed as seen in Fig. 27c-e to realize HSMC of different workpiece materials such as graphite and alloys [229]. The PCD tools were made by either ultrafast laser machining (Fig. 27c,d) [229] or additive manufacturing (Fig. 27e) [230]. Design of dense cutting tooth (Fig. 27c,e) can help to reduce the cutting force on each edge leading to decreased cutting temperature, which is then beneficial for improving machined surface quality and prolonging tool life.

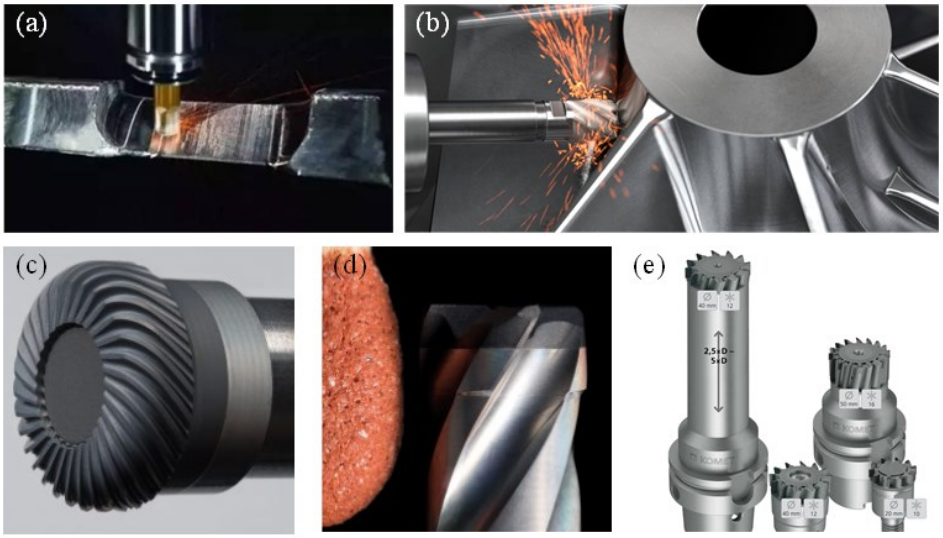

Fig. 27. Advanced integral high speed cutting tools. (a,b) Ceramic end milling tools [224,225]. (c) PCD torus milling tool [229]. (d) PCD end milling tool [229]. (e) PCD face milling tools [230].

Compared with conventional milling tools, the grooves space of additively manufactured milling tools can be significantly shortened. For a milling tool with diameter of 32 mm, the number of grooves and cutting edges have been increased from six to ten, resulting in a feed rate that can be up to 50% higher than conventional tools [230]. In addition, the ability to optimize the paths of coolant channels for the additively manufactured milling tools ensures that each cutting edge can be supplied precisely with coolant through a separate channel. Meanwhile, the flexible design of external cutting tool structures helps to ensure that chips are removed reliably from the tool rake face. Under these favorable effects, the additively manufactured milling tools can effectively improve the cutting performance during HSMC process.

8. Future research directions

The relevant research on HSMC in such aspects as material removal mechanism, machined surface integrity, cutting force and cutting temperature, cutting tool, and workpiece material are summarized in Fig. 28. To provide more detailed information about the recent research progress on this topic, only literatures published after the 1990s are addressed here. The increasing number of studies reported in recent years indicates that the research on HSMC is still attracting significant attention worldwide. In particular, since the 2000s, a higher focus has been placed on the study of machined surface integrity and material removal mechanism during machining of different workpiece materials (four typical metals are presented in Fig. 28) at high cutting speeds. Meanwhile, high speed cutting tools have attracted more attention because they constitute an important factor for promoting the increase in cutting speed. Studies on the cutting force and cutting temperature of HSMC are also being conducted to answer the fundamental questions discussed in the above sections. It can be asserted that HSMC is yet to be an established technology, and that the research on HSMC would also be impelled by the fast development of processing equipment and broad industrial demand.

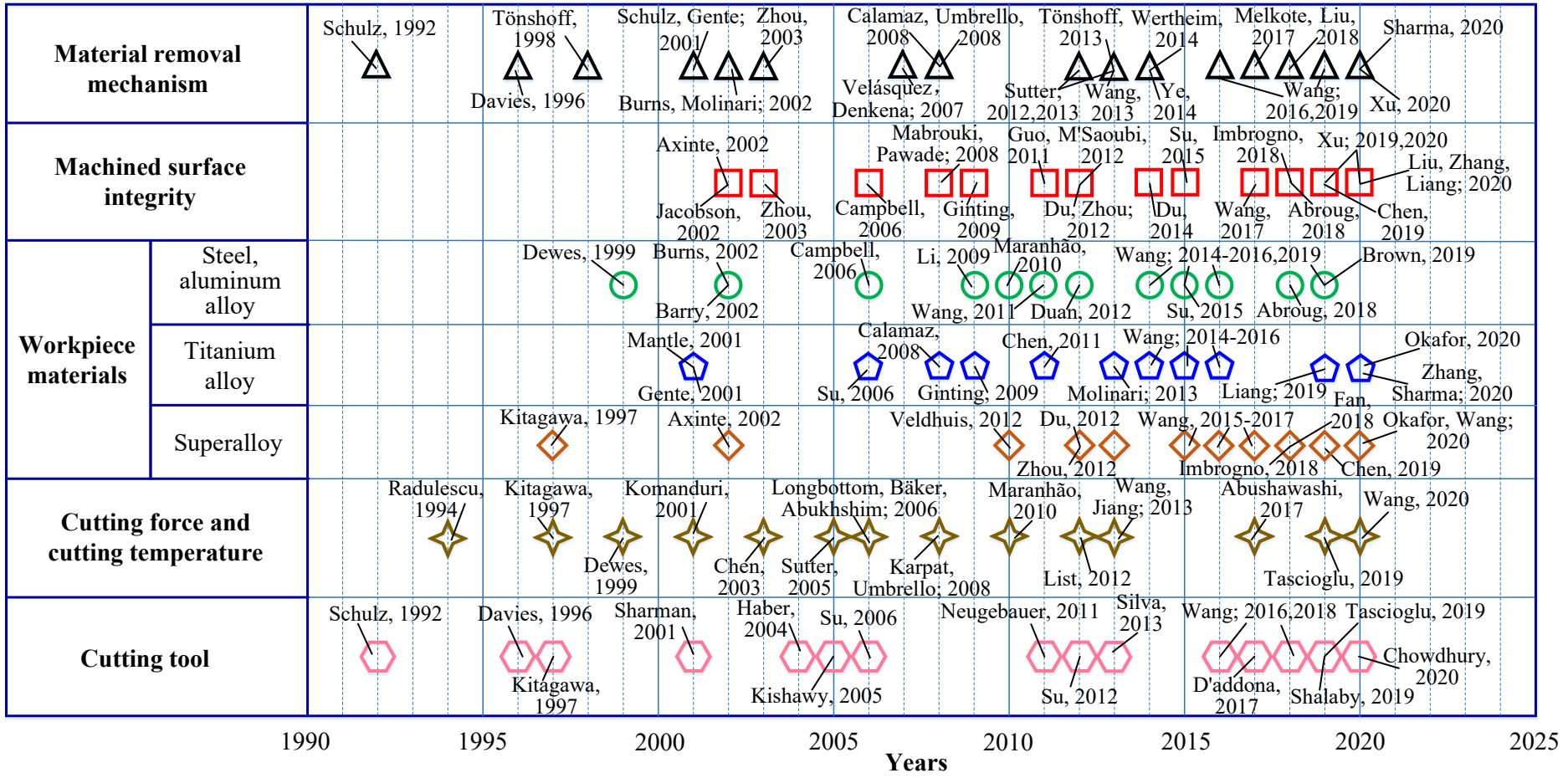

Fig. 28. The development of HSMC from several different research aspects.

Based on the review and above summary, the potential research directions of HSMC to be focused on are as follows.

(1) Material removal mechanism during HSMC

The cutting speed used in manufacturing processes is growing at an increasing pace. Similar to Moore's law, the cutting speed and associated material removal rate increase by approximately 100% every two years (as indicated by the data shown in Fig. 1) with the development of high speed machine tools and ultra-hard cutting tools [9,231,232]. Meanwhile, new advanced engineering materials such as metal matrix and ceramic matrix composite materials have emerged and are being gradually applied in industries. The continuous increase in cutting speed and the new engineering materials may generate different mechanisms (e.g., ductile-to-brittle transition) of material removal behavior, which deserves more research efforts in the future.

The present research on the material removal mechanism during HSMC is mainly limited to two-dimensional cutting mode. The material removal behavior during three-dimensional cutting that is widely used in practical applications lacks enough research. Correspondingly, dynamic deformation and fracture behavior of workpiece materials under the coupled loadings of high strain rate and more complicated stress state need to be studied. More general material models adaptable for three-dimensional HSMC are urgent to be developed. In addition, in-situ observation and measurement of material deformation with the aid of digital image correlation techniques would also be a research focus, as they can provide the most

direct evidence and data basis for material deformation modeling compared with speculation and postmortem examination.

(2) Machined surface integrity generated at high cutting speeds

The evaluation of machined surface integrity has evolved from traditional macro parameters, such as the surface roughness and surface defects, to micro and nano level parameters such as crystalline features and phase transformations. Advanced material characterization tools, including TEM and EBSD, enable us to obtain deeper insights into the mechanisms underlying the material removal and machined surface formation during HSMC. To reveal the relationships among inherent attributes of workpiece materials, processing parameters during HSMC, and evolution of machined surface properties will be a potential breakthrough direction.

Furthermore, the present evaluation system of machined surface integrity generated by HSMC is aimed mainly at isotropic metallic materials. A more general evaluation system is required to assess the machined surface integrity of a wider range of materials, particularly anisotropic composite materials [71,105,106].

(3) Process modeling of HSMC

The present studies on the cutting force and cutting temperature during HSMC are based mainly on experiments and empirical modeling, while theoretical process modeling is still limited. Some issues have not been understood clearly, such as (i) conditions for the existence of Salomon's curve during HSMC, (ii) dependence of process modeling on the thermal-physical-mechanical properties of workpiece materials, and (iii) relationships among the cutting conditions, process parameters

(i.e., cutting force and cutting temperature), and material deformation behavior. Especially, the generation and distribution of cutting heat during HSMC and the cutting temperatures of workpiece and cutting tool need to be theoretically modeled and predicted more precisely. The accurate measurement of the cutting temperature and deformation fields within an extremely small deformation zone at ultra-high cutting speeds is also a great challenge to be tackled.

(4) High speed cutting tools

Under the demand of eco-friendly manufacturing, the development of new advanced cutting tool materials and structures as well as tool coatings that can achieve high cutting speeds without coolant is being pursued by both academia and industries. Ultrafast laser machining [229] and additive manufacturing [230] provide new solutions for fabricating ultra-hard cutting tools with dense tooth structures that can effectively improve the cutting speed. Integral ultra-hard cutting tools such as solid ceramic cutting tools or PCD tools adaptable for HSMC has attracted more attention and would be a research hotspot in the near future.

(5) Application and performance evaluation of HSMC

Considering that different evaluation parameters for the performance of HSMC may not be in favorable conditions simultaneously, a trade-off between the pros and cons of HSMC must be determined reasonably in practical applications. Research on HSMC considering practical service conditions of machined components is a prerequisite to make such as a balance.

Furthermore, developing more adaptable hybrid/combined processes, such as

hybrid machining and post-treatment strengthening, will always be pursued by both academia and industries. Such hybrid/combined processes will be important to ensure different machined surface integrity parameters in satisfied conditions simultaneously, including the geometrical integrity (i.e., the surface roughness and defects), microstructural integrity (i.e., grain size and orientation, phase transformation) and mechanical integrity (i.e., residual stress and microhardness).

Based on the above discussion, the potential research directions are summarized in Fig. 29, which is expected to provide useful suggestions to relevant research fields of HSMC. Multi-objectives of high quality, high efficiency, and high performance will be pursued in the future with the application of HSMC.

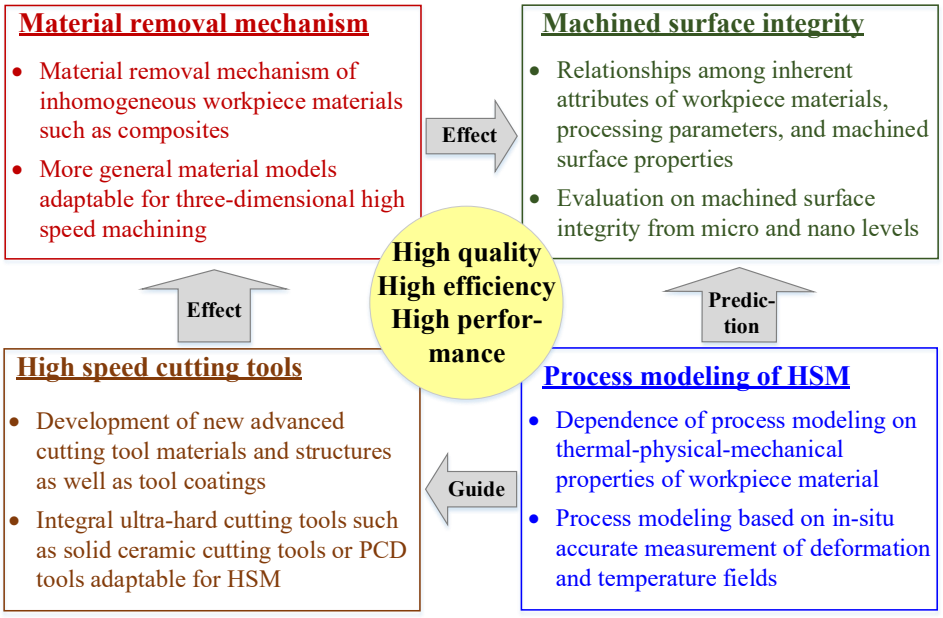

Fig. 29. Potential research directions of HSMC.

9. Conclusions

Through reviewing the advancements of high speed metal cutting (HSMC), the material removal mechanism, machined surface integrity, cutting force and cutting temperature, as well as tool wear behavior during HSMC are summarized and

discussed. The pros and cons of HSMC are elaborated based on the above aspects. The deficiencies in the present research on HSMC and the challenges for application of HSMC in industries are highlighted. Certain potential future directions for research on HSMC are discussed. The main conclusions drawn are as following.

- HSMC can be defined as machining with a cutting speed higher than that for ASB formation, whereas UHSMC can be defined as machining with a cutting speed higher than that for fragmented chip formation induced by workpiece material embrittlement. A consensus has been reached that the "high speed" in HSMC is preferably referred to a combined economic and performance target rather than merely a technical parameter. Different setups to achieve high cutting speeds have been developed, and they have played an important role in both fundamental research and industrial application of HSMC.
- Workpiece materials present distinctly different dynamic behaviors during HSMC compared to their static properties, owing to the high loading rate applied by the cutting tool. Different material models that consider the combined effects of strain, strain rate, and temperature have been established to describe the material deformation and fracture behavior at high cutting speeds. With the increase in cutting speed, chip morphology generally evolves from continuous to serrated and then to fragmented. Different prediction models have been developed for serrated and fragmented chips formation. The variation of material dynamic properties

at high cutting speeds is the underlying mechanism responsible for the transition of chip morphologies. The cutting energy consumption of brittle regime machining in UHSMC can be decreased by more than 19% compared with ductile regime machining in HSMC, which indicates the advantage of UHSMC in terms of energy savings.

- Various surface defects and different surface topographies on the machined surface are generated in HSMC compared to low-speed machining. Less surface defects and lower surface roughness can be obtained at a specific range of high cutting speeds, and the speed range depends on the workpiece material, cutting mode, and cutting tool used. Ultrafine grain layer and phase transformation are produced by severe plastic deformation on the machined surface during HSMC of different workpiece materials.
- With increasing the cutting speed, although larger compressive residual stresses are generated at a deeper subsurface due to severer plastic deformation, a thin layer exhibiting very high tensile residual stresses is generally induced on the superficial surface, which may become a hidden danger in service. The high cutting speeds may not improve all surface integrity parameters (e.g., the residual stress, the surface topography, and the microstructural alteration, etc.) simultaneously. Optimized cutting speed need to be determined based on a balanced surface quality.
- The cutting force can be reduced in the cutting speed range of HSMC due to thermal softening caused by chip plastic deformation that is beneficial for

weakening material deformation resistance. Brittle fracture of removed layer material can also help to keep the cutting force at a low level when the cutting speed increases to the range of UHSMC. The friction coefficient at the tool-chip interface presents a decreasing trend with increasing the cutting speed. Different opinions have been proposed about the existence of Salomon's cutting temperature curve. It indicates that interrupted machining may be a necessary condition for the tenability of Salomon's assumption, and the time ratio of cutting to non-cutting is a significant parameter that affect the variation of cutting temperature.

- Severe tool wear under extreme thermal-mechanical loading conditions is one of the most critical challenges for application of HSMC in industries. Understanding tool wear behavior and associated wear mechanism can instruct design and fabrication of cutting tools adaptable for HSMC, and recommend suitable tools for machining of specific work materials.
- HSMC has been applied successfully in industrial manufacture of different mechanical components. It has presented prominent advantages in the fabrication of components that require the removal of a high volume of material. The speed range used in industries has been improved significantly by the advancements in ultra-hard cutting tools that can achieve higher cutting speeds. Meanwhile, with the development of advanced engineering materials that display higher strength and toughness,

the high-efficient machining of mechanical components made of these materials presents further challenges for HSMC.

References

[1] A. Yadav, S.C. Jayswal, Modelling of flexible manufacturing system: a review, Int. J. Prod. Res. 56(7) (2018) 2464-2487.

[2] D. Dudzinski, A. Devillez, A. Moufki, D. Larrouquere, V. Zerrouki, J. Vigneau, A review of developments towards dry and high speed machining of Inconel 718 alloy, Int. J. Mach. Tools Manuf. 44(4) (2004) 439-456.

[3] H. Schulz, T. Moriwaki, High-speed machining, CIRP Ann. 41(2) (1992) 637-643.

[4] K. Gupta, J.P. Davim, (Eds.) High-Speed Machining, Academic Press (2020).

[5] Machining Market to Reach $414.17 Billion by 2022, Says Beroe Inc. https://www.prnewswire.com/news-releases/machining-market-to-reach-414-17-billion-by-2022--says-beroe-inc-300939464.html.

[6] T.G. Molnar, S. Berezvai, A.K. Kiss, D. Bachrathy, G. Stepan, Experimental investigation of dynamic chip formation in orthogonal cutting, Int. J. Mach. Tools Manuf. 145 (2019) 103429.

[7] C.A. Van Luttervelt, T.H.C. Childs, I.S. Jawahir, F. Klocke, P.K. Venuvinod, Y. Altintas, E. Armarego, D. Dornfeld, I. Grabec, J. Leopold, B. Lindstrom, D. Lucca, T. Obikawa, T. Shirakashi, H. Sato, Present situation and future trends in

modelling of machining operations progress report of the CIRP Working Group ‘Modelling of Machining Operations’, CIRP Ann. 47(2) (1998) 587-626.

[8] C. Maranhão, J.P. Davim, Finite element modelling of machining of AISI 316 steel: numerical simulation and experimental validation, Simul. Model. Pract. Th. 18(2) (2010) 139-156.

[9] V.P. Astakhov, Tribology of Metal Cutting. Elsevier, 2006.

[10] C.J. Salomon, Process for machining metals of similar acting materials when being worked by cutting tools, German Patent No. 523594, 1931.

[11] R. Wertheim, High-speed cutting, CIRP Encyclopedia of Production Engineering (2014) 632-654.

[12] R.S. Pawade, S.S. Joshi, P.K. Brahmankar, Effect of machining parameters and cutting edge geometry on surface integrity of high-speed turned Inconel 718, Int. J. Mach. Tools Manuf. 48(1) (2008) 15-28.

[13] J. Du, Z. Liu, Effect of cutting speed on surface integrity and chip morphology in high-speed machining of PM nickel-based superalloy FGH95, Int. J. Adv. Manuf. Technol. 60(9-12) (2012) 893-899.

[14] A.L. Mantle, D.K. Aspinwall, Surface integrity of a high speed milled gamma titanium aluminide, J. Mater. Process. Technol. 118(1-3) (2001) 143-150.

[15] B. Wang, Z. Liu, Influences of tool structure, tool material and tool wear on machined surface integrity during turning and milling of titanium and nickel alloys: a review, Int. J. Adv. Manuf. Technol. 98(5-8) (2018) 1925-1975.

[16] V. Thévenot, L. Arnaud, G. Dessein, G. Cazenave-Larroche, Influence of material removal on the dynamic behavior of thin-walled structures in peripheral milling, Mach. Sci. Technol. 10(3) (2006) 275-287.

[17] A.C. Okafor, Cooling and machining strategies for high speed milling of titanium and nickel super alloys, In High Speed Machining. Elsevier, Academic Press (2020) 127-161.

[18] B. Wang, S.N. Melkote, S. Saraogi, P. Wang, Effect of scratching speed on phase transformations in high-speed scratching of monocrystalline silicon, Mater. Sci. Eng. A 772 (2020) 138836.

[19] D.A. Axinte, R.C. Dewes, Surface integrity of hot work tool steel after high speed milling-experimental data and empirical models, J. Mater. Process. Technol. 127(3) (2002) 325-335.

[20] M. Rahman, Z.G. Wang, Y.S. Wong, A review on high-speed machining of titanium alloys, JSME Int. J. Series C, Mech. Syst. Mach. Element. Manuf. 49(1) (2006) 11-20.

[21] R. King, Handbook of High-Speed Machining Technology. Springer Science & Business Media, 2013.

[22] J.M. Longbottom, J.D. Lanham, A review of research related to Salomon's hypothesis on cutting speeds and temperatures, Int. J. Mach. Tools Manuf. 46(14) (2006) 1740-1747.

[23] H. Schulz, E. Abele, A. Sahm, Material aspects of chip formation in HSC machining, CIRP Ann. 50(1) (2001) 45-48.

[24] ISO 1940/1, Mechanical vibration - Balance quality requirements for rotors in a constant (rigid) state, 2003.

[25] G. Arndt, Ultra-high-speed machining: a review and an analysis of cutting forces, Proc. Inst. Mech. Eng. 187(1) (1973) 625-634.

[26] G. Icks, Machine dependent limits of high speed turning, Dr.-Ing. Diss., University Stuttgart, 1981.

[27] K. Tuffentsammer, G. Icks, Lathe criteria for the turning at ultra-high cutting speeds, Proceed. 10th NAMRC. (1982) 374.

[28] H. Schulz, High speed cutting - A technology with future, Werkstatt und Betrieb, 127(7-8) (1994) 539-541.

[29] H.K. Tönshoff, B. Karpuschewski, C. Lapp, P. Andrae, New machine techniques for high-speed machining, In International Seminar on improving Machine Tool Performance, 1 (1998) 65-76.

[30] H.K. Tönshoff, B. Denkena, Basics of Cutting and Abrasive Processes. Springer, Berlin, Heidelberg, 2013.

[31] A. Molinari, C. Musquar, G. Sutter, Adiabatic shear banding in high speed machining of Ti-6Al-4V: experiments and modeling, Int. J. Plast. 18(4) (2002) 443-459.

[32] R.F. Recht, Catastrophic thermoplastic shear, ASME J. Appl. Mech. 86 (1964) 186-193.

[33] R. Komanduri, T. Schroeder, J. Hazra, B.F. Von Turkovich, D.G. Flom, On the

catastrophic shear instability in high-speed machining of an AISI 4340 steel, ASME J. Eng. Ind. 104(2) (1982) 121-131.

[34] M.A. Davies, Y. Chou, C.J. Evans, On chip morphology, tool wear and cutting mechanics in finish hard turning, CIRP Ann. 45(1) (1996) 77-82.

[35] B. Denkena, R. Ben Amor, L. De Leon-Garcia, J. Dege, Material specific definition of the high speed cutting range, Int. J. Mach. Mach. Mater. 2(2) (2007) 176-185.

[36] B. Wang, Z. Liu, G. Su, X. Ai, Brittle removal mechanism of ductile materials with ultrahigh-speed machining. ASME J. Manuf. Sci. Eng. 137(6) (2015) 061002.

[37] B. Wang, Z. Liu, G. Su, Q. Song, X. Ai, Investigations of critical cutting speed and ductile-to-brittle transition mechanism for workpiece material in ultra-high speed machining, Int. J. Mech. Sci. 104 (2015) 44-59.

[38] B. Wang, Z. Liu, Q. Yang, Investigations of yield stress, fracture toughness, and energy distribution in high speed orthogonal cutting, Int. J. Mach. Tools Manuf. 73 (2013) 1-8.

[39] J. Tlusty, High-speed machining, CIRP Ann. 42(2) (1993) 733-738.

[40] S. Smith, J. Tlusty, Current trends in high-speed machining, ASME J. Manuf. Sci. Eng. 119(4B) (1997) 664-666.

[41] T.L. Schmitz, R.R. Donalson, Predicting high-speed machining dynamics by substructure analysis, CIRP Ann. 49(1) (2000) 303-308.

[42] M.R. Movahhedy, P. Mosaddegh, Prediction of chatter in high speed milling including gyroscopic effects, Int. J. Mach. Tools Manuf. 46(9) (2006) 996-1001.

[43] S. Sharma, A. Meena, Microstructure induced shear instability criterion during high-speed machining of Ti-6Al-4V, ASME J. Manuf. Sci. Eng. 143(6) (2020) 061001.

[44] G.G. Ye, Y. Chen, S.F. Xue, L.H. Dai, Critical cutting speed for onset of serrated chip flow in high speed machining, Int. J. Mach. Tools Manuf. 86 (2014) 18-33.

[45] L.B. Zhou, J. Shimizu, A. Muroya, E. Hiroshi, Material removal mechanism beyond plastic wave propagation rate, Precis. Eng. 27(2) (2003) 109-116.

[46] G. Sutter, A. Molinari, G. List, X. Bi, Chip flow and scaling laws in high speed metal cutting, ASME J. Manuf. Sci. Eng. 134(2) (2012) 021005.

[47] G. Sutter, G. List, Very high speed cutting of Ti-6Al-4V titanium alloy-change in morphology and mechanism of chip formation, Int. J. Mach. Tools Manuf. 66 (2013) 37-43.

[48] G.G. Ye, S.F. Xue, W. Ma, M.Q. Jiang, Z. Ling, X.H. Tong, L.H. Dai, Cutting AISI 1045 steel at very high speeds, Int. J. Mach. Tools Manuf. 56 (2012) 1-9.

[49] L.B. Wuertemberger, Predicting the Wear of High Speed Rocket Sleds. Air Force Institute of Technology, (2012) No. AFIT-ENY-12-D-02.

[50] D. Xu, Z. Liao, D. Axinte, M. Hardy, A novel method to continuously map the surface integrity and cutting mechanism transition in various cutting conditions, Int. J. Mach. Tools Manuf. 151 (2020) 103529.

[51] D. Xu, Z. Liao, D. Axinte, M. Hardy, R. M'Saoubi, A quick method for evaluating the thresholds of workpiece surface damage in machining, CIRP Ann. 68(1) (2019) 61-64.

[52] V. Nguyen, S. Melkote, A. Deshamudre, M. Khanna, D. Walker, PVDF sensor based monitoring of single-point cutting, J. Manuf. Process. 24 (2016) 328-337.

[53] M.C. Kang, J.S. Kim, J.H. Kim, A monitoring technique using a multi-sensor in high speed machining, J. Mater. Process. Technol. 113(1-3) (2001) 331-336.

[54] R.E. Haber, J.E. Jiménez, C.R. Peres, J.R. Alique, An investigation of tool-wear monitoring in a high-speed machining process, Sensor. Actuat. A: Phys. 116(3) (2004) 539-545.

[55] B. Wang, Z. Liu, Acoustic emission signal analysis during chip formation process in high speed machining of 7050-T7451 aluminum alloy and Inconel 718 superalloy, J. Manuf. Process. 27 (2017) 114-125.

[56] T.D. Marusich, M. Ortiz, Modelling and simulation of high-speed machining. Int. J. Numer. Meth. Eng. 38(21) (1995) 3675-3694.

[57] D. Umbrello, Finite element simulation of conventional and high speed machining of Ti6Al4V alloy, J. Mater. Process. Technol. 196(1-3) (2008) 79-87.

[58] G. Chen, C. Ren, X. Yang, X. Jin, T. Guo, Finite element simulation of high-speed machining of titanium alloy (Ti-6Al-4V) based on ductile failure model, Int. J. Adv. Manuf. Technol. 56(9-12) (2011) 1027-1038.

[59] S.N. Melkote, W. Grzesik, J. Outeiro, J. Rech, V. Schulze, H. Attia, P.J. Arrazola,

R. M'Saoubi, C. Saldana, Advances in material and friction data for modelling of metal machining, CIRP Ann. 66(2) (2017) 731-754.

[60] G.T. Gray III, High-strain-rate testing of materials: The Split-Hopkinson Pressure Bar. Charact. Mater. (2002) 1-15.

[61] B. Wang, Z. Liu, Q. Song, Y. Wan, X. Ren, A modified Johnson-Cook constitutive model and its application to high speed machining of 7050-T7451 aluminum alloy, ASME J. Manuf. Sci. Eng. 141(1) (2019) 011012.

[62] O.S. Lee, M.S. Kim, Dynamic material property characterization by using split Hopkinson pressure bar (SHPB) technique, Nucl. Eng. Des. 226(2) (2003) 119-125.

[63] J. Peirs, P. Verleysen, J. Degrieck, F. Coghe, The use of hat-shaped specimens to study the high strain rate shear behaviour of Ti-6Al-4V, Int. J. Impact Eng. 37(6) (2010) 703-714.

[64] B. Wang, X. Xiao, V.P. Astakhov, Z. Liu, The effects of stress triaxiality and strain rate on the fracture strain of Ti6Al4V, Eng. Fract. Mech. 219 (2019) 106627.

[65] D. Rittel, S. Lee, G. Ravichandran, A shear-compression specimen for large strain testing, Exp. Mech. 42(1) (2002) 58-64.

[66] A. Dorogoy, D. Rittel, A. Godinger, Modification of the shear-compression specimen for large strain testing, Exp. Mech. 55(9) (2015) 1627–1639.

[67] B. Wang, Z. Liu, Investigations on deformation and fracture behavior of

workpiece material during high speed machining of 7050-T7451 aluminum alloy, CIRP J. Manuf. Sci. Technol. 14 (2016) 43-54.

[68] G.R. Johnson, W.H. Cook, A constitutive model and data for metals subjected to large strains, high strain rates and high temperatures, In: Proceedings of the seventh international symposium on ballistics, Hague, Netherlands. (1983) 541-547.

[69] X. Wang, C. Huang, B. Zou, H. Liu, H. Zhu, J. Wang, Dynamic behavior and a modified Johnson-Cook constitutive model of Inconel 718 at high strain rate and elevated temperature, Mater. Sci. Eng. A 580 (2013) 385-390.

[70] A. Banerjee, S. Dhar, S. Acharyya, D. Datta, N. Nayak, Determination of Johnson Cook material and failure model constants and numerical modelling of Charpy impact test of armour steel, Mater. Sc. Eng. A 640 (2015) 200-209.

[71] Q. Wu, W. Xu, L. Zhang, Machining of particulate-reinforced metal matrix composites: An investigation into the chip formation and subsurface damage, J. Mater. Processing Technol. 274 (2019) 116315.

[72] U. Andrade, M.A. Meyers, K.S. Vecchio, A.H. Chokshi, Dynamic recrystallization in high-strain, high-strain-rate plastic deformation of copper, Acta Metall. Mater. 42 (1994) 3183-3195.

[73] X.L. Fu, X. Ai, S. Zhang, Y. Wan, Constitutive equation for 7050 aluminum alloy at high temperatures, Mater. Sci. Forum 532 (2006) 125-128.

[74] M. Calamaz, D. Coupard, F. Girot, A new material model for 2D numerical

simulation of serrated chip formation when machining titanium alloy Ti-6Al-4V, Int. J. Mach. Tools Manuf. 48 (2008) 275-288.

[75] J.Y. Sheikh-Ahmad, J.A. Bailey, A constitutive model for commercially pure titanium, ASME J. Eng. Mater. Tech. 117 (1995) 139-144.

[76] G. Li, M. Wang, C. Duan, Adiabatic shear critical condition in the high-speed cutting, J. Mater. Process. Technol. 209(3) (2009) 1362-1367.

[77] N.E. Ugodilinwa, M. Khoshdarregi, O.A. Ojo, Analysis and constitutive modeling of high strain rate deformation behavior of Haynes 282 aerospace superalloy, Mater. Today Commun. 20 (2019) 100545.

[78] Y.B. Bao, T. Wierzbicki, On fracture locus in the equivalent strain and stress triaxiality space, Int. J. Mech. Sci. 46 (2004) 81-98.

[79] Y. Abushawashi, X. Xiao, V. Astakhov, Practical applications of the "energy-triaxiality" state relationship in metal cutting, Mach. Sci. Technol. 21(1) (2017) 1-18.

[80] B. Wang, Z. Liu, Evaluation on fracture locus of serrated chip generation with stress triaxiality in high speed machining of Ti6Al4V, Mater. Des. 98 (2016) 68-78.

[81] S. Buchkremer, F. Klocke, D. Veselovac, 3D FEM simulation of chip breakage in metal cutting, Int. J. Adv. Manuf. Technol. 82(1-4) (2016) 645-661.

[82] V.P. Astakhov, Mechanical properties of engineering materials: relevance in design and manufacturing, In Introduction to Mechanical Engineering, Springer,

Cham, (2018) 3-41.

[83] B. Wang, X. Xiao, V.P. Astakhov, Z. Liu, A quantitative analysis of the transition of fracture mechanisms of Ti6Al4V over a wide range of stress triaxiality and strain rate, Eng. Fract. Mech. 231 (2020) 107020.

[84] B. Wang, Z. Liu, Investigations on the chip formation mechanism and shear localization sensitivity of high-speed machining Ti6Al4V, Int. J. Adv. Manuf. Technol. 75(5-8) (2014) 1065-1076.

[85] C.E. Campbell, L.A. Bendersky, W.J. Boettinger, R. Ivester, Microstructural characterization of Al-7075-T651 chips and work pieces produced by high-speed machining, Mater. Sci. Eng. A, 430(1-2) (2006) 15-26.

[86] J.P. Velásquez, B. Bolle, P. Chevrier, G. Geandier, A. Tidu, Metallurgical study on chips obtained by high speed machining of a Ti-6 wt.% Al-4 wt.% V alloy, Mater. Sci. Eng. A, 452 (2007) 469-474.

[87] X.M. Zhang, K. Zhang, D. Zhang, J. Outeiro, H. Ding, New in situ imaging-based methodology to identify the material constitutive model coefficients in metal cutting process, ASME J. Manuf. Sci. Eng. 141(10) (2019) 101007.

[88] A. Molinari, X. Soldani, M.H. Miguélez, Adiabatic shear banding and scaling laws in chip formation with application to cutting of Ti-6Al-4V, J. Mech. Phys. Solid. 61(11) (2013) 2331-2359.

[89] B. Wang, Z. Liu, Serrated chip formation mechanism based on mixed mode of

ductile fracture and adiabatic shear, Proc. Inst. Mech. Eng. Part B: J. Eng. Manuf. 228(2) (2014) 181-190.

[90] T.J. Burns, M.A. Davies, On repeated adiabatic shear band formation during high-speed machining, Int. J. Plast. 18(4) (2002) 487-506.

[91] X. Yang, B. Zhang, Material embrittlement in high strain-rate loading, Int. J. Extreme Manuf. 1(2) (2019) 022003.

[92] E. Ceretti, M. Lucchi, T. Altan, FEM simulation of orthogonal cutting: serrated chip formation, J. Mater. Process. Technol. 95(1-3) (1999) 17-26.

[93] Y.B. Guo, D.W. Yen, A FEM study on mechanisms of discontinuous chip formation in hard machining, J. Mater. Process. Technol. 155 (2004) 1350-1356.

[94] T. Özel, The influence of friction models on finite element simulations of machining, Int. J. Mach. Tools Manuf. 46(5) (2006) 518-530.

[95] B. Wang, Z. Liu, Shear localization sensitivity analysis for Johnson-Cook constitutive parameters on serrated chips in high speed machining of Ti6Al4V, Simul. Model. Pract. Th. 55 (2015) 63-76.

[96] B. Wang, Z. Liu, X. Hou, J. Zhao, Influences of cutting speed and material mechanical properties on chip deformation and fracture during high-speed cutting of Inconel 718, Materials 11(4) (2018) 461.

[97] T. Von Karman, P. Duwez, The propagation of plastic deformation in solids, J. Appl. Phys. 21(10) (1950) 987-994.

[98] V.D. Kuznetsov, Super-high-speed cutting of metals, Iron Age 155 (1945) 66-69.

[99] B. Wang, Z. Liu, Q. Song, Y. Wan, Z. Shi, Proper selection of cutting parameters and cutting tool angle to lower the specific cutting energy during high speed machining of 7050-T7451 aluminum alloy, J. Clean. Prod. 129 (2016) 292-304.

[100] B. Wang, Z. Liu, Q. Song, Y. Wan, X. Ren, An approach for reducing cutting energy consumption with ultra-high speed machining of Super Alloy Inconel 718, Int. J. Precis. Eng. Manuf. - Green Technol. 7(1) (2020) 35-51.

[101] C.Z. Duan, L.C. Zhang, Adiabatic shear banding in AISI 1045 steel during high speed machining: mechanisms of microstructural evolution, Mater. Sci. Eng. A 532 (2012) 111-119.

[102] H. Liu, J. Zhang, X. Xu, W. Zhao, Experimental study on fracture mechanism transformation in chip segmentation of Ti-6Al-4V alloys during high-speed machining, J. Mater. Process. Technol. 257 (2018) 132-140.

[103] Y. Idell, J. Wiezorek, G. Facco, A. Kulovits, M.R. Shankar, Geometric dynamic recrystallization of austenitic stainless steel through linear plane-strain machining, Philos. Mag. 100(9) (2020) 1102-1128.

[104] X. Liang, Z. Liu, B. Wang, Dynamic recrystallization characterization in Ti-6Al-4V machined surface layer with process-microstructure-property correlations, Appl. Surf. Sci. 530 (2020) 147184.

[105] Z. Liao, A. Abdelhafeez, H. Li, Y. Yang, O.G. Diaz, D. Axinte, State-of-the-art of surface integrity in machining of metal matrix composites, Int. J. Mach. Tools Manuf. 143 (2019) 63-91.

[106] R. Bejjani, M. Balazinski, H. Attia, P. Plamondon, G. L'Espérance, Chip formation and microstructure evolution in the adiabatic shear band when machining titanium metal matrix composites, Int. J. Mach. Tools Manuf. 109 (2016) 137-146.

[107] S.N. Melkote, R. Liu, P. Fernandez-Zelaia, T. Marusich, A physically based constitutive model for simulation of segmented chip formation in orthogonal cutting of commercially pure titanium, CIRP Ann. 64(1) (2015) 65-68.

[108] S. Imbrogno, S. Rinaldi, D. Umbrello, L. Filice, R. Franchi, A. Del Prete, A physically based constitutive model for predicting the surface integrity in machining of Waspaloy, Mater. Des. 152 (2018) 140-155.

[109] D. Kumar, S. Idapalapati, W. Wang, S. Narasimalu, Effect of surface mechanical treatments on the microstructure-property-performance of engineering alloys, Materials 12(16) (2019) 2503.

[110] Y. Hua, Z. Liu, B. Wang, X. Hou, Surface modification through combination of finish turning with low plasticity burnishing and its effect on fatigue performance for Inconel 718, Surf. Coat. Technol. 375 (2019) 508-517.

[111] M. Suraratchai, J. Limido, C. Mabru, R. Chieragatti, Modelling the influence of machined surface roughness on the fatigue life of aluminium alloy, Int. J.

Fatigue 30(12) (2008) 2119-2126.

[112] G. Su, Z. Liu, L. Li, B. Wang, Influences of chip serration on micro-topography of machined surface in high-speed cutting, Int. J. Mach. Tools Manuf. 89 (2015) 202-207.

[113] Z. Zhang, Z. Wang, W. Wang, R. Jiang, Y. Xiong, Investigation on surface quality of high-speed cutting titanium alloy Ti6Al4V based on Split-Hopkinson pressure bar. Proc. Inst. Mech. Eng. Part B: J. Eng. Manuf. 234(10) (2020) 1293-1301.

[114] J. Zhou, V. Bushlya, P. Avdovic, J.E. Ståhl, Study of surface quality in high speed turning of Inconel 718 with uncoated and coated CBN tools, Int. J. Adv. Manuf. Technol. 58(1-4) (2012) 141-151.

[115] F. Abroug, E. Pessard, G. Germain, F. Morel, A probabilistic approach to study the effect of machined surface states on HCF behavior of a AA7050 alloy, Int. J. Fatigue 116 (2018) 473-489.

[116] J.M. Zhou, V. Bushlya, J.E. Stahl, An investigation of surface damage in the high speed turning of Inconel 718 with use of whisker reinforced ceramic tools, J. Mater. Process. Technol. 212(2) (2012) 372-384.

[117] Z. Chen, R.L. Peng, J. Zhou, R. M'Saoubi, D. Gustafsson, J. Moverare, Effect of machining parameters on cutting force and surface integrity when high-speed turning AD 730™ with PCBN tools, Int. J. Adv. Manuf. Technol. 100(9) (2019) 2601-2615.

[118] A. Ginting, M. Nouari, Surface integrity of dry machined titanium alloys, Int. J. Mach. Tools Manuf. 49(3-4) (2009) 325-332.

[119] X. Liang, Z. Liu, Tool wear behaviors and corresponding machined surface topography during high-speed machining of Ti-6Al-4V with fine grain tools, Trib. Int. 121 (2018) 321-332.

[120] R. M'Saoubi, T. Larsson, J. Outeiro, Y. Guo, S. Suslov, C. Saldana, S. Chandrasekar, Surface integrity analysis of machined Inconel 718 over multiple length scales, CIRP Ann. 61(1) (2012) 99-102.

[121] H.A. Kishawy, M.A. Elbestawi, Effects of process parameters on material side flow during hard turning, Int. J. Mach. Tools Manuf. 39 (1999) 1017-1030.

[122] B. Shiari, R.E. Miller, D.D. Klug, Multiscale simulation of material removal processes at the nanoscale, J. Mech. Phys. Solids 55 (2007) 2384-2405.

[123] Y. Guo, C. Saldana, W.D. Compton, S. Chandrasekar, Controlling deformation and microstructure on machined surfaces, Acta Mater. 59(11) (2011) 4538-4547.

[124] Q. Wang, Z. Liu, B. Wang, Q. Song, Y. Wan, Evolutions of grain size and micro-hardness during chip formation and machined surface generation for Ti-6Al-4V in high-speed machining, Int. J. Adv. Manuf. Technol. 82(9-12) (2016) 1725-1736.

[125] J.P. Velásquez, A. Tidu, B. Bolle, P. Chevrier, J.J. Fundenberger, Sub-surface and surface analysis of high speed machined Ti-6Al-4V alloy, Mater. Sci. Eng.

A 527(10-11) (2010) 2572-2578.

[126] R. Neugebauer, K.D. Bouzakis, B. Denkena, F. Klocke, A. Sterzing, A.E. Tekkaya, R. Wertheim, Velocity effects in metal forming and machining processes, CIRP Ann. 60(2) (2011) 627-650.

[127] B. Zhang, J. Yin, The 'skin effect'of subsurface damage distribution in materials subjected to high-speed machining, Int. J. Extreme Manuf. 1(1) (2019) 012007.

[128] H. Liu, J. Zhang, B. Xu, X. Xu, W. Zhao, Prediction of microstructure gradient distribution in machined surface induced by high speed machining through a coupled FE and CA approach, Mater. Des. 196 (2020) 109133.

[129] L.S. Tóth, Y. Estrin, R. Lapovok, C. Gu, A model of grain fragmentation based on lattice curvature, Acta Mater. 58 (2010) 1782-1794.

[130] R. Ding, Z.X. Guo, Microstructural evolution of a Ti-6Al-4V alloy during β-phase processing: experimental and simulative investigations, Mater. Sci. Eng. A 365 (2004) 172-179.

[131] D.A. Axinte, P. Andrews, W. Li, N. Gindy, P.J. Withers, T.H.C. Childs, Turning of advanced Ni based alloys obtained via powder metallurgy route, CIRP Ann. 55(1) (2006) 117-120.

[132] M. Brown, P. Crawforth, R. M'Saoubi, T. Larsson, B. Wynne, A. Mantle, H. Ghadbeigi, Quantitative characterization of machining-induced white layers in Ti-6Al-4V, Mater. Sci. Eng. A 764 (2019) 138220.

[133] J. Barry, G. Byrne, TEM study on the surface white layer in two turned hardened steels, Mater. Sci. Eng. A 325(1-2) (2002) 356-364.

[134] J. Du, Z. Liu, S. Lv, Deformation-phase transformation coupling mechanism of white layer formation in high speed machining of FGH95 Ni-based superalloy, Appl. Surf. Sci. 292 (2014) 197-203.

[135] S.C. Veldhuis, G.K. Dosbaeva, A. Elfizy, G.S. Fox-Rabinovich, T. Wagg, Investigations of white layer formation during machining of powder metallurgical Ni-based ME 16 superalloy, J. Mater. Eng. Perform. 19(7) (2010) 1031-1036.

[136] A. Wusatowska-Sarnek, B. Dubiel, A. Czyrska-Filemonowicz, P. Bhowal, N.B. Salah, J. Klemberg-Sapieha, Microstructural characterization of the white etching layer in nickel-based superalloy, Metall. Mater. Trans. A 42(12) (2011) 3813-3825.

[137] Z. Liao, M. Polyakov, O.G. Diaz, D. Axinte, G. Mohanty, X. Maeder, J. Michler, M. Hardy, Grain refinement mechanism of nickel-based superalloy by severe plastic deformation-Mechanical machining case, Acta Mater. 180 (2019) 2-14.

[138] X. Yan, S. Yin, C. Chen, C. Huang, R. Bolot, R. Lupoi, M. Kuang, We. Ma, C. Coddet, H. Liao, M. Liu, Effect of heat treatment on the phase transformation and mechanical properties of Ti6Al4V fabricated by selective laser melting, J. Alloy. Compd. 764 (2018) 1056-1071.

[139] Q. Wang, Z. Liu, D. Yang, A.U.H. Mohsan, Metallurgical-based prediction of stress-temperature induced rapid heating and cooling phase transformations for high speed machining Ti-6Al-4V alloy, Mater. Des. 119 (2017) 208-218.

[140] M.A.S. Torres, H.J.C. Voorwald, An evaluation of shot peening, residual stress and stress relaxation on the fatigue life of AISI 4340 steel, Int. J. Fatigue 24(8) (2002) 877-886.

[141] Y.B. Guo, A.W. Warren, F. Hashimoto, The basic relationships between residual stress, white layer, and fatigue life of hard turned and ground surfaces in rolling contact, CIRP J. Manuf. Sci. Technol. 2(2) (2010) 129-134.

[142] J.G. Li, S.Q. Wang, Distortion caused by residual stresses in machining aeronautical aluminum alloy parts: recent advances, Int. J. Adv. Manuf. Technol. 89(1-4) (2017) 997-1012.

[143] R.M.N. Fleury, E. Salvati, D. Nowell, A.M. Korsunsky, F. Silva, Y.H. Tai, The effect of surface damage and residual stresses on the fatigue life of nickel superalloys at high temperature, Int. J. Fatigue 119 (2019) 34-42.

[144] Y. Hua, Z. Liu, B. Wang, J. Jiang, Residual stress regenerated on low plasticity burnished Inconel 718 surface after initial turning process, ASME J. Manuf. Sci. Eng. 141(12) (2019) 121004.

[145] A. Weidner, T. Lippmann, H. Biermann, Crack initiation in the very high cycle fatigue regime of nitrided 42CrMo4 steel, J. Mater. Res. 32(23) (2017) 4305-4316.

[146] M. Jacobson, P. Dahlman, F. Gunnberg, Cutting speed influence on surface integrity of hard turned bainite steel, J. Mater. Process. Technol. 128 (2002) 318-323.

[147] C. Schlauer, R.L. Peng, M. Odén, Residual stresses in a nickel-based superalloy introduced by turning, Mater. Sci. Forum 404-407 (2002) 173-178.

[148] L. Guerville, J. Vigneau, Influence of machining conditions on residual stresses, in: D. Dudzinski, A. Molinari, H. Schulz (Eds.), Metal Cutting and High Speed Machining, Kluwer Academic Plenum Publishers (2002) 201-210.

[149] S. Derrien, J. Vigneau, High speed milling of difficult to machine alloys, in: A. Molinari, H. Schulz, H. Schulz (Eds.), Proceedings of the First French and German Conference on High Speed Machining, University of Metz, France, 1997.

[150] I.S. Jawahir, E. Brinksmeier, R. M'Saoubi, D.K. Aspinwall, J.C. Outeiro, D. Meyer, D. Umbrello, A.D. Jayal, Surface integrity in material removal processes: recent advances, CIRP Ann. 60(2) (2011) 603-626.

[151] M. Mohammadpour, M.R. Razfar, R.J. Saffar, Numerical investigating the effect of machining parameters on residual stresses in orthogonal cutting, Simul. Model. Pract. Th. 18(3) (2010) 378-389.

[152] T. Özel, D. Ulutan, Prediction of machining induced residual stresses in turning of titanium and nickel based alloys with experiments and finite element simulations, CIRP Ann. 61(1) (2012) 547-550.

[153] F. Wang, Z.Y. Liu, Y.B. Guo, J. Zhao, Z.Q. Liu, Efficient multiscale modeling and validation of residual stress field in cutting, ASME J. Manuf. Sci. Eng. 139(9) (2017) 091004.

[154] T. Mabrouki, F. Girardin, M. Asad, J.F. Rigal, Numerical and experimental study of dry cutting for an aeronautic aluminium alloy (A2024-T351), Int. J. Mach. Tools Manuf. 48(11) (2008) 1187-1197.

[155] M. Daoud, J.F. Chatelain, A. Bouzid, Effect of rake angle-based Johnson-Cook material constants on the prediction of residual stresses and temperatures induced in Al2024-T3 machining, Int. J. Mech. Sci. 122 (2017) 392-404.

[156] F. Valiorgue, J. Rech, H. Hamdi, P. Gilles, J.M. Bergheau, 3D modelling of residual stresses induced in finish turning of an AISI 304L stainless steel, Int. J. Mach. Tools Manuf. 53 (2012) 77-90.

[157] Y. Fan, T. Wang, Z. Hao, X. Liu, S. Gao, R. Li, Surface residual stress in high speed cutting of superalloy Inconel718 based on multiscale simulation, J. Manuf. Process. 31 (2018) 480-493.

[158] D. Yang, Z. Liu, X. Ren, P. Zhuang, Hybrid modeling with finite element and statistical methods for residual stress prediction in peripheral milling of titanium alloy Ti-6Al-4V, Int. J. Mech. Sci. 108 (2016) 29-38.

[159] P.A. Colegrove, H.E. Coules, J. Fairman, F. Martina, T. Kashoob, H. Mamash, L.D. Cozzolino, Microstructure and residual stress improvement in wire and arc additively manufactured parts through high-pressure rolling, J. Mater. Process.

Technol. 213(10) (2013) 1782-1791.

[160] A.H. Mahmoudi, A. Ghasemi, G.H. Farrahi, K. Sherafatnia, A comprehensive experimental and numerical study on redistribution of residual stresses by shot peening, Mater. Des. 90 (2016) 478-487.

[161] A. Marcon, S.N. Melkote, M. Yoda, Effect of nozzle size scaling in co-flow water cavitation jet peening, J. Manuf. Process. 31 (2018) 372-381.

[162] F. Klocke, S. Hoppe, Mechanisms of chip formation in high speed cutting. Sci. Fundament. HSC 1 (2001) 1-10.

[163] H.W. Hoffmeister, A. Gente, T.H. Weber, Chip formation at titanium alloys under cutting speed of up to 100 m/s, in: 2nd International Conference on High Speed Machining, PTW Darmstadt University, (1999) 21-28.

[164] A. Gente, H.W. Hoffmeister, C.J. Evans, Chip formation in machining Ti6Al4V at extremely high cutting speeds, CIRP Ann. Manuf. Technol. 50 (2001) 49-52.

[165] S. Hoppe, Experimental and numerical analysis of chip formation in metal cutting, Ph.D. Thesis, Fakultät für Maschinenwesen der Rheinisch-Westfälischen Technischen Hochschule Aachen, 2003.

[166] J. Barry, G. Byrne, D. Lennon, Observations on chip formation and acoustic emission in machining Ti-6Al-4V alloy, Int. J. Mach. Tools Manuf. 41 (2001) 1055-1070.

[167] H.J. Illgner, Hochgeschwindigkeitsfräsen schwer zerspanbarer Legierungen,

Ph.D. Thesis, TH Darmstadt, Carl Hanser Verlag, 1990.

[168] S. Larbi, Contribution à l'étude de l'usinage à grandes vitesses de matériaux métalliques par simulation sur un banc d'essai à base de barres de Hopkinson, Ph.D. Thesis, Université de Nantes, 1990.

[169] M. Cotterell, G. Byrne, Characterisation of chip formation during orthogonal cutting of titanium alloy Ti-6Al-4V, CIRP J. Manuf. Sci. Technol. 1 (2008) 81-85.

[170] E. Uhlmann, M.G. Von Der Schulenburg, R. Zettier, Finite element modeling and cutting simulation of Inconel 718, CIRP Ann. 56(1) (2007) 61-64.

[171] M. Bäker, Finite element simulation of high-speed cutting forces, J. Mater. Process. Technol. 176(1-3) (2006) 117-126.

[172] B. Rao, Y.C. Shin, Analysis on high-speed face-milling of 7075-T6 aluminum using carbide and diamond cutters, Int. J. Mach. Tools Manuf. 41(12) (2001) 1763-1781.

[173] G. Sutter, A. Molinari, Analysis of the cutting force components and friction in high speed machining, ASME J. Manuf. Sci. Eng. 127 (2005) 245-250.

[174] W.N. Findley, R.M. Reed, The influence of extreme speeds and rake angles in metal cutting, ASME J. Eng. Ind. 85(2) (1963) 49-67.

[175] Y. Tanaka, H. Tsuwa, M. Kitano, Cutting mechanism in ultra-high-speed machining, Trans. ASME (1967) paper No 67-PROD-14.

[176] R.F. Recht, A dynamic analysis of high speed machining, High Speed

Machining, edited by R. Komanduri, et al., ASME, New York, (1984) 83-93.

[177] N.A. Abukhshim, P.T. Mativenga, M.A. Sheikh, Heat generation and temperature prediction in metal cutting: A review and implications for high speed machining, Int. J. Mach. Tools Manuf. 46(7-8) (2006) 782-800.

[178] R. Komanduri, Z.B. Hou, Thermal modeling of the metal cutting process-Part II: temperature rise distribution due to frictional heat source at the tool-chip interface, Int. J. Mech. Sci. 43(1) (2001) 57-88.

[179] Y. Karpat, T. Özel, Analytical and thermal modeling of high-speed machining with chamfered tools, ASME J. Manuf. Sci. Eng. 130(1) (2008) 011001.

[180] N.A. Abukhshim, P.T. Mativenga, M.A. Sheikh, Investigation of heat partition in high speed turning of high strength alloy steel, Int. J. Mach. Tools Manuf. 45(15) (2005) 1687-1695.

[181] G. List, G. Sutter, A. Bouthiche, Cutting temperature prediction in high speed machining by numerical modelling of chip formation and its dependence with crater wear, Int. J. Mach. Tools Manuf. 54 (2012) 1-9.

[182] T. Kitagawa, A. Kubo, K. Maekawa, Temperature and wear of cutting tools in high-speed machining of Inconel 718 and Ti-6Al-6V-2Sn, Wear 202(2) (1997) 142-148.

[183] F.J. McGee, An assessment of high-speed machining, SME Tech., MR 78-648 (1978) 22.

[184] F.J. McGee, High speed machining study: methods for aluminum workpieces,

Amer. Mach. 123(3) (1979) 121-126.

[185] R.C. Dewes, E. Ng, K.S. Chua, P.G. Newton, D.K. Aspinwall, Temperature measurement when high speed machining hardened mould/die steel, J. Mater. Process. Technol. 92 (1999) 293-301.

[186] R. Komanduri, D.G. Flom, M. Lee. Highlights of the DARPA advanced machining research program, ASME J. Eng. Ind. 107(4) (1985) 325-335.

[187] R. Radulescu, S.G. Kapoor, An analytical model for prediction of tool temperature fields during continuous and interrupted cutting, ASME J. Eng. Ind. 116(2) (1994) 135-143.

[188] H. Schultz, High speed milling of aluminium alloys, In Proceedings of the Winter Annual Meeting of the ASME, High Speed Machining, New Orleans, (1984) 241-244.

[189] I.F. Dagiloke, A. Kaldos, S. Douglas, B. Mills, High-speed machining: an approach to process analysis, J. Mater. Process. Technol. 54(1-4) (1995) 82-87.

[190] M. Chen, F. Sun, H. Wang, R. Yuan, Z. Qu, S. Zhang, Experimental research on the dynamic characteristics of the cutting temperature in the process of high-speed milling, J. Mater. Process. Technol. 138(1-3) (2003) 468-471.

[191] D. O'sullivan, M. Cotterell, Temperature measurement in single point turning, J. Mater. Process. Technol. 118(1-3) (2001) 301-308.

[192] Z. Palmai, Cutting temperature in intermittent cutting, Period. Polytech. Mech. Eng. 31(1) (1987) 61-78.

[193] D.J. Richardson, M.A. Keavey, F. Dailami, Modelling of cutting induced workpiece temperatures for dry milling, Int. J. Mach. Tools Manuf. 46(10) (2006) 1139-1145.

[194] M.C. Shaw, Energy conversion in cutting and grinding, CIRP Ann. 45(1) (1996) 101-104.

[195] Sandviken Cormorant, Modem metal cutting-A practical handbook, 1994.

[196] V.P. Astakhov, A treatise on material characterization in the metal cutting process, Part 1: A novel approach and experimental verification, J. Mater. Process. Technol. 96(1-3) (1999) 22-33.

[197] F. Jiang, Z. Liu, Y. Wan, Z. Shi, Analytical modeling and experimental investigation of tool and workpiece temperatures for interrupted cutting 1045 steel by inverse heat conduction method, J. Mater. Process. Technol. 213(6) (2013) 887-894.

[198] M. Rahman, Z.G. Wang, Y.S. Wong, A review on high-speed machining of titanium alloys, JSME Int. J. Series C, Mech. Syst. Mach. Element. Manuf. 49(1) (2006) 11-20.

[199] H. Su, P. Liu, Y. Fu, J. Xu, Tool life and surface integrity in high-speed milling of titanium alloy TA15 with PCD/PCBN tools, Chin. J. Aeronaut. 25(5) (2012) 784-790.

[200] M.A. Shalaby, S.C. Veldhuis, Wear and tribological performance of different ceramic tools in dry high speed machining of Ni-Co-Cr precipitation hardenable

aerospace superalloy, Trib. Trans. 62(1) (2019) 62-77.

[201] A. Sharman, R.C. Dewes, D.K. Aspinwall, Tool life when high speed ball nose end milling Inconel 718™, J. Mater. Process. Technol. 118(1-3) (2001) 29-35.

[202] Z.Q. Liu, X. Ai, H. Zhang, Z.T. Wang, Y. Wan, Wear patterns and mechanisms of cutting tools in high-speed face milling, J. Mater. Process. Technol. 129(1-3) (2002) 222-226.

[203] H.A. Kishawy, M. Dumitrescu, E.G. Ng, M.A. Elbestawi, Effect of coolant strategy on tool performance, chip morphology and surface quality during high-speed machining of A356 aluminum alloy, Int. J. Mach. Tools Manuf. 45(2) (2005) 219-227.

[204] A. Ginting, M. Nouari, Experimental and numerical studies on the performance of alloyed carbide tool in dry milling of aerospace material, Int. J. Mach. Tools Manuf. 46(7-8) (2006) 758-768.

[205] R.B. da Silva, Á.R. Machado, E.O. Ezugwu, J. Bonney, W.F. Sales, Tool life and wear mechanisms in high speed machining of Ti-6Al-4V alloy with PCD tools under various coolant pressures, J. Mater. Process. Technol. 213(8) (2013) 1459-1464.

[206] E. Tascioglu, A. Gharibi, Y. Kaynak, High speed machining of near-beta titanium Ti-5553 alloy under various cooling and lubrication conditions, Int. J. Adv. Manuf. Technol. 102(9-12) (2019) 4257-4271.

[207] V.D. Calatoru, M. Balazinski, J.R.R. Mayer, H. Paris, G. L'Espérance,

Diffusion wear mechanism during high-speed machining of 7475-T7351 aluminum alloy with carbide end mills, Wear 265(11-12) (2008) 1793-1800.

[208] D.M. D'addona, S.J. Raykar, M.M. Narke, High speed machining of Inconel 718: tool wear and surface roughness analysis, Procedia CIRP 62 (2017) 269-274.

[209] K.H. Arnold, A. Stoll, Economic and energy-efficient cutting assisted by high-pressure cooling, Using the Example of Titanium Alloys, Sustainable Production for Resource Efficiency and Ecomobility, ICMC, Proceedings, (2010) 231-246.

[210] X. Liang, Z. Liu, W. Liu, B. Wang, G. Yao, Surface integrity analysis for high-pressure jet assisted machined Ti-6Al-4V considering cooling pressures and injection positions, J. Manuf. Process. 40 (2019) 149-159.

[211] Y. Su, N. He, L. Li, X.L. Li, An experimental investigation of effects of cooling/lubrication conditions on tool wear in high-speed end milling of Ti-6Al-4V, Wear 261(7-8) (2006) 760-766.

[212] Y. Kaynak, H.E. Karaca, R.D. Noebe, I.S. Jawahir, Tool-wear analysis in cryogenic machining of NiTi shape memory alloys: A comparison of tool-wear performance with dry and MQL machining, Wear 306(1-2) (2013) 51-63.

[213] N. Tapoglou, M.I.A. Lopez, I. Cook, C.M. Taylor, Investigation of the influence of CO_2 cryogenic coolant application on tool wear, Procedia CIRP 63 (2017) 745-749.

[214] P.C. Jindal, A.T. Santhanam, U. Schleinkofer, A.F. Shuster, Performance of PVD TiN, TiCN, and TiAlN coated cemented carbide tools in turning, Int. J. Refract. Metal. Hard Mater. 17(1-3) (1999) 163-170.

[215] K. Tönshoff, B. Karpuschewski, A. Mohfeld, T. Leyendecker, G. Erkens, H.G. Fuss, R. Wenke, Performance of oxygen-rich TiAlON coatings in dry cuttings applications, Surf. Coat. Technol. 108-109 (1998) 535-542.

[216] H. Schulz, J. Dörr, I.J. Rass, M. Schulze, T. Leyendecker, G. Erkens, Performance of oxide PVD-coatings in dry cutting operations, Surf. Coat. Technol. 146 (2001) 480-485.

[217] K. Bobzin, High-performance coatings for cutting tools, CIRP J. Manuf. Sci. Technol. 18 (2017) 1-9.

[218] M.S.I. Chowdhury, B. Bose, K. Yamamoto, L.S. Shuster, J. Paiva, G.S. Fox-Rabinovich, S.C. Veldhuis, Wear performance investigation of PVD coated and uncoated carbide tools during high-speed machining of TiAl6V4 aerospace alloy, Wear 446 (2020) 203168.

[219] B. Navinsek, P. Panjan, M. Cekada, D.T. Quinto, Interface characterization of combination hard/solid lubricant coatings by specific methods, Surf. Coat. Technol. 154 (2002) 194-203.

[220] K.K. Gajrani, S. Suresh, M.R. Sankar, Environmental friendly hard machining performance of uncoated and MoS_2 coated mechanical micro-textured tungsten carbide cutting tools, Trib. Int. 125 (2018) 141-155.

[221] P. Bałon, J. Szostak, B. Kiełbasa, E. Rejman, R. Smusz, Application of high speed machining technology in aviation, In AIP Conference Proceedings, 1960(1) (2018) 070003.

[222] W. Zhao, Q. Shen, B. Wang, Z. Liu, CNC programming and machining technology for 5-axis milling of turbine blisk, Aeronaut. Manuf. Technol. 60(15) (2017) 58-63.

[223] D. Grguraš, M. Kern, F. Pušavec, Cutting performance of solid ceramic and carbide end milling tools in machining of nickel based alloy Inconel 718 and stainless steel 316L, Adv. Prod. Eng. Manag. 14(1) (2019) 27-38.

[224]https://www.kennametal.com/us/en/site-search.html?query=:relevance:allCategories.

[225]https://www.sandvik.coromant.com/en-gb/products/coromill_316/pages/default.aspx.

[226] D. Grguraš, M. Kern, F. Pušavec, Suitability of the full body ceramic end milling tools for high speed machining of nickel based alloy Inconel 718, Procedia CIRP 77 (2018) 630-633.

[227] H. Zhang, J. Dang, W. Ming, X. Xu, M. Chen, Q. An, Cutting responses of additive manufactured Ti6Al4V with solid ceramic tool under dry high-speed milling processes, Ceram. Int. 46(10) (2020) 14536-14547

[228] B. Wang, Z. Liu, Cutting performance of solid ceramic end milling tools in machining hardened AISI H13 steel, Int. J. Refract. Metal. Hard Mater. 55

(2016) 24-32.

[229] C.A. Dold, G. Eberle, C. Heger, Digitization for highly accurate 3D laser processing of customer-specific tools: digital generation of micro tools in coatable carbide and ultra-hard materials and aspects of autonomous production, Photon. Views 17(2) (2020) 38-42.

[230]https://www.renishaw.com/en/komet-group-innovates-cutting-tools-using-metal-3d-printing-technology--42311.

[231] B. Carlsson, The development and use of machine tools in historical perspective, J. Econ. Behav. Organiz. 5(1) (1984) 91-114.

[232] K. De Decker, How sustainable is digital fabrication, Low-Tech Magaz. (2014) March 25.